The postcranial anatomy and osteohistology of Terrestrisuchus gracilis (Archosauria, Crocodylomorpha) from the Late Triassic of Wales

Spiekman, Stephan N. F.; Butler, Richard J.; Maidment, Susannah C. R.

Link to publication on Research at Birmingham portal

The postcranial anatomy and osteohistology of *Terrestrisuchus gracilis* (Archosauria, Crocodylomorpha) from the Late Triassic of Wales

by STEPHAN N. F. SPIEKMAN[1,2,3,*] (iD), RICHARD J. BUTLER[2] (iD) *and* SUSANNAH C. R. MAIDMENT[1,2] (iD)

[1]Fossil Reptiles, Amphibians & Birds Section, Natural History Museum, Cromwell Road, London SW7 5BD, UK; stephanspiekman@gmail.com
[2]School of Geography, Earth & Environmental Sciences, University of Birmingham, Edgbaston, Birmingham B15 2TT, UK
[3]Staatliches Museum für Naturkunde Stuttgart, Rosenstein 1, 70191 Stuttgart, Germany
*Corresponding author

Abstract: The earliest crocodylomorphs, known as non-crocodyliform crocodylomorphs, first appeared during the Late Triassic. In contrast to extant crocodylians, which are all semi-aquatic, early crocodylomorphs represent terrestrial taxa with a fully erect posture and in most cases a small body size. Their gracile skeletons suggest an active mode of life, possibly similar to contemporaneous, bipedal theropod dinosaurs. Despite this remarkable body plan, the postcranial morphology of early crocodylomorphs has rarely been documented in detail, restricting our ability to infer aspects of their functional morphology and evolution. Here, we provide a detailed description of the postcranium of *Terrestrisuchus gracilis*, a small-bodied crocodylomorph from the Late Triassic of Pant-y-Ffynnon Quarry (southern Wales, UK), including a description of long bone tissues based on histological thin sections. Almost all elements of the postcranial skeleton have been preserved. The skeleton of *Terrestrisuchus gracilis* is highly gracile, even for a non-crocodyliform crocodylomorph. Osteological correlates of the appendicular skeleton suggest that *Terrestrisuchus gracilis* had a digitigrade, quadrupedal posture. A quantitative analysis of limb robustness corroborates that *Terrestrisuchus gracilis* was a quadruped. Histological analysis suggests that all sampled specimens were skeletally immature and had fast growth at the time of death, as indicated by the lack of an external fundamental system and the predominance of fibrolamellar bone. The bone tissue is similar to that recently described for *Saltoposuchus connectens* and certain non-crocodylomorph pseudosuchians, but differs from *Hesperosuchus agilis* and crocodyliforms, in which parallel-fibred bone is more prevalent.

Key words: *Terrestrisuchus*, Crocodylomorpha, Triassic, postcranial osteology, quadrupedality, bone histology.

M ODERN crocodylians are all semi-aquatic predators with limited morphological disparity compared with their deep time crocodylomorph relatives (Brochu 2003; Stubbs *et al.* 2021). Aquatic propulsion of modern taxa is predominantly driven by lateral undulation of the body and tail (Fish 1984), whereas on land the relatively short limbs are held in a position that can be broadly summarized as semi-erect (Parrish 1987; Gatesy 1991; Reilly & Elias 1998; Wiseman *et al.* 2021). During the Mesozoic, crocodylomorphs occupied a much wider range of habitats and had diverse body plans (e.g. Buckley *et al.* 2000; Stubbs *et al.* 2013, 2021; Godoy *et al.* 2019).

Crocodylomorphs first evolved from early pseudosuchian archosaur precursors during the Late Triassic. These early non-crocodyliform crocodylomorphs (often referred to as 'sphenosuchians') were all terrestrial and, although some large-bodied taxa are known (Nesbitt *et al.* 2005; Drymala & Zanno 2016), they were predominantly small-bodied and gracile (Irmis *et al.* 2013). They had long limbs that were held directly below the body in an erect and digitigrade posture (Parrish 1987; Sereno 1991; Sereno & Wild 1992; Cuff *et al.* 2022). Some authors have suggested that *Terrestrisuchus gracilis* and other non-crocodyliform crocodylomorphs might have been (facultative) bipeds (Seymour *et al.* 2004; Benton 2021; Gônet *et al.* 2023), interpretations that have been disputed by others (Crush 1980, 1984; Irmis *et al.* 2013; Cuff *et al.* 2022; Pintore *et al.* 2022). Histological investigations also indicate that at least some taxa (including *Terrestrisuchus* sp.) had fibrolamellar bone indicative of fast growth (de Ricqlès *et al.* 2003, 2008; de Buffrénil & Quilhac 2021; Spiekman 2023). This suggests a considerably higher basal metabolic rate than in modern crocodylians, which is congruent with data from other Triassic archosaurs, including several non-crocodylomorph pseudosuchians (Legendre *et al.* 2016; Klein *et al.* 2017; Botha *et al.* 2023).

Even among non-crocodyliform crocodylomorphs, the limbs of the saltoposuchids (*sensu* Spiekman 2023) are particularly gracile and elongate relative to their body size (Crush 1984; Gow & Kitching 1988; Irmis *et al.* 2013; Spiekman 2023). Known from nearly 200 specimens, the saltoposuchid *Terrestrisuchus gracilis* represents one of the most completely preserved non-crocodyliform crocodylomorphs. Due to its phylogenetic position as a crocodylomorph that is only distantly related to crocodyliforms, *Terrestrisuchus gracilis* is crucial for understanding the early evolution of the clade and the acquisition of crocodylomorph synapomorphies, such as extensive braincase pneumaticity (Leardi *et al.* 2020; Spiekman 2023; Spiekman *et al.* 2023). *Terrestrisuchus gracilis* was previously described by Crush (1980, 1984) and Allen (2010), whereas its cranial morphology was recently documented in detail, aided by digital reconstructions derived from x-ray micro-computed tomography (x-ray μCT) (Spiekman *et al.* 2023). *Terrestrisuchus gracilis* is known from the Late Triassic fissure fill locality of Pant-y-Ffynnon Quarry in southern Wales (Crush 1984). The known Pant-y-Ffynnon fauna is composed of small-bodied tetrapods (Whiteside *et al.* 2016; Keeble *et al.* 2018) that, besides *Terrestrisuchus gracilis*, includes the coelophysoid theropod *Pendraig milnerae* (Spiekman *et al.* 2021), the sauropodomorph *Pantydraco caducus*, which might represent the juvenile form of *Thecodontosaurus antiquus* (Galton *et al.* 2007; Ballell *et al.* 2020), the enigmatic pseudosuchian *Aenigmaspina pantyffynnonensis* (Patrick *et al.* 2019), and the rhynchocephalians *Clevosaurus cambrica*, *Clevosaurus* sp. and *Diphydontosaurus* sp. (Keeble *et al.* 2018).

Most studies of crocodylomorphs, ranging from taxonomic descriptions and morphological character matrices to investigations of macroevolutionary patterns, either exclusively or predominantly focus on cranial anatomy (e.g. Stubbs *et al.* 2013; Toljagić & Butler 2013; Mannion *et al.* 2019; Groh *et al.* 2020; Stubbs *et al.* 2021). Consequently, postcranial features are comparatively much less well understood, despite being crucial for inferring evolutionary innovation, functional morphology, taxonomy and phylogeny (e.g. Pol *et al.* 2012; Leardi *et al.* 2015; Godoy *et al.* 2016; Rio *et al.* 2020). Here, we describe the postcranial anatomy of *Terrestrisuchus gracilis* in detail, and include a histological investigation of its limb bones, and an analysis of its stance (quadrupedal vs bipedal) based on humeral and femoral circumferences.

MATERIAL & METHOD

X-ray micro-computed tomography

For this study, two specimens underwent x-ray μCT scanning using a Nikon Metrology XT H 225 ST (Fernandez 2024). The craniomandibular remains of the first specimen, NHMUK PV R 7591a, consisting of a partial skull and mandible, a caudal vertebra, and the anterior part of the cervical column, were treated in Spiekman *et al.* (2023). Here, digital renderings of the anterior cervical column, including the atlas and axis, are included and described. For the second specimen, the holotype NHMUK PV R 7557, the isolated tarsal elements of the right ankle (NHMUK PV R 7557d), comprising the astragalus, calcaneum and distal tarsals 3 and 4, were scanned. The four tarsal elements were imaged individually to maximize the resolution, fine-tuning parameters for each acquisition accordingly. The parameters for all five scans (including that of NHMUK PV R 7591a) are listed in Table S1.

The μCT data were segmented in Avizo v2020.1 (https://www.thermofisher.com). The resulting surface files were subsequently exported into Blender v3.2 (https://blender.org), where texture and colour were applied to the bones. The elements were digitally re-assembled into their inferred *in vivo* positions. The ball and socket joint formed between the astragalus and calcaneum in *Terrestrisuchus gracilis* represents a highly detailed early example of the 'crocodile-normal' (*sensu* Cruickshank 1979) or crurotarsal ankle joint (Turner & Gatesy 2023). This joint forms the primary ankle articulation in pseudosuchians, including extant crocodylians, in which the astragalus forms a relatively inflexible crus with the tibia and fibula, and the calcaneum similarly forms a rotational unit with the distal tarsals and the pes (Schaeffer 1941; Parrish 1987; Sereno 1991; Turner & Gatesy 2023). Although limited mobility is also present in other planes, the primary rotation of the astragalus–calcaneum joint is along the dorsiflexion–plantarflexion axis in *Alligator mississippiensis*, which has a similar crurotarsal ankle joint to *Terrestrisuchus gracilis* (Turner & Gatesy 2023), and this rotation was modelled for *Terrestrisuchus gracilis* here. Images of the tarsal elements, as well as videos showing the flexion and extension of the astragalus–calcaneum joint (Appendix S1), were rendered in Blender v3.2.

Histology

One femur (NHMUK PV R 37865) and three tibiae (NHMUK PV R 37652, 37664 and 37653) were sampled for histological analysis. Sections of the limb bones were taken at roughly mid-shaft, and thin sections were prepared in accordance with standard histological practices for fossil bone (Sander 2000; Padian & Lamm 2013). The thin sections were examined using a Leica DM CB2 polarizing microscope connected to a Windows PC. Images of the slides were taken using an Axio Imager M2 with an AxioCam HR RS camera.

Analysis of stance

The stance of *Terrestrisuchus* has been the subject of debate in the literature (e.g. Crush 1980; Seymour *et al.* 2004; Pintore *et al.* 2022; Gônet *et al.* 2023). In order to examine whether *Terrestrisuchus* was most likely to be bipedal or quadrupedal, we added it to the dataset of McPhee *et al.* (2018). Linear discriminant analysis of this dataset, which contains femoral and humeral shaft circumferences of a range of mammalian and reptilian (including dinosaur) taxa, demonstrates that there is a relationship between quadrupedality and shaft robustness that can be used to make inferences about stance. We measured the humeral circumference of the holotype of *Terrestrisuchus*, NHMUK PV R 7557 (7.96 mm). The femur of the same specimen is preserved in a slab and thus the circumference cannot be directly measured; we therefore measured the diameter of the shaft (2.88 mm) and calculated circumference assuming that the shaft was cylindrical, giving a circumference of 9.11 mm. We added these data to the McPhee *et al.* (2018) dataset, and plotted it using ggplot2 in R v4.0.4 (Wickham 2016).

Institutional abbreviations. AMNH, American Museum of Natural History, New York NY, USA; CMNH, Carnegie Museum of Natural History, Pittsburgh PA, USA; NHMUK, Natural History Museum, London, UK; SMNS, Staatliches Museum für Naturkunde Stuttgart, Stuttgart, Germany; UCMP, University of California Museum of Paleontology, Berkeley CA, USA; YPM, Yale Peabody Museum, New Haven CT, USA.

SYSTEMATIC PALAEONTOLOGY

ARCHOSAURIA Cope, 1869–1870 *sensu* Gauthier & Padian (2020)
PSEUDOSUCHIA Zittel, 1887
CROCODYLOMORPHA (Hay, 1930) *sensu* Nesbitt (2011)
(= Crocodilomorphi name emend. Walker 1970)
SALTOPOSUCHIDAE Crush, 1984 *sensu* Spiekman (2023)

Terrestrisuchus gracilis Crush, 1984

Holotype. NHMUK PV R 7557a–h, an associated skeleton comprising a largely complete but disarticulated skull, the axis, dorsal, sacral and caudal vertebrae, as well as associated ribs, osteoderms and gastralia, and an appendicular skeleton comprising a left scapula, both ilia and pubes, the distal end of the left humerus, the radius and ulna of both forelimbs, a well-preserved left and poorly preserved right carpus and manus, both femora, and the right tibia, fibula, tarsus and pes.

Referred material. Close to 200 specimens can be referred to *Terrestrisuchus gracilis*, consisting of both associated and isolated remains. A full overview of all referred specimens is provided in the supporting information of Spiekman *et al.* (2023).

Diagnosis. The diagnosis was recently revised by Spiekman *et al.* (2023): '*Terrestrisuchus gracilis* is a small-sized non-crocodyliform crocodylomorph distinguished by the following combination of character states (autapomorphies in non-crocodyliform crocodylomorphs, in part based on the phylogenetic analysis in Spiekman (2023), are indicated with *; traits that are potentially ontogenetically variable are indicated with †): squamosal without a longitudinal crest on the dorsal surface (also absent in *Litargosuchus leptorhynchus*)†; transverse width of anterior process of squamosal wider than supratemporal fenestra (also present in *Saltoposuchus connectens* and *Litargosuchus leptorhynchus*); absence of sagittal crest on parietal (also absent in *Litargosuchus leptorhynchus* and *Kayentasuchus walkeri*)†; presence of a large quadrate fenestra (also present in *Saltoposuchus connectens* and *Almadasuchus figarii*); perilymphatic loop of the otoccipital extends approximately as far ventrally as the subcapsular buttress in lateral view*; presence of an otic bulla on the otoccipital*; enlarged, heavily pneumatized parabasisphenoid body (also present in *Junggarsuchus sloani*, *Almadasuchus figarii*, and *Macelognathus vagans*); elongate anterior process on the lateral head of the ectopterygoid (also present in *Saltoposuchus connectens* and *Junggarsuchus sloani*); retroarticular process elongated, triangular shaped, and dorsally facing*; large pneumatic cavity with dorsal and ventral openings in articular*; distinct postzygodiapophyseal laminae on posterior cervical and anterior dorsal vertebrae (also present in *Hesperosuchus agilis*); narrow teardrop-shaped, poorly sculptured paramedian osteoderms*; proximal end of radius with a medial process (also present in *Hesperosuchus agilis*); proximal ends of metacarpals overlap*; metacarpal I more slender than other metacarpals (also present in *Junggarsuchus sloani*); lateral condyle of distal end of femur projected further distally than medial condyle (also present in *Macelognathus vagans*); tibia longer than femur (also present in *Hallopus victor* and *Macelognathus vagans*); pedal digit V with two phalanges (at least one phalanx also present in *Hesperosuchus agilis*).'

Ontogenetic assessment. The ontogenetic age of the material assigned to *Terrestrisuchus gracilis* was recently assessed in detail in Spiekman *et al.* (2023) based on external skeletal markers, and these interpretations are summarized in brief here. Based on the presence of unfused parietals and unfused neurocentral sutures in most postaxial vertebrae of the *Terrestrisuchus gracilis* specimens, as well as the presence of large pneumatic openings in the articulars of the lower jaw of NHMUK PV R 7591, a feature shared with juvenile individuals of *Alligator mississippiensis* (Dufeau & Witmer 2015), *Terrestrisuchus gracilis* is considered to be represented by skeletally immature specimens (Spiekman *et al.* 2023). Conversely, osteoderms are known to ossify a considerable time after hatching in at least some crocodylomorphs (Vickaryous & Hall 2008; de Buffrénil *et al.* 2015; Griffin *et al.* 2021) and in *Alligator mississippiensis* this ossification occurs asynchronously (Vickaryous & Hall 2008). Given that osteoderms are preserved in all *Terrestrisuchus gracilis* specimens that include partially articulated vertebrae and these osteoderms have the same morphology and relative size in these specimens, this suggests that the osteoderms were fully developed and that these specimens therefore do not represent early juvenile or perinatal individuals. The results of the histological analysis provide further evidence that all known specimens are skeletally

immature, based on the absence of an external fundamental system in the three studied sections. For further details, see the histological discussion below.

Although some have attributed the diminutive size of the fauna at Pant-y-Ffynnon Quarry and other Late Triassic to Early Jurassic fissure fill deposits from the Bristol Channel Area to insular dwarfism (Keeble *et al.* 2018; Ballell *et al.* 2020; Skinner *et al.* 2020; Lovegrove *et al.* 2021), others have argued that this is the result of a taphonomic bias against the preservation of larger animals, which would not have fallen or washed into the fissures (Galton & Kermack 2010). The other Pant-y-Ffynnon archosaur species for which the relative ontogenetic age of their referred specimens has been assessed, the theropod *Pendraig milnerae* and sauropodomorph *Pantydraco caducus*, are also both exclusively known from skeletally immature specimens (Galton & Kermack 2010; Ballell *et al.* 2020; Spiekman *et al.* 2021). The absence of demonstrably mature individuals known for these taxa, in particular for *Terrestrisuchus gracilis*, which is by far the most common archosaur from Pant-y-Ffynnon Quarry with almost 200 specimens, appears to support the latter hypothesis. None of the currently known *Terrestrisuchus gracilis* specimens would have exceeded 1 m in total body length. However, this evidence remains conjectural, and neither hypothesis has been rigorously tested to date (Lovegrove *et al.* 2021; Spiekman *et al.* 2021).

Locality & horizon. Upper Triassic (Carnian–Rhaetian) fissure fill deposits of Pant-y-Ffynnon Quarry in southern Wales (Spiekman *et al.* 2023).

Postcranial description

The material assigned to *Terrestrisuchus gracilis* is extensive and composed of specimens ranging from isolated, fragmentary elements to partially complete and articulated skeletons. Elements of all parts of the postcranium are present among the material. The distribution of the various postcranial elements among the specimens assigned to *Terrestrisuchus gracilis* is listed in Appendix S2 and the entire hypodigm of the species is provided in the supporting information of Spiekman *et al.* (2023).

Axial skeleton

Atlas–axis complex. The atlas–axis complex is predominantly described based on the µCT data of NHMUK PV R 7591 first presented in Spiekman *et al.* (2023) (Fig. 1A–D, F). In NHMUK PV R 7591, two blocky bones are preserved anterior to the axis. These are the atlas pleurocentrum and intercentrum, the former forming a completely fused co-ossification with the axis intercentrum, which is thus absent as a separate element (Korneisel *et al.* 2022). The left atlantal neural arch is an anteroposteriorly elongated, curved element and found in close association with its articular surface of the left side of the axis. A poorly preserved, plate-like bone preserved directly dorsal to the left atlantal neural arch could represent the left proatlas. On the right side of the axis, three elongate, thin bones are preserved, but due to their disarticulation and limited morphological detail they cannot be identified confidently (Fig. 1G, coloured in grey). None of these elements corresponds in size to the right atlantal neural arch. Two sets of paired ribs are preserved ventral to the axis, clearly indicating that the atlas bore ribs in *Terrestrisuchus gracilis*. Atlantal ribs have also been described for *Hesperosuchus agilis* (Colbert 1952) and *Junggarsuchus sloani* (albeit with a very short shaft in this taxon, Ruebenstahl *et al.* 2022) and are also present in extant crocodylians (Hoffstetter & Gasc 1969; Korneisel *et al.* 2022). With the aid of the µCT data, the atlas–axis complex and the articulation of its various element can be described in detail.

The atlas intercentrum is a complex, somewhat bean-shaped bone that has three main surfaces (Fig. 1A–D). The largest of these is the posterodorsal surface. It is concave in posteroventral view and forms the articular surface for the ventral part of the bulbous anterior expansion of the atlas pleurocentrum. Both the ventral and dorsal margins of the posterodorsal surface are transversely concave, with the dorsal margin being particularly deeply excavated. This latter end of the posterodorsal surface also forms the posterodorsal margin of the second surface of the atlas intercentrum, which faced predominantly dorsally and slightly anteriorly. This surface is deeply concave in anteroventral view and formed the articular surface of the posteroventral part of the occipital condyle of the basioccipital of the skull (Fig. 1C–D). This surface is lateromedially wide, extending across almost the entire width of the bone, but anteroposteriorly short. The anteroventral margin of this articular surface is slightly convex, and it also forms the anterodorsal margin of the third and final surface of the atlas intercentrum. This surface faces anteroventrally and is not an articular facet (Fig. 1A, C). It is very slightly concave in anterodorsal view. In addition to these three surfaces, a smaller, excavated, and anterolaterally facing surface is present on each side of the atlas intercentrum. On each ventrolateral end the atlas intercentrum bears a slight expansion. These expansions have a slightly concave articular surface that is mainly directed laterally, but also slightly

FIG. 1. Selected elements of the atlas–axis complex of *Terrestrisuchus gracilis*. A–D, digitally reconstructed and reassembled atlas–axis complex of NHMUK PV R 7591, including third cervical and fraction of the fourth cervical and associated ribs in: A, left lateral view; B, anterior view; C, slightly anteriorly angled left lateral view, including articulation with the basioccipital and right otoccipital; D, angled left anterolateral view; note that the right atlas neural arch and tentative proatlas represent mirrored copies of the left. E, axis NHMUK PV R 7557g in right lateral view. F–G, the digitally reconstructed skull and associated postcranial elements of NHMUK PV R 7591, including the atlas–axis complex, in: F, left lateral or ventral view; G, right lateral view. *Abbreviations*: atic, atlas intercentrum; atlr, atlantal rib; atna, atlas neural arch; atpl, atlas pleurocentrum; ax, axis; axr, axial rib; bo, basioccipital; cev, cervical vertebra; cr, cervical rib; l., left; ll, longitudinal lamina; ns, neural spine; ot, otoccipital; os, osteoderm; poz, postzygapophysis; prat, proatlas; prz, prezygapophysis; r., right; srf, single rib facet. Scale bars represent: 10 mm (A–D, F, G); 5 mm (E).
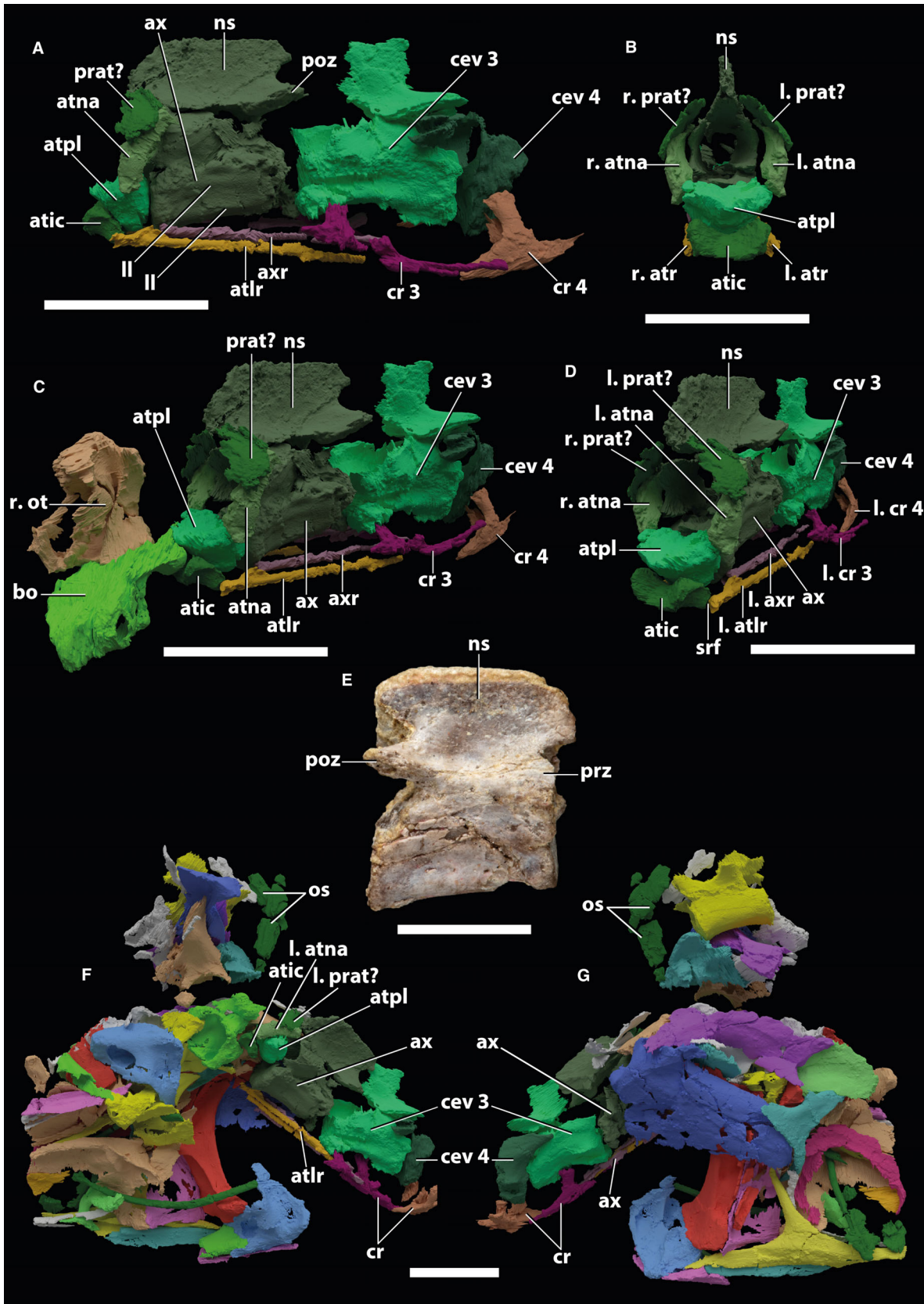
posteriorly. These represent the articular facets for the atlantal ribs, which thus articulated with the atlas intercentrum, as is also the condition in extant crocodylians, *Hesperosuchus agilis* (AMNH FARB 6758), and probably in *Carnufex carolinensis* and *Protosuchus richardsoni* (Colbert & Mook 1952; Drymala & Zanno 2016). In *Hesperosuchus agilis* the atlas intercentrum was previously mistaken for the atlas (pleuro)centrum (Colbert 1952), which is missing in AMNH FARB 6758.

The atlas pleurocentrum (= odontoid) is more than twice the size of the atlas intercentrum (Fig. 1A–D). It is a robust bone that is also composed of three main surfaces. The surface facing dorsally is slightly concave in anterior view (Fig. 1B) and it is continuous with the dorsal surface of the centrum of the axis and with the dorsal surface of the occipital condyle of the skull. It thus forms part of the ventral floor of the neural canal as it exits the skull through the foramen magnum (Fig. 1C). This dorsal surface gradually tapers to a rounded tip anteriorly, which forms the anterodorsal end of the odontoid process. The anterior surface of the atlas pleurocentrum, which is roofed dorsally by the odontoid process, is curved so that it faces anteriorly along the midline and laterally at its posterolateral end on either side (Fig. 1B, D). It forms the articular surface with the atlas intercentrum ventrally and part of the occipital condyle of the basioccipital dorsally. The posterior surface of the atlas pleurocentrum forms the articular surface with the anterior surface of the axial centrum (Fig. 1A). It is slightly convex in lateral view, with its dorsal end extending further posteriorly than its ventral end. The ventral margin of the atlas pleurocentrum is gently convex in anterior view. There are no apparent articular surfaces on the lateral sides of the atlas pleurocentrum for the articulation of the atlantal neural arches, but this is where they would have articulated, as in extant crocodylians and *Hesperosuchus agilis* (Colbert 1952; Hoffstetter & Gasc 1969).

The atlantal neural arch is poorly preserved. It is a curved bone with an expanded, bulbous anteroventral end and a lateromedially thin posterior end (Fig. 1A–D). The bulbous anteroventral end articulated with the atlas pleurocentrum, whereas the posterodorsal end articulated along its medial side with the poorly developed prezygapophysis of the axis (Fig. 1A–B). The medial side of the shaft of the neural arch is distinctly concave, and its lateral side is correspondingly strongly convex (Fig. 1B). In lateral view the atlantal neural arch curved distinctly anteroventrally to posterodorsally, with a convex anterodorsal margin and a concave posteroventral margin (Fig. 1A). The element tentatively identified as the left proatlas is preserved on the dorsolateral side of the left atlantal neural arch. It is a lateromedially thin plate of bone that is dorsoventrally taller than anteroposteriorly long. In both its relative position and shape, it could correspond to a proatlas as seen in extant crocodylians (Hoffstetter & Gasc 1969; Korneisel *et al.* 2022) and as suggested for *Sphenosuchus acutus* (Walker 1990). However, due to the disarticulation of NHMUK PV R 7591, and the presence of several other, unidentified, plate-like bones near this proatlas, this identification cannot be made unequivocally (Fig. 1F).

The axis neural arch and centrum are fused without any discernible suture (Fig. 1A, E). The axis is considerably shorter anteroposteriorly than the succeeding postaxial cervical vertebrae (Fig. 1A). The anterior articular surface of the centrum is mostly flat, but slightly concave dorsally. The dorsal margin of the anterior articular surface is somewhat flattened, whereas the remaining margin, including the ventral portion, is continuously convex and subcircular. The posterior articular surface of the centrum is gently concave (Fig. 1E). The axis centrum bears a faint keel along the midline on its ventral surface, similar to the anterior postaxial cervical vertebrae (see below). In lateral view the ventral surface of the axis is very slightly concave, but much less so than the succeeding postaxial cervical vertebrae (Fig. 1A). The lateral surface of the centrum is flattened and has a slight concavity, which is framed between faint dorsal and ventral, longitudinal laminae (Fig. 1A). On the lateroventral side of the anterior end of the centrum, a roughened thickening represents the articular facet of the axial rib (Fig. 1A). The prezygapophyses of the axis are strongly reduced compared with those of the postaxial cervical vertebrae. They are represented only by a slight, convex anterior projection of the neural arch ventral to the neural spine, and no lateral expansion is discernible (Fig. 1D–E). In contrast, the postzygapophyses are well developed, albeit still reduced compared with the postzygapophyses of the anterior postaxial cervical vertebrae (Fig. 1A). The neural spine of the axis extends for the entire anteroposterior length of the neural arch. Its dorsal margin is mostly straight, but it curves gradually anteroventrally near its anterior end. The posterior end of the dorsal margin of the neural spine forms an acute angle with the posterior margin in lateral view, and the posterior margin is distinctly oriented anteroventrally to posterodorsally (Fig. 1E).

The atlantal ribs are holocephalous and straight. They are elongate, extending to at least the anterior half of the third cervical vertebra (Fig. 1A). The axial ribs are dichocephalous but their tubercular and capitular heads are poorly developed and placed much closer together than in the anterior postaxial cervical ribs. No free-ending anterior process is present on the axial ribs. Both axial ribs extend to approximately the anteroposterior mid-length of the third cervical vertebra, therefore extending only slightly further posteriorly than the atlantal ribs (Fig. 1A).

Postaxial cervical vertebrae & ribs. The postaxial cervical vertebrae are approximately twice as long anteroposteriorly as their posterior articular surface is tall dorsoventrally, similar to that in other crocodylomorphs (e.g. Colbert 1952; Lecuona *et al.* 2016), but contrasting with the comparatively shorter cervical vertebrae seen in crocodyliform notosuchians and thalattosuchians (Georgi & Krause 2010; Pol *et al.* 2012; Johnson *et al.* 2020). The postaxial cervical vertebrae are amphicoelous, with both the anterior and posterior articular surfaces of the centrum being concave (Fig. 2). The neurocentral suture can be clearly observed in the postaxial cervical vertebrae (Figs 2, 3).

The ventral margins of the centra of the postaxial cervical vertebrae are concave in lateral view. In the anterior cervical vertebrae this concavity is asymmetrical, being strongly concave on its anterior portion and gradually concave posteriorly (Fig. 2A). Consequently, the deepest excavation of the concavity is positioned anterior to the anteroposterior mid-point of the centrum in these elements. In addition, in these vertebrae the anteroventral margin of the centrum is positioned slightly higher (i.e. further dorsally) than the posteroventral margin of the centrum
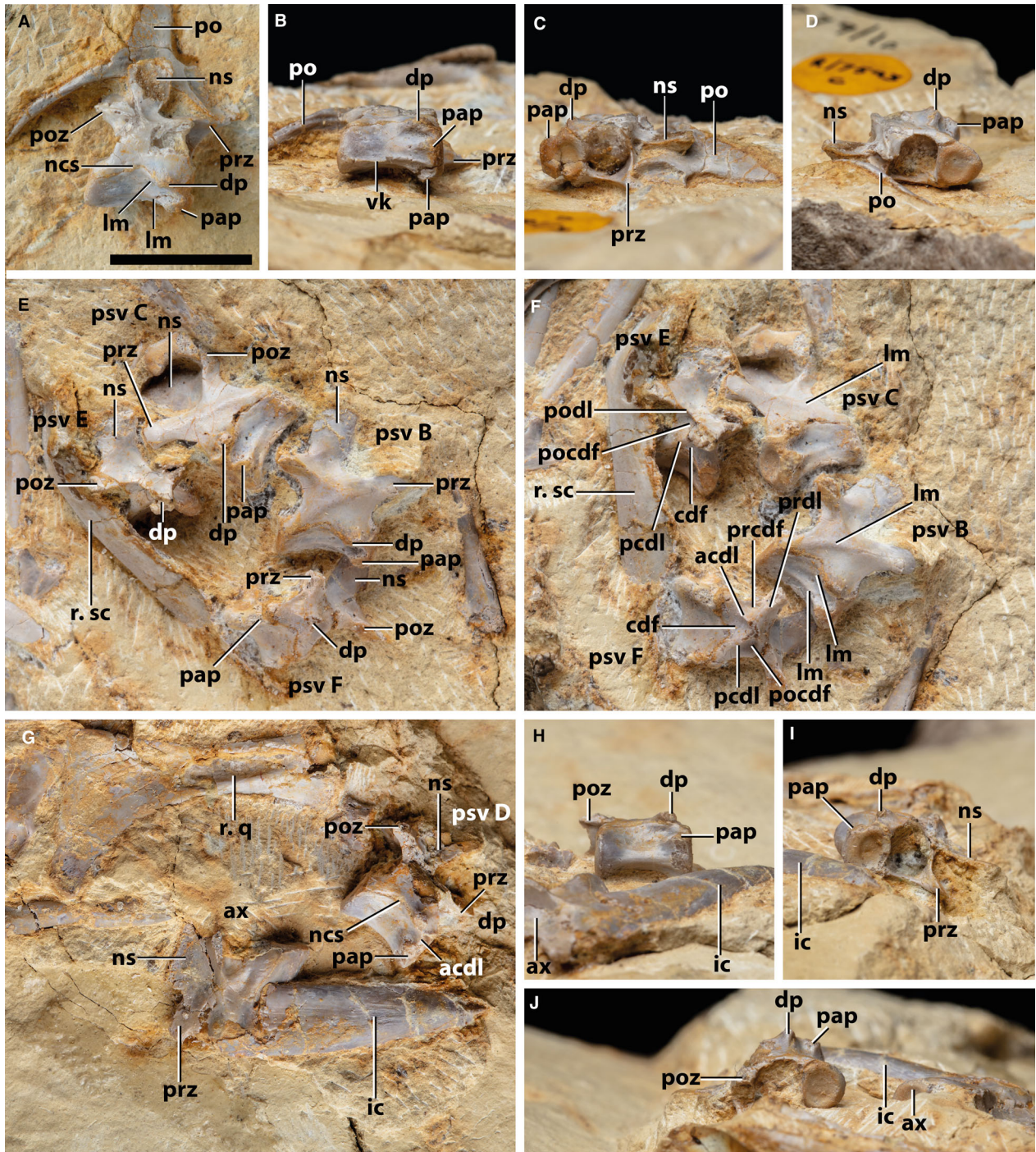
FIG. 2. Cervical and possibly anterior dorsal vertebrae of NHMUK PV R 7593 and associated elements. Because the vertebrae are disarticulated the exact position in the vertebral column could not be established (see text). Therefore, the vertebrae are labelled A–F, with A being the inferred anteriormost and F the posteriormost presacral vertebra preserved. A–D, presacral vertebra A in: A, right lateral; B, ventral; C, anterior; D, posterior view. E–F, presacral vertebrae B–C and E–F in lateral or angled lateral view. G, axis, exposed in left lateral view, presacral vertebra D, exposed in right lateral view, and associated elements. H–J, presacral vertebra D in: H, ventral; I, anterior; J, posterior view. *Abbreviations*: acdl, anterior centrodiapophyseal lamina; ax, axis; cdf, centrodiapophyseal fossa; dp, diapophysis; ic, interclavicle; lm, lamina; ncs, neurocentral suture; ns, neural spine; pcdl, posterior centrodiapophyseal lamina; pap, parapophysis; po, postorbital; pocdf, postzygapophyseal centrodiapophyseal fossa; podl, postzygodiapophyseal lamina; poz, postzygapophysis; prcdf, prezygapophyseal centrodiapophyseal fossa; prdl, prezygodiapophyseal lamina; prz, prezygapophysis; psv, presacral vertebra; q, quadrate; r., right; sc, scapula; vk, ventral keel. Scale bar represents 10 mm.

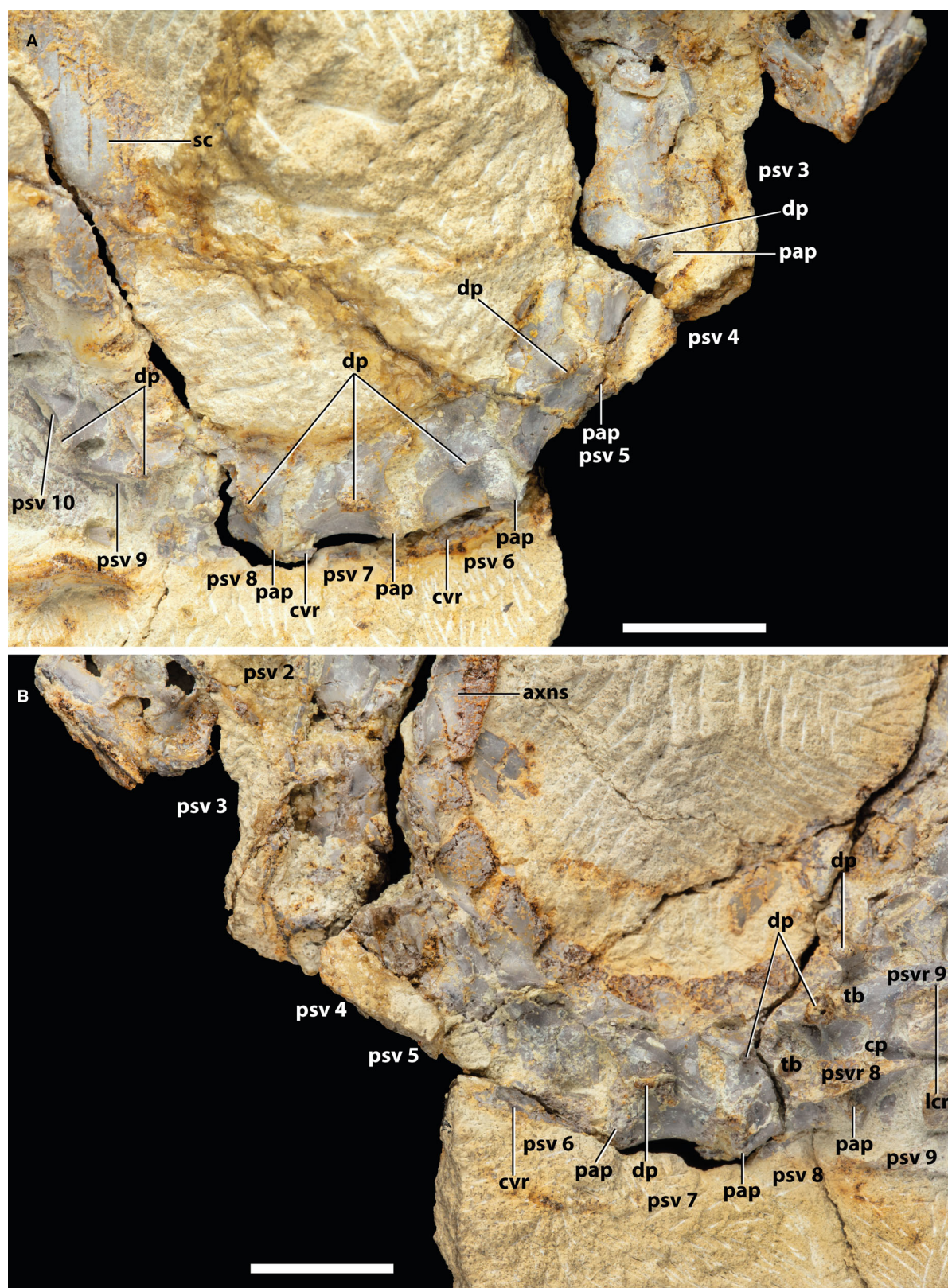**F I G . 3 .** Cervical region of NHMUK PV R 7591 in: A, right lateral; B, left lateral view. *Abbreviations*: axns, axis neural spine; cp; capitulum; cvr, cervical rib; dp, diapophysis; lcr, longitudinal crest; pap, parapophysis; psv, presacral vertebra; psvr, presacral rib; sc, scapula; tb, tuberculum. Scale bars represent 10 mm.

relative to the horizontal plane, as is the case in most archosaurs but not *Trialestes romeri* (Lecuona *et al.* 2016). This concavity becomes less pronounced posteriorly, but is still slightly present in the seventh cervical vertebra of NHMUK PV R 7591 (Fig. 3B). In vertebra F of NHMUK PV R 7593 (posterior cervical or anterior dorsal vertebra) this concavity is virtually symmetrical in lateral view (Fig. 2E–F). The anteroventral and posteroventral margins of the centrum are positioned at the same horizontal level in cervical vertebra 7 in NHMUK PV R 7591, while in vertebra F of NHMUK PV R7593a the anteroventral margin is positioned slightly lower (i.e. ventral) than the posteroventral margin in the horizontal plane. This transition from asymmetrical to virtually symmetrical ventral margins of the centra in lateral view from the anterior to posterior cervical vertebrae is also present in *Hesperosuchus agilis* and *Dibothrosuchus elaphros* (Colbert 1952; Wu & Chatterjee 1993).

In all postaxial cervical vertebrae of *Terrestrisuchus gracilis*, the anterior articular surface of the centrum is slightly wider lateromedially than tall dorsoventrally (Fig. 2C, I), whereas the posterior articular surface is subcircular (Fig. 2D, J). Both are clearly demarcated by a pronounced outer rim. Vertebra A of NHMUK PV R 7593a (anterior cervical vertebra) bears a thin ventral keel, which is quite distinct posteriorly but broken anteriorly (Fig. 2B). As such it appears as a ventral expansion on the posterior portion of the centrum, which was misinterpreted as a small hypapophysis by Crush (1980). A ventral keel in cervical vertebra 3 of *Sphenosuchus acutus* was also interpreted as a hypapophysis by Walker (1990). However, hypapophyses, which occur in some cervical vertebrae of extant crocodylians (Hoffstetter & Gasc 1969), are absent in all cervical vertebrae of *Terrestrisuchus gracilis*. Among non-crocodyliform crocodylomorphs, unambiguous hypapophyses are present only in *Junggarsuchus sloani* (Ruebenstahl *et al.* 2022). Anteriorly the ventral surface of vertebra A of NHMUK PV R 7593a forms a shallow longitudinally directed depression between the keel and the parapophysis on each side of the vertebra. Cervical vertebra 6 of NHMUK PV R 7591 has a shallow longitudinal groove instead of a keel on its ventral surface, and both a keel and groove are absent in more posterior vertebrae, in contrast to *Dromicosuchus grallator*, which bears a ventral keel on all cervical vertebrae (Sues *et al.* 2003). In all postaxial cervical vertebrae the centrum is somewhat lateromedially constricted at its anteroposterior midpoint compared with the articular faces. This constriction is subtle in anterior cervical vertebrae, but posteriorly the centra become gradually narrower lateromedially (i.e. the centra are pinched) and the lateral surfaces of the centra become more distinctly concave at their anteroposterior midpoint.

In vertebrae A and B of NHMUK PV R 7593 (anterior cervical vertebrae), the diapophysis is positioned almost as far anteriorly as the parapophysis, and the diapophysis is positioned partially on the centrum, on its dorsolateral margin close to the anterior edge of the centrum (Fig. 2A, E). As such, the diapophysis is positioned only slightly dorsal to the parapophysis. The articular facet of the diapophysis is roughly oval in outline, being longer anteroposteriorly than tall dorsoventrally, whereas that of the parapophysis is considerably larger and triangular, tapering posteriorly. The articular facet of the diapophysis faces lateroventrally and that of the parapophysis predominantly

laterally. Anteriorly, the parapophysis is confluent with the lateral margin of the anterior articular surface of the centrum. The lateral surface of the centrum between the para- and diapophysis is distinctly concave. Thin laminae project from both the para- and diapophysis in a posterior direction (Fig. 2A, F). The lamina of the parapophysis curves posteriorly along the lateroventral surface of the centrum and fully fades away only on the posterior portion of the centrum. It becomes gradually shorter in subsequent vertebrae, before completely disappearing in cervical vertebra 7 of NHMUK PV R 7591. The lamina of the diapophysis is more posterodorsally oriented and is considerably shorter, not quite reaching the anteroposterior mid-length of the centrum. In vertebrae B and C of NHMUK PV R 7593a (anterior to mid-cervical vertebrae), a low, slightly curved lamina is projected across the lateral surface of the neural arch between the prezygapophysis and the posteroventral corner of the lateral surface of the neural arch (Fig. 2F).

The diapophysis is gradually placed further posteriorly and dorsally in subsequent cervical vertebrae. It also projects gradually further laterally, with laminae projecting along the lateral surface of the vertebra from it. An anterior centrodiapophyseal lamina (*sensu* Wilson 1999) can first be discerned in vertebra D of NHMUK PV R 7593b (mid or posterior cervical vertebra; Fig. 2G) and it becomes more prominent in subsequent vertebrae. Vertebrae E (posterior cervical vertebra) and F (posterior cervical or anterior dorsal vertebra) additionally also possess distinct prezygodiapophyseal, postzygodiapophyseal and posterior centrodiapophyseal laminae (*sensu* Wilson 1999; Fig. 2F). Posterior and ventral to the diapophysis, these laminae form two fossae, a postzygapophyseal centrodiapophyseal fossa and centrodiapophyseal fossa, respectively (*sensu* Wilson *et al.* 2011; Fig. 2F). A weakly demarcated prezygapophyseal centrodiapophyseal fossa is also present in vertebra F. These laminae are also present in the posterior cervical vertebrae of *Hesperosuchus agilis* and *Carnufex carolinensis* (Colbert 1952; Drymala & Zanno 2016). In vertebra D the articular facet of the diapophysis is still oval and oriented slightly lateroventrally (Fig. 2G–H). In vertebrae E and F the articular facet of the diapophysis faces laterally and it is no longer directly adjacent to the neurocentral suture (Fig. 2E). In these two vertebrae the parapophysis still has a triangular articular facet and it is confluent with the anterior margin of the centrum, but it is positioned more dorsally on the centrum, with its dorsal portion being placed on the neural arch.

In all postaxial cervical vertebrae the prezygapophyses are directed anterodorsally from the neural arch. Their articular facets face dorsomedially, and those of the postzygapophyses ventrolaterally. In vertebrae A–C of NHMUK PV R 7593 the prezygapophysis is strongly developed and extends considerably anteriorly beyond the anterior margin of the centrum (Fig. 2A, E, F), as in the anterior cervical vertebrae of *Hesperosuchus agilis*, *Sphenosuchus acutus* and *Trialestes romeri* (Colbert 1952; Walker 1990; Lecuona *et al.* 2016), but unlike the less strongly developed prezygapophyses of the anterior cervical vertebrae of *Dromicosuchus grallator* (Sues *et al.* 2003). It extends only slightly beyond the anterior margin of the centrum in vertebra D (Fig. 2G), and barely reaches beyond this margin in vertebra E and F (Fig. 2E). The postzygapophysis, in contrast, does not

project, or barely projects, posteriorly beyond the posterior margin of the centrum in vertebrae A–D, whereas it is almost fully projected beyond this margin in vertebrae E and F. The postzygapophyses do not possess epipophyses in any of the cervical vertebrae, as in other crocodylomorphs (e.g. Georgi & Krause 2010; Lecuona *et al.* 2016). A hypantrum–hyposphene articulation between the vertebrae was absent in *Terrestrisuchus gracilis* (Fig. 2D, J), as in all known crocodylomorphs (Stefanic & Nesbitt 2019). Other forms of accessory intervertebral articulations as seen in *Carnufex carolinensis* and several non-crocodylomorph paracrocodylomorphs (Drymala & Zanno 2016) are similarly absent. The neural canal is roughly subcircular in anterior view (Fig. 2C) and subrectangular in posterior view (Fig. 2D, J). It is slightly taller dorsoventrally than lateromedially wide both anteriorly and posteriorly. A clear but shallow fossa is present on the neural arch at the base of the neural spine in lateral view in all cervical vertebrae.

The neural spines of all postaxial cervical vertebrae are similar in that they are positioned on the posterior half of the neural arch and are strongly concave at the base of the anterior margin, as in *Carnufex carolinensis* and *Sphenosuchus acutus* and in the anterior cervical vertebrae of *Hesperosuchus agilis* (Colbert 1952; Walker 1990; Drymala & Zanno 2016). In contrast, the neural spine occupies most of the anteroposterior length of the dorsal surface of the neural arch in *Trialestes romeri* and *Dibothrosuchus elaphros*, and in the posterior cervical vertebrae of *Hesperosuchus agilis* (Colbert 1952; Wu & Chatterjee 1993; Lecuona *et al.* 2016). In lateral view the neural spines are oriented slightly anterodorsally, and both the anterior and posterior margin are roughly straight on their distal halves. The neural spines are slightly taller than half the anteroposterior length of the centrum of the corresponding vertebra (Table S2), and as such they are similar in relative height to the cervical vertebrae of *Sphenosuchus acutus* (Walker 1990), but considerably taller than those of *Trialestes romeri* (Lecuona *et al.* 2016), and shorter than those of *Saltoposuchus connectens*, *Hesperosuchus agilis*, *Carnufex carolinensis* and *Dibothrosuchus elaphros* (Colbert 1952; Wu & Chatterjee 1993; Drymala & Zanno 2016; Spiekman 2023). The neural spines are lateromedially thin and do not laterally expand, contrary to certain non-crocodylomorph pseudosuchians such as erpetosuchids and the only other known pseudosuchian from Pant-y-Ffynnon Quarry, *Aenigmaspina pantyffynnonensis* (Patrick *et al.* 2019), in which this is most clearly expressed. Among non-crocodyliform crocodylomorphs, *Hesperosuchus agilis* has posterior cervical vertebrae that have a narrow distal lateral expansion of their neural spine (Colbert 1952). The neural spines of *Terrestrisuchus gracilis* maintain roughly the same height and anteroposterior length along the cervical series. The distal ends of the neural spines are slightly and continuously convex in lateral view and very slightly slanted anterodorsally to posteroventrally in lateral view (Fig. 3B).

As in other archosaurs, the cervical ribs are thin and oriented parallel to the cervical column. Cervical ribs 3 and 4 are dichocephalous, with the tuberculum being considerably more elongate than the capitulum (Fig. 1). They have a short but distinct anterior free-ending process as in other crocodylomorphs, including crocodyliforms (e.g. Hoffstetter & Gasc 1969; Leardi *et al.* 2015; Lecuona *et al.* 2016; Johnson *et al.* 2020). In the

anterior cervical ribs, the capitulum and tuberculum are set at an acute angle to each other, resulting in a V-shaped outline of the cervical rib head in anterior or posterior view. Thin laminae are projected posteriorly from the base of both the capitulum and tuberculum, with a concave gully formed between them. The articular surfaces of both rib facets are oval, being longer anteroposteriorly than wide lateromedially. The eighth cervical rib differs strongly from preceding cervical ribs in that the proximal portion of the shaft, as well as the preserved tuberculum, is flattened and wide (Fig. 3B). Posteriorly, this wide, plate-like surface becomes gradually narrower, before transitioning into a thin shaft with a subcircular cross-section as in the preceding ribs at approximately the anteroposterior level of the diapophysis of presacral vertebra 9. This rib also differs from preceding ribs in that its shaft is oriented posteroventrally and slightly laterally. Like the preceding cervical ribs, the shaft is short (i.e. it does not project posteriorly behind the left scapulocoracoid that covers it) and straight. It is unclear whether this rib also bore an anterior, free-ending process. The left rib of presacral vertebra 9 is much closer in morphology to the ribs of the dorsal vertebrae. It is elongate, strongly curved ventrally, and it projects far posterior to the left scapulocoracoid (Fig. 3B). The orientation of this rib is subparallel to the subsequent dorsal ribs. In contrast to the preceding ribs, the tuberculum is shorter than the capitulum (Fig. 3B). The tuberculum is oriented roughly in the same plane as the shaft, whereas the capitulum projects ventrally from the main body of the rib and curves ventrolaterally. The proximal part of the shaft is considerably dorsoventrally wider than the posterior shaft. A sharp longitudinal crest is projected on the ventral portion of the anterior surface of the proximal portion of the shaft. In these features, presacral rib 9 is also very similar to subsequent dorsal ribs (see below).

The transition between the cervical and dorsal series of the vertebral column is often difficult to establish based on fossil material. Crush (1980) suggested that the exact number of cervical vertebrae of *Terrestrisuchus gracilis* could not be determined, given that he defined cervical vertebrae 'as those whose ribs do not reach the sternum' (Crush 1980, p. 128), and this information is not available in the known material. Indeed, in extant crocodylians the ninth presacral rib is similar in morphology and orientation to that of the subsequent dorsal ribs, but it does not reach the sternum. Nevertheless, the ninth presacral of crocodylians is unambiguously a cervical vertebra (Hoffstetter & Gasc 1969; Mansfield & Abzhanov 2010). Therefore, the identity of the ninth presacral vertebra in *Terrestrisuchus gracilis* as either a cervical or dorsal vertebra remains ambiguous despite the strong morphological similarities of its ribs to dorsal ribs. The exact number of cervical vertebrae in other non-crocodyliform crocodylomorphs has also not been established confidently, but it has been assumed to be nine in *Sphenosuchus acutus* and *Dibothrosuchus elaphros* (Walker 1990; Wu & Chatterjee 1993).

Dorsal vertebrae & ribs. As explained above, the identity of presacral vertebra 9 as a cervical or dorsal vertebra cannot be unambiguously established. However, all presacral vertebrae posterior to this element almost certainly represent dorsal vertebrae. The neurocentral suture is unfused in all known dorsal vertebrae of *Terrestrisuchus gracilis*. The exact dorsal vertebral count

cannot be established because no specimen preserves a complete dorsal series, but it is likely to have been 15 or 16 as in other crocodylomorphs.

The anterior dorsal vertebrae are morphologically very similar to the posterior cervical vertebrae (Figs 4, 5A–F). The centrum has a concave ventral margin that is symmetrical in lateral view, as in other non-crocodyliform crocodylomorphs (e.g. *Trialestes romeri*, *Pseudhesperosuchus jachaleri*; Bonaparte 1972; Lecuona *et al.* 2016). There is no indication of a median keel on the ventral margin of the anterior dorsal centrum (Fig. 5C), in contrast to *Trialestes romeri* and *Macelognathus vagans* (Göhlich *et al.* 2005; Lecuona *et al.* 2016). In both the anterior dorsal and mid-dorsal vertebrae the anterior and posterior articular surfaces of the centrum are subequal in height and both surfaces are subcircular in outline (Fig. 5E, F, K, L). In the anterior dorsal vertebra NHMUK PV R 37874 the anterior surface is flat to very slightly concave, whereas the posterior surface is more strongly concave and marked by a distinct rim. In the mid-dorsal vertebra NHMUK PV R 37894 this situation is reversed, with the anterior surface being more concave than the virtually flat posterior surface and the former being rimmed by a distinct margin. In lateral view, the ventral portion of the posterior margin of the centrum is somewhat thickened and rugose (Fig. 5G–H). The posterior articular surface is slightly concave and rimmed in presacral vertebra 17 of NHMUK PV 7591 (Fig. 4B). In ventral view, the centra are constricted, being almost twice as wide at their ends as at their anteroposterior midpoint (Fig. 5C, I). The centra lack a hypapophysis, contrary to extant crocodylians. A hypapophysis is present in the anterior dorsal vertebrae of *Macelognathus vagans* and *Junggarsuchus sloani* (Clark *et al.* 2004; Göhlich *et al.* 2005). Crush (1980, 1984) suggested that the dorsal vertebrae slightly increase in length posteriorly, but this is not unambiguously supported by our measurements (Table S2).

As in *Carnufex carolinensis* (Drymala & Zanno 2016), the pre- and postzygapophyses do not extend very far beyond the centrum in the anterior dorsal vertebrae (Figs 4A, 5A–B). In contrast, the pre- and postzygapophyses are considerably more elongate in *Trialestes romeri*, *Dibothrosuchus elaphros* and *Hesperosuchus agilis*, with the prezygapophyses being directed distinctly anterodorsally and the postzygapophyses posterodorsally (Colbert 1952; Wu & Chatterjee 1993; Lecuona *et al.* 2016). The articular facet of the prezygapophysis faces mostly dorsally and slightly medially, and that of the postzygapophysis faces mostly ventrally and slightly laterally (Fig. 5). The postzygapophyses do not bear epipophyses (Fig. 5A, B, G, H). An accessory intervertebral articulation, such as a hyposphene–hypantrum articulation (Stefanic & Nesbitt 2019), is also absent in the dorsal vertebrae (Fig. 5F–L), unlike in *Carnufex carolinensis* (Drymala & Zanno 2016). The neural spine was similar in relative height to that seen in *Saltoposuchus connectens*, *Hesperosuchus agilis*, *Junggarsuchus sloani*, *Macelognathus vagans* and *Trialestes romeri* (Colbert 1952; Clark *et al.* 2004; Göhlich *et al.* 2005; Lecuona *et al.* 2016; Spiekman 2023), and thus not markedly tall as in *Dibothrosuchus elaphros* and *Carnufex carolinensis* (Wu & Chatterjee 1993; Drymala & Zanno 2016). The distal end of the neural spine is not laterally expanded (Fig. 5E–F), similar to *Carnufex carolinensis* and *Saltoposuchus connectens* (Drymala &

Zanno 2016; Spiekman 2023), but in contrast to *Hesperosuchus agilis*, *Dibothrosuchus elaphros* and *Trialestes romeri*, which bear a narrow spine table on their anterior dorsal vertebrae (Colbert 1952; Wu & Chatterjee 1993; Lecuona *et al.* 2016).

In the anterior dorsal vertebrae, the parapophysis is positioned at the anterior margin of the neural arch, distinctly ventral to the prezygapophysis (Fig. 5A–B). A very low lamina is projected anteroventrally to posterodorsally between the para- and diapophysis, the paradiapophyseal lamina (*sensu* Wilson 1999; Fig. 5A). As in all dorsal vertebrae, the parapophysis is only very minorly laterally projected from the neural arch. The diapophysis is placed on an anteroposteriorly elongate transverse process that projects far laterally (Fig. 5D–F). It is positioned on the same dorsoventral level as the pre- and postzygapophyses (Fig. 5A–B). The articular facet of the diapophysis is oval, being anteroposteriorly longer than dorsoventrally tall. There is no fossa at the base of the diapophysis on its dorsal surface, in contrast to *Trialestes romeri* (Lecuona *et al.* 2016). The parapophyses are too poorly preserved to determine the morphology of their articular facet. The diapophysis is connected at its base to both zygapophyses by thin, well developed laminae on either side, the prezygodiapophyseal lamina anteriorly and postzygodiapophyseal lamina posteriorly (Fig. 5A–B), as in other non-crocodyliform crocodylomorphs (e.g. *Carnufex carolinensis*, *Trialestes romeri*, *Hesperosuchus agilis*; Colbert 1952; Drymala & Zanno 2016; Lecuona *et al.* 2016). Anterior to the diapophysis, a prezygapophyseal centrodiapophyseal fossa (*sensu* Wilson *et al.* 2011) is formed that is demarcated by the prezygodiapophyseal lamina dorsally and paradiapophyseal lamina posteroventrally. In addition to the low paradiapophyseal lamina that is projected anteroventrally from the diapophysis, a low posteroventrally directed lamina is also present in anterior dorsal vertebrae, the posterior centrodiapophyseal lamina (Fig. 5A). The postzygapophyseal centrodiapophyseal fossa is framed anteroventrally by this lamina, and dorsally by the postzygodiapophyseal lamina. This fossa is positioned directly posterior to the diapophysis. In addition to this, a centrodiapophyseal fossa is placed ventral to the diapophysis, which is framed between the paradiapophyseal lamina anterodorsally and the posterior centrodiapophyseal lamina posterodorsally. In anterior view a clear intraprezygapophyseal lamina, as well as spinoprezygapophyseal laminae, are also present in anterior dorsal vertebrae (Fig. 5E), and these laminae demarcate a clear and deeply excavated spinoprezygapophyseal fossa. In posterior view an intrapostzygapophyseal lamina and spinopostzygapophyseal laminae are also present (Fig. 5F). A spinopostzygapophyseal fossa was probably also developed, but this region is covered in sediment. All of these laminae and fossae are restricted to the neural arch (i.e. they do not extend onto the centrum).

The parapophysis gradually moves further dorsally on the neural arch further posterior along the dorsal series. In presacral vertebra 14 of NHMUK PV R 7591b and mid-dorsal vertebra NHMUK PV R 37894 the parapophysis is confluent with the base of the prezygapophysis (Figs 4B, 5G–H). Here, the articular facet of the parapophysis is oval, being very slightly longer anteroposteriorly than tall dorsoventrally. The facet of the diapophysis is also oval, but it is relatively more elongate anteroposteriorly and shorter dorsoventrally than the parapophysis.

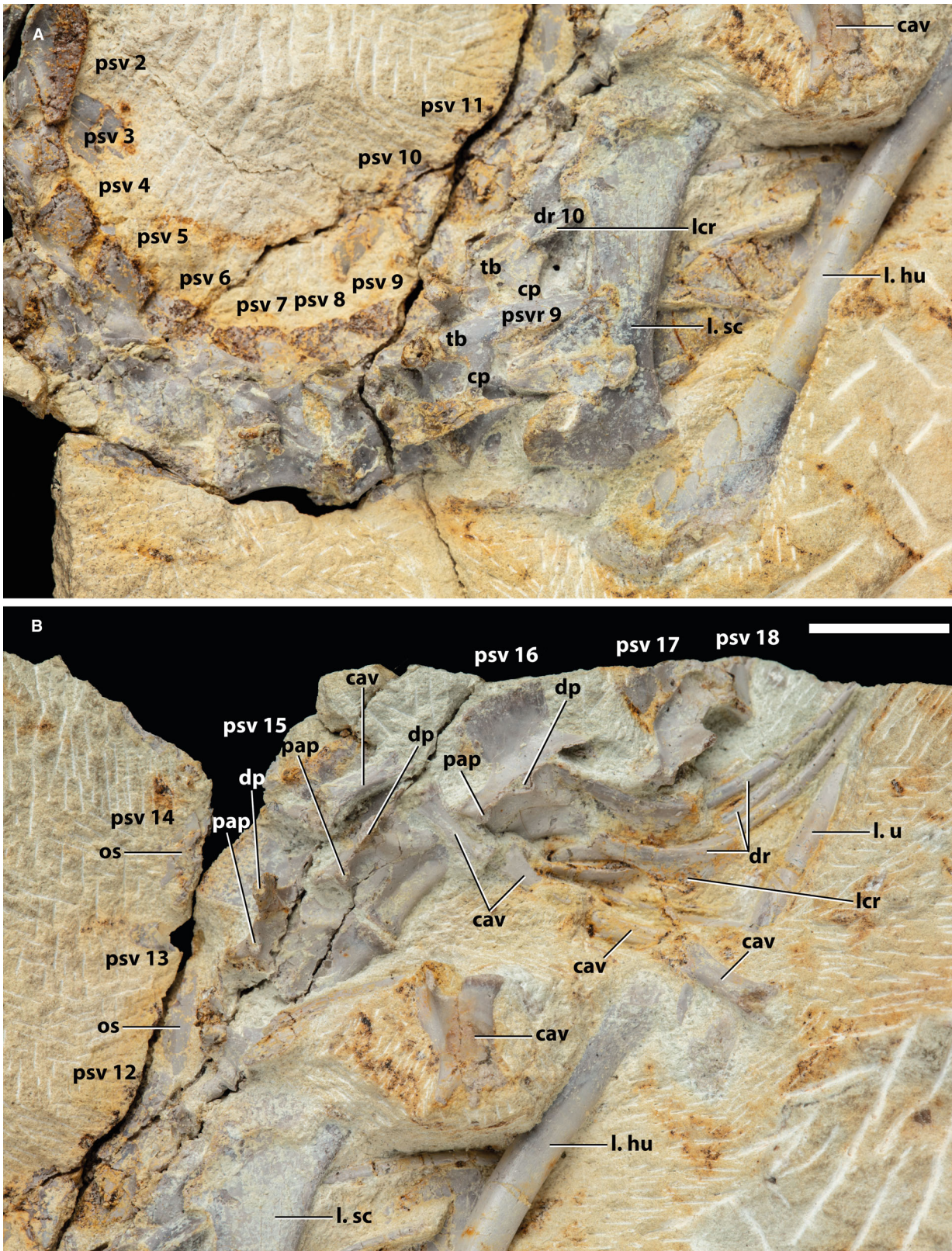**FIG. 4.** Dorsal vertebral region of NHMUK PV R 7591. A, anterior dorsal region; B, mid-dorsal region; both in left lateral view. *Abbreviations*: cav, caudal vertebra; cp, capitulum; dp, diapophysis; dr, dorsal rib; hu, humerus; l., left; lcr, longitudinal crest; os, osteoderm; pap, parapophysis; psv, presacral vertebra; psvr, presacral rib; sc, scapula; tb, tuberculum; u, ulna. Scale bar represents 10 mm.

The para- and diapophysis are still connected through a paradiapophyseal lamina (*sensu* Wilson 1999), which is nearly horizontally oriented in this specimen, being very slightly anteroventrally to posterodorsally directed (Fig. 5H). The posterior centrodiapophyseal lamina and postzygodiapophyseal laminae are similar in development and orientation as in the anterior dorsal vertebrae (Fig. 5G–H), and consequently the postzygapophyseal centrodiapophyseal fossa, which is demarcated by these laminae, is also similar. A centrodiapophyseal fossa is present, but it is extended further anterodorsally than in the anterior dorsal vertebrae. A prezygapophyseal centrodiapophyseal fossa is absent. A spinoprezygapophyseal lamina is present in presacral vertebra 15 of NHMUK PV R 7591b (Fig. 4B). A clear spinopostzygapophyseal lamina and an intrapostzygapophyseal lamina, which form the margins of a deeply excavated spinopostzygapophyseal fossa, are preserved in the isolated vertebra NHMUK PV R 37874 (Fig. 5L). The neural spines have a similar morphology to those of the anterior dorsal vertebrae. In lateral view the margin of the neural spine is deeply concave at its anterior base and slightly concave at its posterior base (Fig. 4B). The distal half of the anterior margin is somewhat anterodorsally directed and that of the posterior margin is very slightly posterodorsally directed. As such, the neural spine is somewhat fan shaped in lateral view, being anteroposteriorly longer at its distal end than at its base, with this expansion being most prominent anteriorly, as in *Junggarsuchus sloani* (Ruebenstahl *et al.* 2022). The distal margin of the neural spine is slightly convex and slightly taller anteriorly than posteriorly.

In the posterior dorsal vertebrae the diapophysis is gradually positioned further anteroventrally on the lateral side of the neural arch towards the parapophysis (Fig. 6). Furthermore, the diapophysis extends gradually less far laterally in the more posterior dorsal vertebrae. The parapophysis remains in approximately the same position on the neural arch in the posterior presacral vertebrae as it was in the mid-dorsal vertebrae. As in the preceding vertebrae, the parapophysis is also only slightly projected laterally from the neural arch in the posterior dorsal vertebrae. However, in the second to last presacral vertebra, in which the parapophysis connects to the diapophysis (Fig. 6A), the parapophysis is extended further laterally comparatively. Although the diapophysis and parapophysis are directly connected in this element, they are still present as distinguishable rib facets, whereas in the last presacral vertebra only a single rib facet remains (Fig. 6). In contrast, in *Dromicosuchus grallator* the para- and diapophysis are already confluent in the 13th presacral vertebra (Sues *et al.* 2003). The articular facets of the para- and diapophysis become gradually dorsoventrally flatter in the posterior dorsal vertebrae and, as such, they appear more elongate. These facets are particularly flattened in the third to last and second to last presacral vertebrae. In the last presacral vertebra, the single rib facet is enlarged and more oval than the two preceding vertebrae, and it has a concave surface.

A clear paradiapophyseal lamina (*sensu* Wilson 1999) is present between the diapophysis and parapophysis of the posterior presacral vertebrae (Fig. 6) until these structures meet in the second to last presacral vertebra. As in the preceding dorsal vertebrae, the posterior dorsal vertebrae up until the third to last presacral vertebra possess a low posterior centrodiapophyseal lamina and postzygodiapophyseal lamina that demarcate a postzygapophyseal centrodiapophyseal fossa (*sensu* Wilson 1999; Wilson *et al.* 2011). A centrodiapophyseal fossa is still present in the third to last presacral vertebra. In contrast to the preceding dorsal vertebrae, the fourth to last and third to last presacral vertebrae bear a short but distinct anterior centroparapophyseal lamina (*sensu* Wilson 1999) that is projected anteroventrally from the parapophysis and which fades away at the anterodorsal tip of the centrum in lateral view (Fig. 6B). It is unclear whether these laminae and fossae also occurred in the two posteriormost presacral vertebrae, because this region is obscured by overlying ribs and matrix in NHMUK PV R 7562. Spinoprezygapophyseal, spinopostzygapophyseal, intraprezygapophyseal and intrapostzygapophyseal laminae, as well as the spinoprezygapophyseal and spinopostzygapophyseal fossae they demarcate, can still be observed in the fourth presacral vertebra counted from posterior. These regions are obscured in more posterior presacral vertebrae by overlying osteoderms.

The anterior dorsal ribs are dichocephalous, with the capitulum being considerably more elongate than the tuberculum (Fig. 4A). The tuberculum is oriented in roughly the same plane as the base of the shaft, whereas the capitulum is projected ventrally from the main portion of the rib, forming an obtuse angle with the tuberculum. The proximal portion of the shaft is anteroposteriorly flattened, as in *Hesperosuchus agilis* (Colbert 1952), with a very sharp and tall longitudinal crest projected along the anterior surface, close to its ventral margin. Proximally, this crest terminates quite abruptly at the level of the base of the capitulum. Its distal extent cannot be determined because it is covered by the scapular blade in the left rib of presacral vertebra 10, whereas it is not adequately preserved in any of the other anterior to mid-dorsal vertebrae (Fig. 4). The crest is directed anteriorly and slightly ventrally. Its dorsal surface is slightly convex, whereas its ventral surface is distinctly concave. The distal portion of the shaft is continuously curved and has an oval cross-section.

In the mid-dorsal ribs (Fig. 4B), the tuberculum is very short and only extends slightly from the shaft. It is separated from the more elongate capitulum by a small concavity on the anterior side of the tuberculum, and, as such, the two rib heads are virtually confluent. As in the anterior dorsal ribs, the proximal portion of the shaft is somewhat flattened, and it has a prominent anteriorly directed crest. This crest is more mound-like in the mid-dorsal ribs compared with the thin flange formed in the anterior dorsal ribs. Because of this crest and the general curvature in this part of the rib, the proximal portion of the rib is roughly boomerang shaped in lateral view, as in *Dromicosuchus grallator* (Sues *et al.* 2003). Further distally in NHMUK PV R 7591b, the shaft becomes narrower. The distal shaft has a slightly more elongate oval cross-section compared with the anterior dorsal ribs. The ribs are more posteriorly directed than the anterior dorsal ribs. This morphology is very similar to that seen in the ribs of the fifth to last and fourth to last presacral vertebrae in NHMUK PV R 7562. In these ribs, the capitulum is much shorter and consequently the capitulum and tuberculum are closely placed together (Fig. 6A). Compared with the ribs associated with presacral vertebra 16 in NHMUK PV R 7591b, the distal ends of these ribs appear to be considerably shorter and more straight distally.
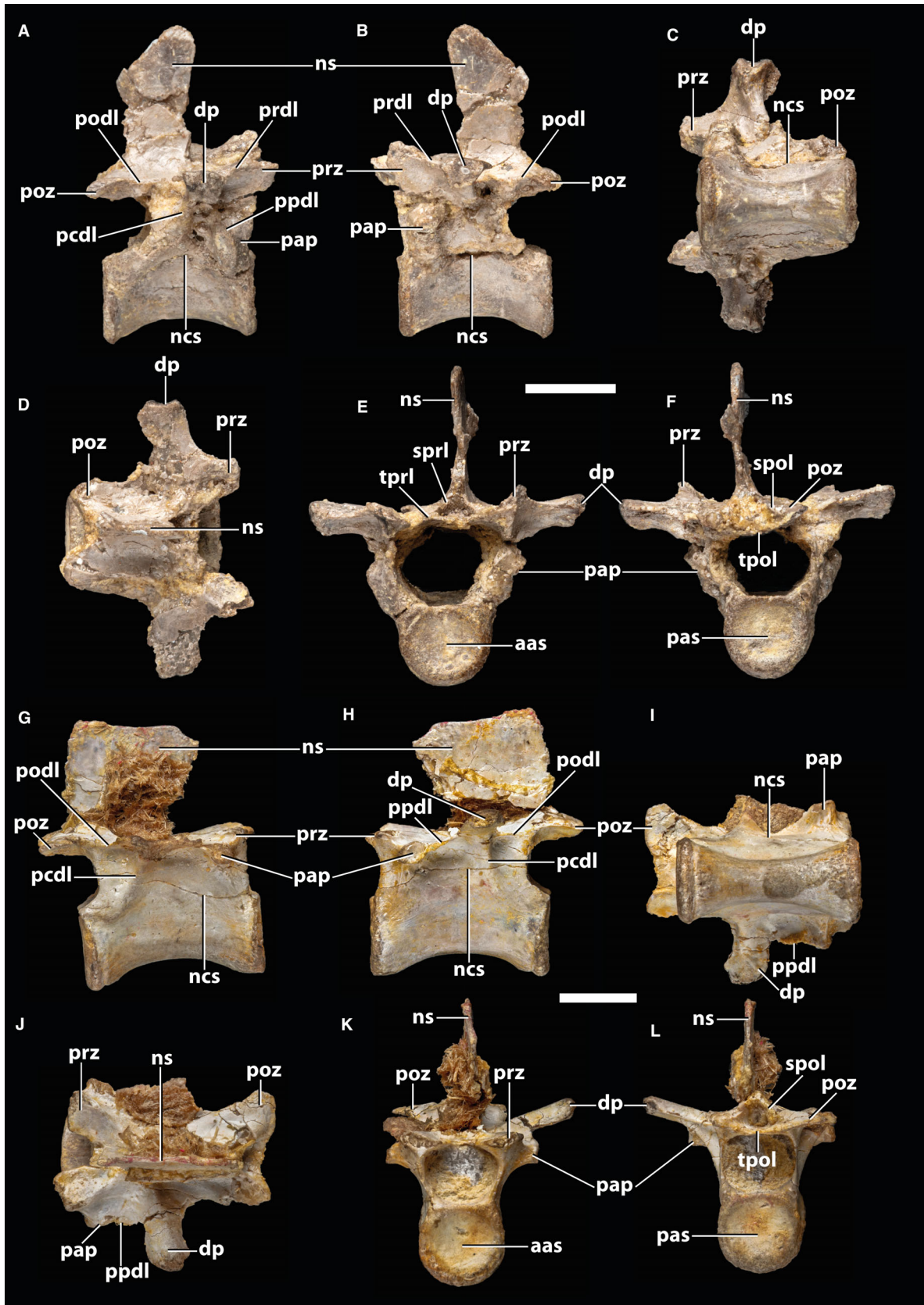
FIG. 5. Selected isolated dorsal vertebrae of *Terrestrisuchus gracilis*. A–F, anterior dorsal vertebra NHMUK PV R 37874 in: A, right lateral; B, left lateral; C, ventral; D, dorsal; E, anterior; F, posterior view. G–L, mid-dorsal vertebra NHMUK PV R 37894 in: G, right lateral; H, left lateral; I, ventral; J, dorsal; K, anterior; L, posterior view. *Abbreviations*: aas, anterior articular surface; dp, diapophysis; ncs, neurocentral suture; ns, neural spine; pap, parapophysis; pas, posterior articular surface; pcdl, posterior centrodiapophyseal lamina; podl, postzygodiapophyseal lamina; poz, postzygapophysis; ppdl, paradiapophyseal lamina; prdl, prezygodiapophyseal lamina; prz, prezygapophysis; spol, spinopostzygapophyseal lamina; sprl, spinoprezygapophyseal lamina; tpol, intrapostzygapophyseal lamina; tprl, intraprezygapophyseal lamina. Scale bars represent 5 mm.
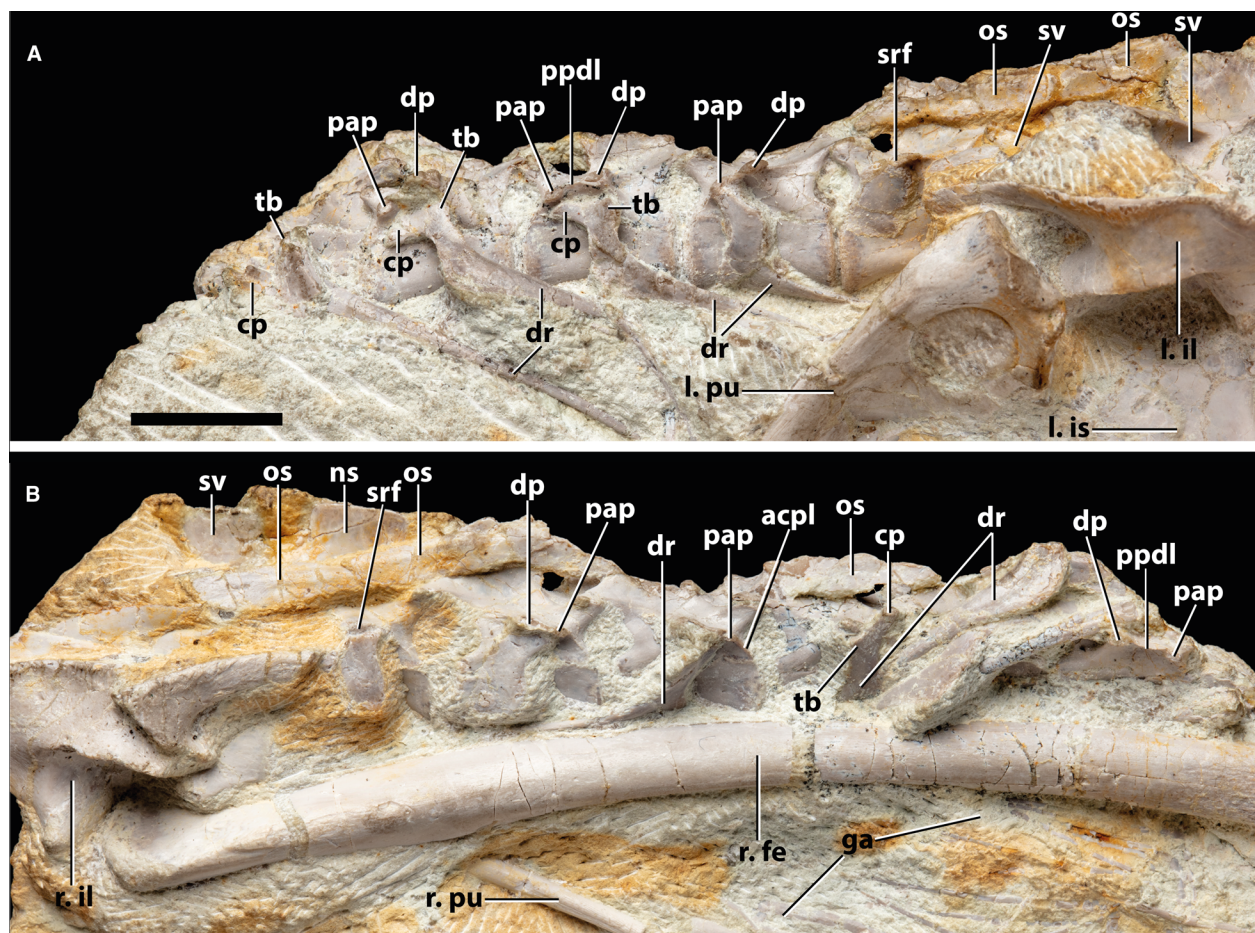

FIG. 6. Dorsal vertebral region of NHMUK PV R 7562 in: A, left lateral; B, right lateral view. *Abbreviations*: acpl, anterior centroparapophyseal lamina; cp, capitulum; dp, diapophysis; dr, dorsal rib; fe, femur; ga, gastralia; il, ilium; is, ischium; l., left; os, osteoderm; pap, parapophysis; ppdl, paradiapophyseal lamina; pu, pubis; r., right; srf, single rib facet; sv, sacral vertebra; tb, tuberculum. Scale bar represents 10 mm.

In contrast to extant crocodylians, which have a distinct lumbar region in which the posterior dorsal vertebrae do not bear ribs (Hoffstetter & Gasc 1969), all dorsal vertebrae of *Terrestrisuchus gracilis* are rib bearing (Fig. 6). All ribs up until the two posteriormost presacral vertebrae bear a clear proximal portion, including articular facets, and a shaft. The ribs of the two posteriormost presacral vertebrae lack a distinct shaft, and instead form only a proximal portion that is rounded off distally and ventrally. The two distinct articular facets present in these two posteriormost presacral ribs are confluent.

Sacral vertebrae. The centrum of the first sacral vertebra is amphiplatyan with both the anterior and posterior articular surfaces being flat to very slightly concave (Fig. 7E–F). The anterior articular surface is oval in anterior view, being considerably lateromedially wider than dorsoventrally tall (Fig. 7E), whereas the posterior articular surface is lateromedially narrower and semi-circular in outline, with a flattened dorsal margin (Fig. 7F). As in the preceding dorsal vertebrae, the ventral margin of the centrum is concave in lateral view (Fig. 7A–B). The opening for the neural canal is oval to rectangular in both anterior and

posterior view, being lateromedially wider than dorsoventrally tall. The pre- and postzygapophyses of the first sacral vertebra are directed anteriorly and posteriorly, respectively, and they extend only slightly beyond the vertebral centrum. The articular surface of the prezygapophysis is oriented mostly dorsally and slightly medially (Fig. 7A, E) and that of the postzygapophyses is directed ventrolaterally (Fig. 7A, B, F). Small but distinct fossae are present between the prezygapophyses anteriorly, and postzygapophyses posteriorly, representing a spinoprezygapophyseal and spinopostzygapophyseal fossa (*sensu* Wilson *et al.* 2011), respectively (Fig. 7E–F). The neural spine of the first sacral vertebra is slightly expanded anteriorly on its distal end, and consequently, its anterior margin would have been somewhat concave at the base in lateral view, as in the preceding dorsal vertebrae (Fig. 7H). The posterior margin of the neural spine is virtually straight in lateral view. The distal margin of the neural spine is unexpanded laterally, as in the presacral vertebrae, and it is straight to slightly convex in lateral view (Fig. 7D).

The sacral ribs are fully fused to the transverse processes in NHMUK PV R 37631 (Fig. 7C–D), but a curved suture is clearly present in the first sacral vertebra of NHMUK PV R 7562 (Fig. 7H) and NHMUK PV R 7557b (Fig. 8B), showing that the transverse process of the vertebra is a short stalk. The sacral ribs of the first sacral vertebra are anteroposteriorly wide and robust. They extend laterally and slightly anteriorly from the neural arch. The dorsal surface of the sacral rib and transverse process is very slightly convex (Fig. 7E–F). In dorsal view the transverse process, as well as the proximal portion of the sacral rib, slightly narrow distally, and both the anterior and posterior margins of the area are straight (Fig. 7D). Further distally the sacral rib widens strongly both anteriorly and posteriorly, with the anterior extension being the most prominent. The anterodistal tip of the sacral rib forms a sharp point in dorsal view (Fig. 8B). Proximal to the rounded posterior margin of the articular facet, the posterior surface of the sacral rib, as well as that of the transverse process of the vertebra, is concave (Fig. 7D). At the base of the process a pit is formed on the posterior surface in its proximodorsal corner, which is roofed dorsally by a thin lamina of the dorsal surface of the transverse process (Fig. 7F). A shallower pit is also formed in the proximoventral corner of the posterior surface. In anterior and posterior view, the distal end of the sacral rib is expanded ventrally (Fig. 7E–F), with the dorsal margin of the process being roughly straight, whereas the ventral margin is distinctly concave.

The articular facet of the rib with the ilium has a deeply excavated concavity on its anterior margin, and therefore it has the outline of an inverted comma in lateral view (Fig. 7A–B). This concave margin forms a groove that continues along the anterior surface to the base of the rib. Dorsally, the anterior projection of the dorsal margin is formed by a thin lamina. This lamina would have articulated with the medial surface of the preacetabular process of the ilium, specifically near the ventral margin of its proximal portion based on an articulation scar on the ilium (see below). The posterior margin is distinctly convex in lateral view, and it is continuous with both the dorsal and ventral margins of the facet (Fig. 7A–B). The facet is most strongly rounded on its posteroventral corner. The articular surface of the sacral rib widens ventrally and forms a broad, oval articular surface on its ventral half, which would have articulated with the anterior half of the acetabular region of the ilium. This surface is flat to very slightly concave and faces ventrolaterally and slightly posteriorly.

The centrum of the second sacral vertebra is not fused to that of the first sacral vertebra, in contrast to the condition in *Trialestes romeri* and *Hallopus victor* (Walker 1970; Lecuona *et al.* 2016). The ventral margin of the centrum is concave as in the preceding vertebrae. The posterior articular surface of the centrum is oval, being lateromedially wider than dorsoventrally tall, with a roughly flat dorsal margin (Fig. 7I). The articular surface is distinctly concave, in contrast to the flattened face of the first sacral vertebra. The posterior end of the centrum of the second sacral vertebra was subequal in width to its anterior end (Fig. 8A) and would have extended slightly further ventrally. The posterior opening of the neural canal is similar to that of the first sacral vertebra (Fig. 7I). The lateral portion of the prezygapophysis is also similar to that of the first sacral vertebra, but no other information is available for the zygapophyses of the second sacral vertebra (Fig. 7H). As in the preceding vertebrae the neural spine is not laterally expanded distally.

The suture between the transverse process and rib is unfused. The transverse process extends less far laterally in the second sacral vertebra compared with the first, and it protrudes only slightly lateral to the centrum (Figs 7I, 8B). In contrast to the slightly curved suture between the transverse process and rib in the first sacral vertebra, the suture of the second sacral vertebra is interdigitating. The ribs of the second sacral vertebra are both laterally longer and anteroposteriorly wider than those of the first sacral vertebra (Fig. 8B; Table S2). The ventral surface of the sacral rib is convex anteriorly at the anteroposterior level of the transverse process, whereas further posteriorly, where the rib forms a flange-like expansion, the ventral surface is concave (Fig. 7J). A similar, elongate, flange-like posterior extension of the distal end of the second sacral rib is present in *Hallopus victor*, *Saltoposuchus connectens* and *Dromicosuchus grallator* (Walker 1970; Sues *et al.* 2003; Spiekman 2023). The anterior margin of the sacral rib is concave in ventral view and the distal

FIG. 7. Selected sacral vertebrae of *Terrestrisuchus gracilis*. A–F, isolated first sacral vertebra NHMUK PV R 37631 in: A, left lateral; B, right lateral; C, ventral; D, dorsal; E, anterior; F, posterior view. G–I, sacral vertebrae and associated elements of NHMUK PV R 7562 in: G, ventral; H, dorsal; I, posterior view. J, second sacral vertebra of NHMUK PV R 37600e in lateral view (note that the ventral side faces up in this image). *Abbreviations*: arts, articular surface; dv, dorsal vertebra; gr, groove; il, ilium; is, ischium; l., left; lam, lamina; ns, neural spine; obf, obturator foramen; os, osteoderm; pofl, posterior flange; poz, postzygapophysis; prz, prezygapophysis; pu, pubis; spozf, spinopostzygapophyseal fossa; sprzf, spinoprezygapophyseal fossa; sut, suture; sv, sacral vertebra. Scale bars represent: 10 mm (A–I); 5 mm (J).
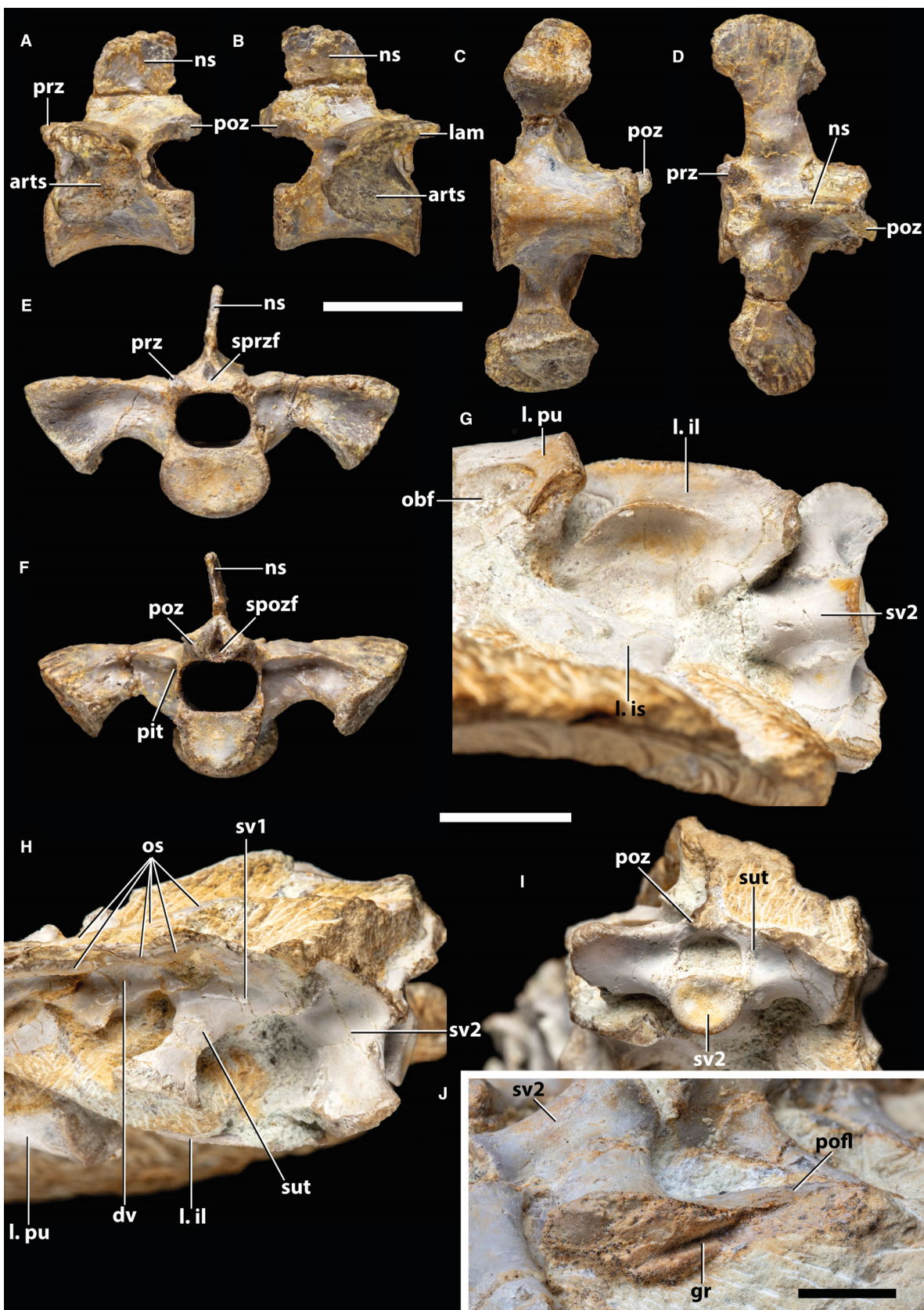
FIG. 8. Selected sacral vertebrae of *Terrestrisuchus gracilis*. A, sacral vertebrae, exposed in ventral view, and associated elements of NHMUK PV R 37600e. B, sacral vertebrae, exposed in dorsal view, and associated elements of NHMUK PV R 7557b. *Abbreviations*: cav, caudal vertebra; chv, chevron; il, ilium; is, ischium; l., left; ot, otoccipital; psv, presacral vertebra; pu, pubis; sut, suture; sv, sacral vertebra. Scale bars represent 10 mm.

end of the rib is slightly expanded anteriorly, with the distal end of the anterior margin forming an acute angle with the lateral margin. The anterior margin does not form a distinct ridge but is rather gently rounded. The posterior margin is thin and sheet like and distally it terminates in a sharp tip. It is slightly convex in posterior view.

The lateral articular surface of the rib is roughly teardrop shaped in lateral view, being anteroposteriorly wider than dorsoventrally tall with a rounded anterior margin and a gradually tapering posterior end (Fig. 7J). The articular surface is oriented anteroventrally to posterodorsally. Posteriorly, the posterior flange is directed slightly posteroventrally. The laterally facing articular surface on the second sacral rib is flat to very slightly convex and characterized by a distinct groove (Fig. 7J). This groove is positioned on the posterior half of the lateral surface, close to its dorsal margin, and it is oriented anterodorsally to posteroventrally. This groove probably articulated with a thin crest at the anteroventral base of the postacetabular process of the ilium (= medial shelf, see below), as was also suggested by Crush (1980, 1984). This interpretation is corroborated by the position of the anterior portion of this medial shelf on the rugose articular facet for the second sacral rib on the medial surface of the ilium. The dorsal margin of this groove on the sacral rib forms the lateral margin of the posterior flange, and it continues posteriorly beyond the groove. Here, the lateral margin of the posterior flange is very thin and its ventral surface would probably have continued its articulation with the medial shelf of the ilium along its postacetabular process, as in *Dromicosuchus grallator* (Sues *et al.* 2003). The lateral margin of the posterior flange is slightly convex in outline (Fig. 8B).

Caudal vertebrae & ribs. Following Crush (1980, 1984), the caudal vertebrae can be subdivided into two main types: the proximal caudal vertebrae that bear transverse processes and ribs, and the distal caudal vertebrae that do not possess transverse processes and ribs. Like the preceding sacral and dorsal vertebrae, the ventral margin of the centrum of the proximal caudal vertebrae is distinctly and symmetrically concave in lateral view (Fig. 9B, C, H, I). The ventral margin does not possess a ventral keel, and the centrum is pinched in ventral view (Fig. 9A). The anterior and posterior sides of the proximal caudal vertebrae are exposed in the isolated proximal caudal vertebrae NHMUK PV R 37769 and NHMUK PV R 37632 (Fig. 9F–G, K–M), which can only tentatively be referred to *Terrestrisuchus gracilis*. The centra of both specimens are amphiplatyan, with the articular surfaces being flat to slightly concave. Both articular surfaces are subcircular, being slightly lateromedially wider than

dorsoventrally tall. Chevrons have a typical V-shaped opening in anterior or posterior view, which reaches until about the mid-length of the total element in the only preserved anterior representative of this element (Fig. 8B).

The prezygapophyses of the proximal caudal vertebrae are positioned slightly ventral to the level of the postzygapophyses (Fig. 9C). The prezygapophyses are predominantly anteriorly and slightly dorsally oriented, and the postzygapophyses are similarly mostly posteriorly and slightly dorsally oriented. Based on NHMUK PV R 37769, the articular surface of the prezygapophysis mainly faced dorsally and slightly medially, and that of the postzygapophysis mostly ventrally and slightly laterally (Fig. 9E). The only preserved neural spine is present in a posterior proximal caudal vertebra (Fig. 9B). It is considerably dorsoventrally shorter than that seen in *Hallopus victor* and *Sphenosuchus acutus*, and those of the tentative proximal caudal vertebrae of *Trialestes romeri* (Walker 1970, 1990; Lecuona *et al.* 2016). It is positioned on the posterior half of the neural arch. It is directed posterodorsally and has a gently rounded distal margin in lateral view. The neural spine is not expanded laterally. A narrow anterodorsally directed process is positioned on the anterior portion of the neural arch. This represents the accessory anterior spine (*sensu* Clark 1986), which is also present in the caudal vertebrae of *Saltoposuchus connectens* (Spiekman 2023), but is apparently absent in *Hallopus victor* and *Sphenosuchus acutus* (Walker 1970, 1990).

The ribs are positioned on the lateral surface of the neural arch, just posterior to its anteroposterior midpoint (Fig. 9C, H, I), as in the proximal caudal vertebra of *Sphenosuchus acutus* (Walker 1990). The ribs project laterally and slightly posteriorly in ventral view (Fig. 9A), as in *Dromicosuchus grallator* and *Sphenosuchus acutus* (Walker 1990; Sues *et al.* 2003). As in the preceding sacral vertebrae, the caudal ribs of NHMUK PV R 37600e are not fused to the vertebra, given that a clear suture with the short transverse process can be observed at their base (Fig. 9A). The ribs gradually taper distally and terminate in a rounded end in dorsal or ventral view. In anterior and posterior view, the ribs of the anterior proximal caudal vertebrae are curved with a convex dorsal and concave ventral margin (Fig. 9F–G). The ribs are flattened, being considerably lateromedially wider than dorsoventrally tall. In NHMUK PV R 37769, a suture between the rib and transverse process is observable only in dorsal view (Fig. 9E), whereas this suture is completely absent in NHMUK PV R 37632 (Fig. 9H–K).

The distal caudal vertebrae are considerably more elongate relative to their height compared with the proximal caudal vertebrae (Table S2), and consequently are cylindrical in shape.
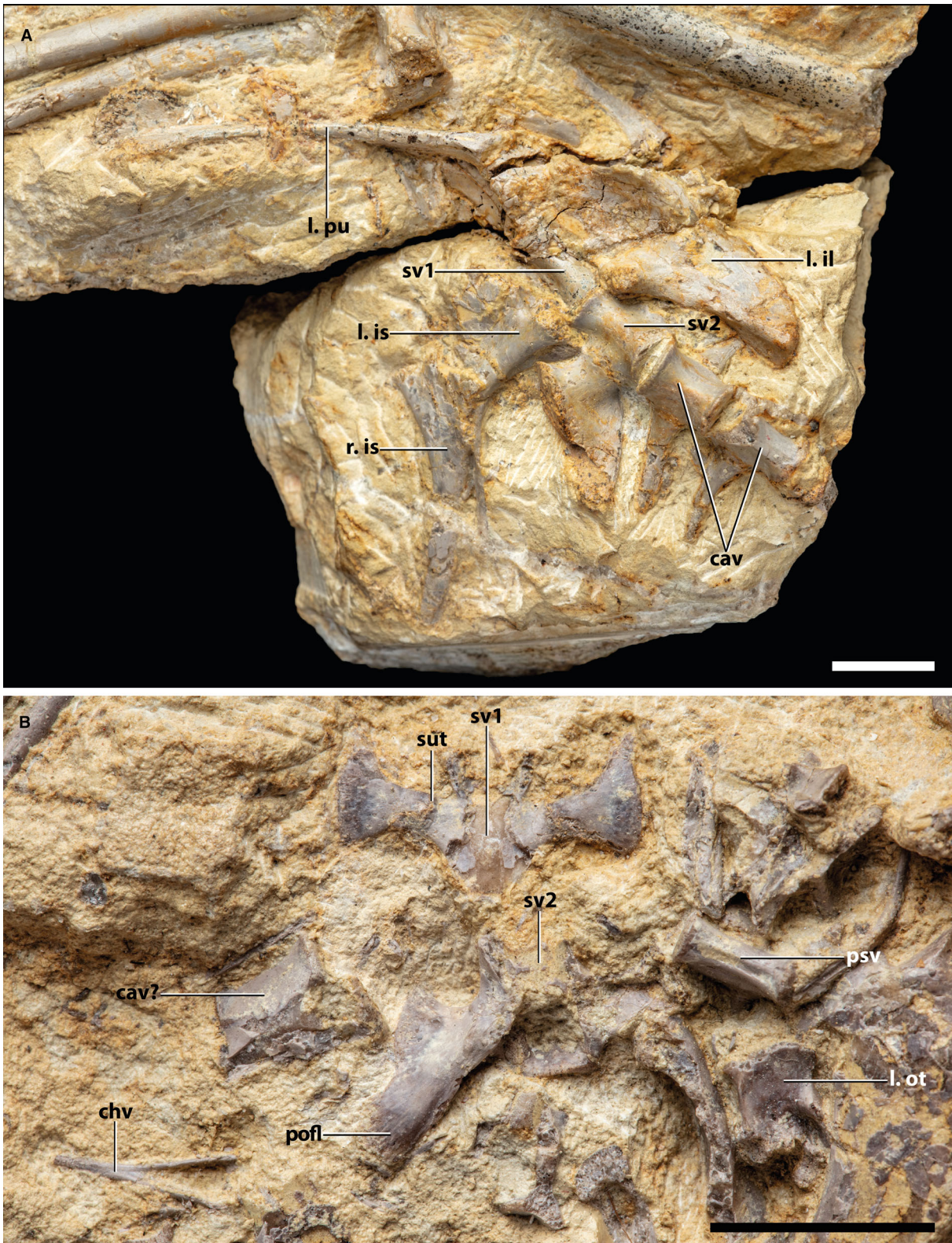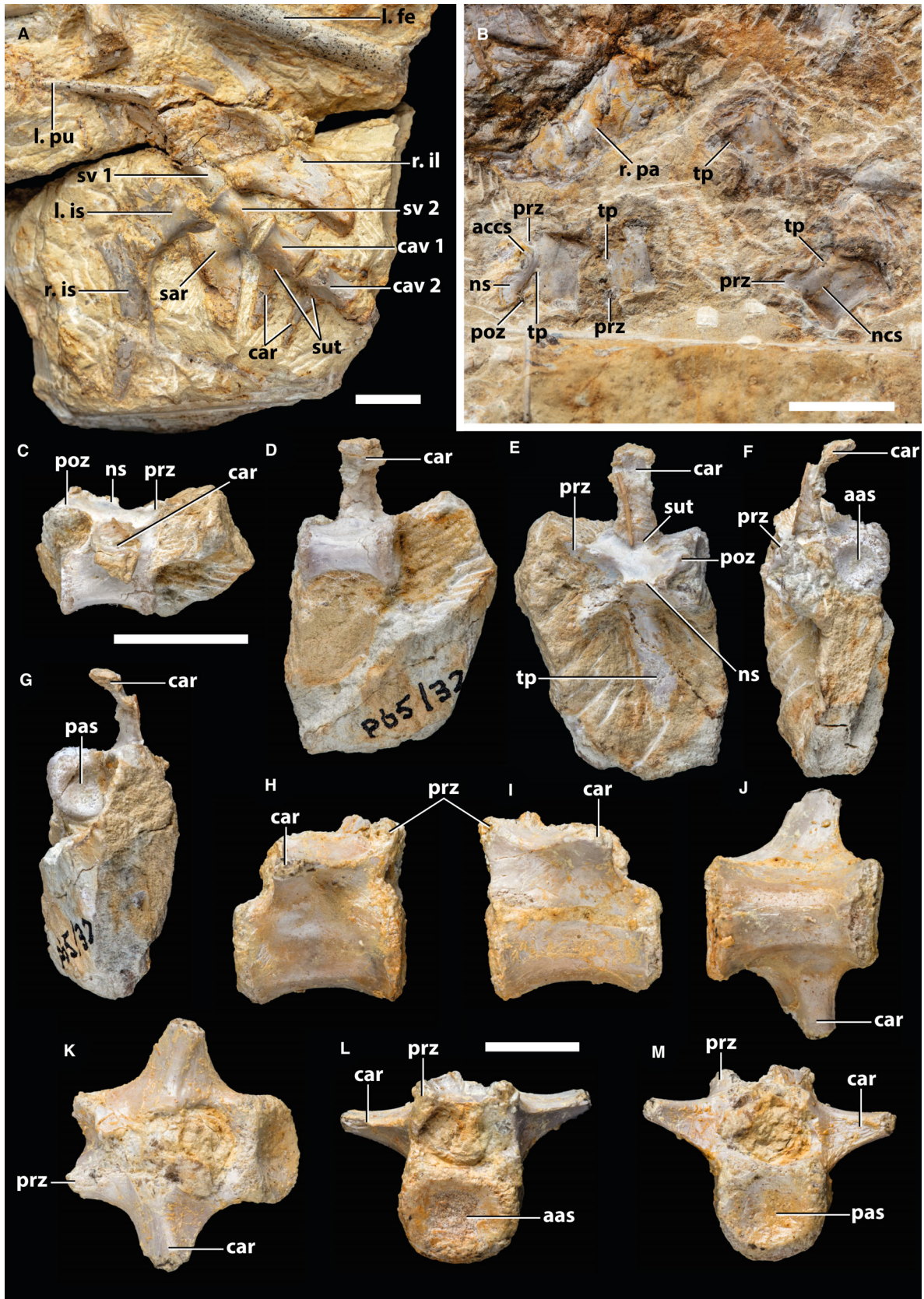
FIG. 9. Selected proximal caudal vertebrae of *Terrestrisuchus gracilis*. A, two proximalmost caudal vertebrae, exposed in ventral view, and associated elements of NHMUK PV R 37600e. B, four disarticulated proximal caudal vertebrae, exposed in lateral and ventrolateral view, of NHMUK PV R 7561. C–G, isolated proximal caudal vertebra NHMUK PV R 37769 in: C, right lateral; D, ventral; E, dorsal; F, anterior; G, posterior view. H–M, isolated proximal caudal vertebra NHMUK PV R 37632 in: H, right lateral; I, left lateral; J, ventral; K, dorsal; L, anterior; M, posterior view. *Abbreviations*: aas, anterior articular surface; accs, accessory anterior spine; car, caudal rib; cav, caudal vertebra; fe, femur; il, ilium; is, ischium; l., left; ncs, neurocentral suture; ns, neural spine; pa, parietal; pas, posterior articular surface; poz, postzygapophysis; prz, prezygapophysis; pu, pubis; r., right; sar, sacral rib; sut, suture; sv, sacral vertebra; tp, transverse process. Scale bars represent: 10 mm (A–G); 5 mm (H–M).
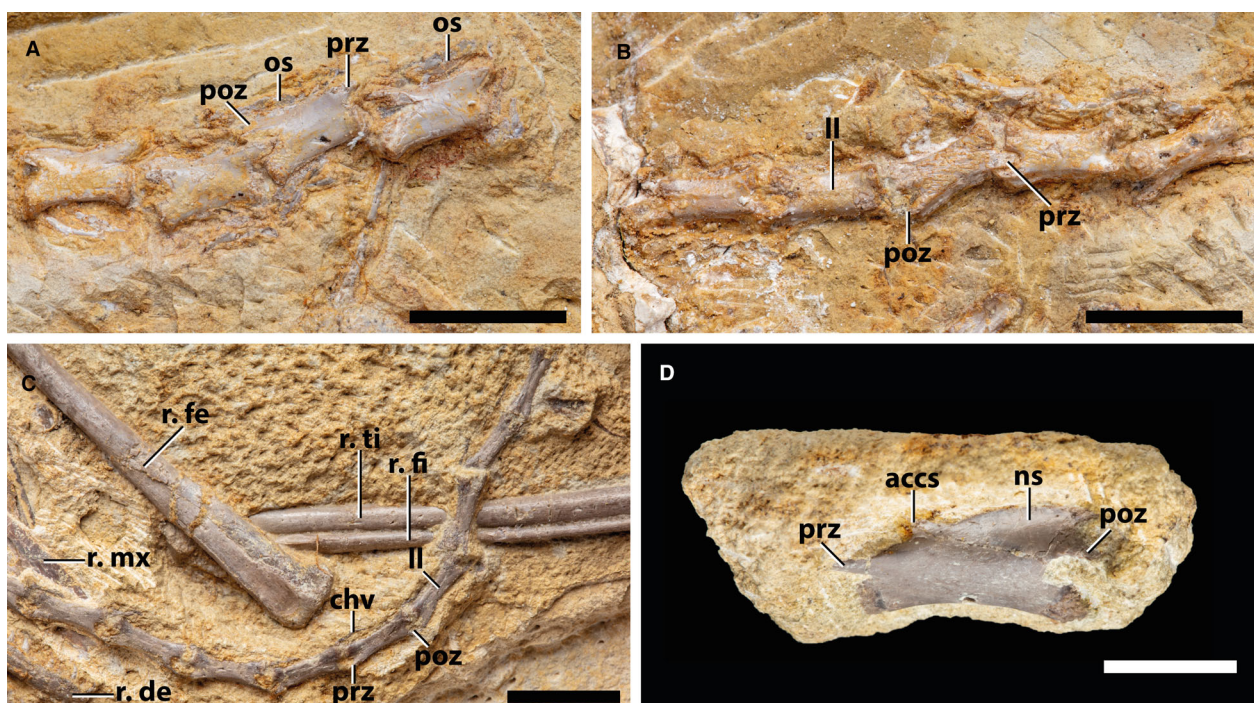
FIG. 10. Selected distal caudal vertebrae of *Terrestrisuchus gracilis*. A, proximal part of distal caudal vertebral column of NHMUK PV R 7571 in lateral view. B, distal part of the distal caudal vertebral column of NHMUK PV R 7571 in lateral view. C, distal caudal vertebral column, exposed in lateral view, and associated elements of NHMUK PV R 7557. D, isolated distal caudal vertebra NHMUK PV R 37896 in left lateral view. *Abbreviations*: accs, accessory anterior spine; chv, chevron; de, dentary; fe, femur; fi, fibula; ll, longitudinal lamina; mx, maxilla; ns, neural spine; os, osteoderm; poz, postzygapophysis; prz, prezygapophysis; r., right; ti, tibia. Scale bars represent: 10 mm (A–C); 5 mm (D).

They are considerably more elongate than the distal caudal vertebrae of *Saltoposuchus connectens* (Spiekman 2023), as was also observed by Sereno & Wild (1992). Clark *et al.* (2000) suggested that this observation was problematic because the terminal caudal vertebrae are not known for *Saltoposuchus connectens*. However, the posteriormost caudal vertebrae of SMNS 12597 are diminutive in size compared with those of the more anterior distal caudal vertebrae in the same articulated series, clearly indicating that the former are positioned close to the end of the tail.

The distal caudal vertebrae of *Terrestrisuchus gracilis* become gradually smaller in size and relatively more elongate posteriorly (Fig. 10C). Their ventral margin is concave in lateral view (Fig. 10), but less so than in the proximal caudal vertebrae. The lateral surface of many distal caudal vertebrae possesses a longitudinal lamina near the transition between the centrum and neural arch (Fig. 10B–C). This lamina is slightly curved, arching slightly ventrally both anteriorly and posteriorly. The lamina is further demarcated by a shallow longitudinal groove positioned directly ventral to it, which is oriented parallel to the lamina on the lateral surface of the vertebra. The prezygapophyses are predominantly oriented anteriorly and very slightly dorsally and the postzygapophyses similarly posteriorly and very slightly dorsally (Fig. 10). Neither extends markedly beyond the centrum. The neural spines are poorly developed and therefore difficult to observe in the distal caudal vertebrae. The neural spine is restricted to the posterior end of the neural arch, forming a

small posterodorsally oriented process that is largely positioned between the postzygapophyses. The accessory anterior spine is also present in the distal caudal vertebrae as a small anterodorsally projecting process (Fig. 10D). The chevrons associated with distal caudal vertebrae are oriented posteriorly to slightly posteroventrally along the ventral margins of the caudal vertebrae (Fig. 10C). These chevrons possess a slight anterior curvature along their lengths. Posteriorly, the chevrons become gradually narrower and shorter in length. The posteriormost chevron is preserved between the 11th and 12th caudal vertebrae, but it is unclear whether chevrons were absent in more distal caudal vertebrae, or merely not preserved.

Crush (1980, 1984) estimated that the total number of caudal vertebrae in *Terrestrisuchus gracilis* was *c.* 71 based on comparisons with extant crocodylians (Crush 1980, pp. 154–155). Due to the high number of caudal vertebrae, Crush (1980, 1984) reconstructed the tail as being very long, with the distal portion dragging along the ground as in extant crocodylians during terrestrial locomotion. The latter aspect of the interpretation is quite unlikely based on the highly elongate limbs of *Terrestrisuchus gracilis* (see also the modified reconstruction of *Terrestrisuchus gracilis* by Sereno & Wild 1992). The caudal vertebral count of Crush (1980, 1984) might also have been inspired by that of *Saltoposuchus connectens*, which was reconstructed as having *c.* 70 caudal vertebrae by Huene (1921). However, as for *Terrestrisuchus gracilis*, no
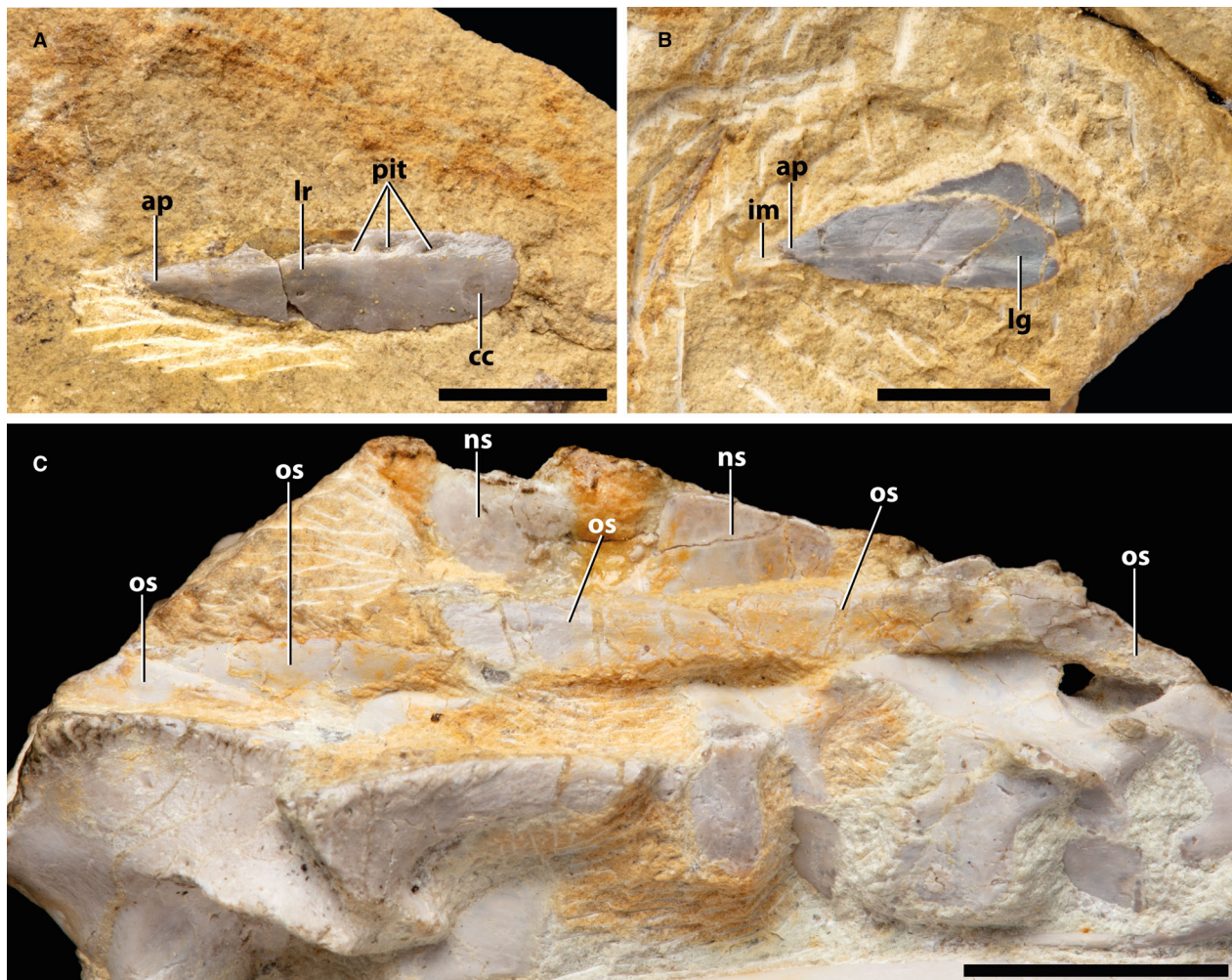
FIG. 11. Selected osteoderms of *Terrestrisuchus gracilis*. A, isolated left osteoderm of NHMUK PV R 37802 in dorsal view. B, two associated left osteoderms of NHMUK PV R 7572a in ventral view. C, articulated right osteoderms and associated elements of NHMUK PV R 7562 in lateral view. *Abbreviations*: ap, anterior process; cc, circular concavity; im, impression; lg, longitudinal groove; lr, longitudinal ridge; ns, neural spine; os, osteoderm. Scale bars represent: 5 mm (A, B); 10 mm (C).

complete caudal series is preserved for *Saltoposuchus connectens*, with only an articulated series of nine proximal and a separate series of 15 distal caudal vertebrae being preserved in SMNS 12597 (Spiekman 2023). In early crocodylomorphs, the caudal vertebral count can be established with some confidence only in the Early Jurassic crocodyliform *Protosuchus richardsoni*, given that AMNH FARB 3024 of this taxon preserves a complete, almost completely articulated tail, which consists of *c.* 35 caudal vertebrae (Colbert & Mook 1952). Colbert (1952) considered the tail of *Hesperosuchus agilis* to possess *c.* 45–50 vertebrae, although this interpretation was provided tentatively. Allen (2010) suggested that the caudal vertebrae count of Crush (1980, 1984) is exaggerated and considered a caudal vertebral count of *c.* 30. Unfortunately, a confident approximation of the caudal vertebral count cannot be made, although it seems likely that the approximation of 72 caudal vertebrae of Crush (1980, 1984) is a considerable overestimation.

Osteoderms. Terrestrisuchus gracilis has osteoderms that are organized in a single paramedian row formed by a pair of scutes placed dorsal to the vertebral column (Fig. 7H). Most early crocodylomorphs have a similarly arranged osteoderm covering (Nesbitt 2011), with the possible exception of *Junggarsuchus sloani*, which might lack osteoderms all together (Clark *et al.* 2004; Ruebenstahl *et al.* 2022). The osteoderms of *Terrestrisuchus gracilis* are clearly present in the cervical and anterior dorsal series (Fig. 4B) and the posterior dorsal and sacral series (Fig. 11C). They are also present in the caudal series (Fig. 10A), and although their exact arrangement is not preserved, it is very likely that the osteoderms also formed a single, paired, paramedian row, as in other early crocodylomorphs, such as *Saltoposuchus connectens* and *Protosuchus richardsoni* (Colbert 1952; Spiekman 2023). The osteoderms form an overlapping articulation, with the posterior end dorsally covering the anterior end of the succeeding osteoderm (Fig. 11C). Medially, the paired osteoderms probably had a simple abutting contact.
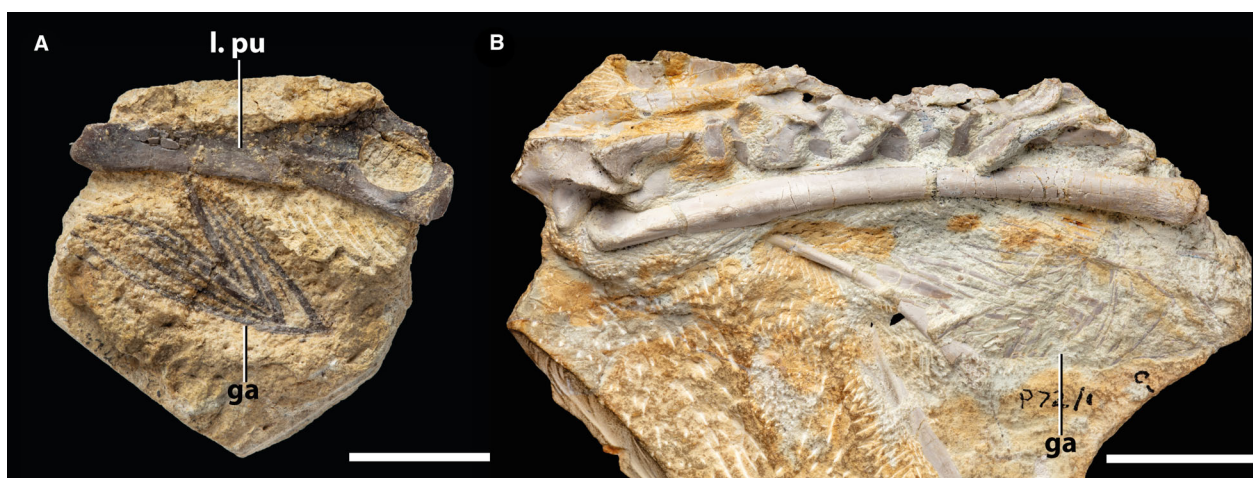
FIG. 12. Selected gastral baskets of *Terrestrisuchus gracilis* in: A, NHMUK PV R 7557f; B, NHMUK PV R 7562. *Abbreviations*: ga, gastralia; l.pu, left pubis. Scale bars represent: 10 mm (A); 20 mm (B).

The osteoderms of *Terrestrisuchus gracilis* are elongate and leaf shaped, being approximately fourfold longer than wide (Fig. 11A–B). The osteoderms of most other non-crocodyliform crocodylomorphs are also anteroposteriorly longer than lateromedially wide, although none is as relatively elongate as those of *Terrestrisuchus gracilis* (Colbert 1952; Wu & Chatterjee 1993; Sues *et al.* 2003; Spiekman 2023). In contrast, the osteoderms of early crocodyliforms such as *Protosuchus richardsoni* and the non-crocodyliform crocodylomorph *Kayentasuchus walkeri* are considerably wider than long (Colbert & Mook 1952; Clark & Sues 2002). Anteriorly, the osteoderms of *Terrestrisuchus gracilis* terminate in an elongate process or peg (Fig. 11B), as in *Saltoposuchus connectens*, *Hesperosuchus agilis* and *Dromicosuchus grallator* (Colbert 1952; Sues *et al.* 2003; Spiekman 2023).

The osteoderms bear a low, relatively wide, longitudinal ridge along most of their length (Fig. 11A). The sculpture of the dorsal surface of the osteoderms is limited to the presence of several small pits, with most of these being positioned medial to the longitudinal ridge (Fig. 11A). This contrasts with the osteoderms of most other crocodylomorphs, which are distinctly sculptured with extensive pits and ridges (e.g. Colbert 1952; Wu & Chatterjee 1993; Clark *et al.* 2000; Sues *et al.* 2003; Hill 2010; Johnson *et al.* 2020; Spiekman 2023), although some other exceptions exist (e.g. Pol 2005). A circular concavity present on the posterolateral portion of the dorsal surface of some of the osteoderms (Fig. 11A) was interpreted as a muscle scar by Crush (1980). We disagree with this interpretation because the placement of a muscle dorsal to an osteoderm is highly unlikely. The osteoderms are asymmetrical; the longitudinal ridge is placed medial to the mid-line of the element, and the lateral margin is convex, whereas the medial margin is straight along most of its length (Fig. 11A–B). From the anterior peg, the osteoderms gradually widen posteriorly for two-thirds of their length. Here, the osteoderm is at its widest, and posterior to this point the osteoderm narrows until the posterior end of the bone, which is almost rectangular in outline. The osteoderms are mostly flat as in *Saltoposuchus connectens* (Spiekman 2023), but in contrast to *Dromicosuchus grallator* and *Kayentasuchus*

walkeri, in which the osteoderms are somewhat ventrally deflected on their lateral side (Clark & Sues 2002; Sues *et al.* 2003). The ventral surface of the osteoderms is mostly flat, but on its posterior end it bears a distinct longitudinal groove (Fig. 11B). This groove is widest posteriorly and narrows anteriorly, and forms the articular surface for the anterior peg of the succeeding osteoderm.

Gastralia. The gastralia of *Terrestrisuchus gracilis* are closely packed together, forming a tight gastral basket (Fig. 12), as in *Sphenosuchus acutus* and CMNH 29894 (Walker 1990; Clark *et al.* 2000). Each gastralium is V shaped, with the two branches of each element forming an acute angle. The cross-section of the gastral shaft is oval, being distinctly lateromedially wider than dorsoventrally tall. The entire extent of the gastral basket is unclear, because no complete gastral baskets are exposed in their natural position relative to the vertebral column.

Appendicular skeleton

Scapula. The scapula is composed of a ventral portion, which includes the articular surfaces for the coracoid and humerus, and a scapular blade. The ventral portion is expanded relative to the scapular blade both anteriorly and posteriorly (Fig. 13A–D). The glenoid fossa is positioned on its posteroventral margin. Its surface is gently concave and oval, being lateromedially wider than anteroposteriorly long (Fig. 13E, G, H). The glenoid fossa faces ventrally, as well as slightly posteriorly and medially. As such, it is very similar to that described for *Junggarsuchus sloani* (Ruebenstahl *et al.* 2022) and seen in *Trialestes romeri* (Lecuona *et al.* 2016). In contrast to *Dromicosuchus grallator* (Sues *et al.* 2003) and *Dibothrosuchus elaphros* (Wu & Chatterjee 1993), a rugose thickening dorsal to the glenoid fossa is absent. The ventral margin of the scapula anterior to the glenoid fossa formed the articular surface with the coracoid. It is lateromedially widest posteriorly, adjacent to the glenoid fossa, and becomes narrower anteriorly, providing the ventral margin with
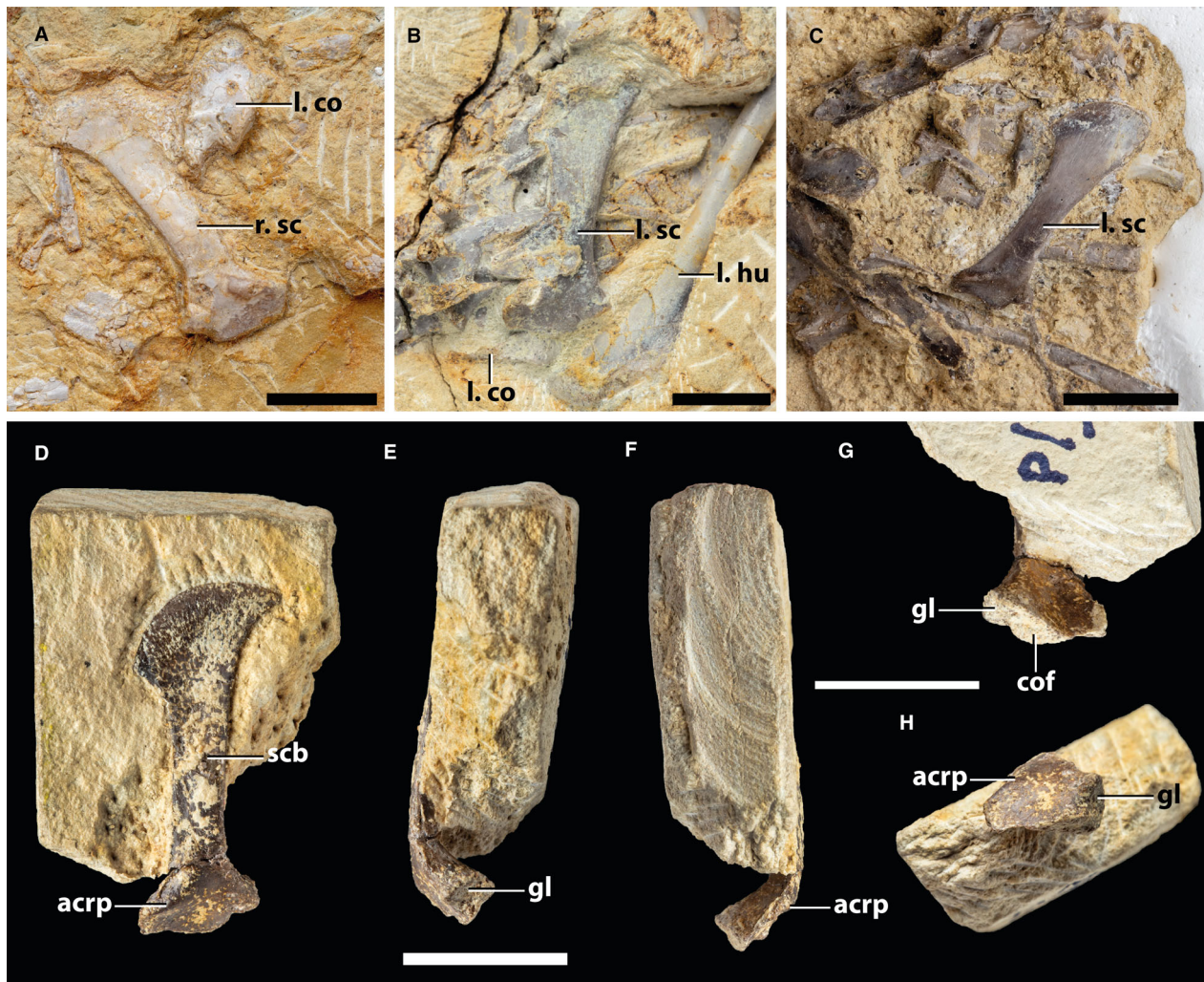
FIG. 13. Selected scapulae of *Terrestrisuchus gracilis*. A, right scapula in lateral view and surrounding elements of NHMUK PV R 7571. B, left scapula in lateral view and surrounding elements of NHMUK PV R 7591. C, left scapula in lateral view and surrounding elements of NHMUK PV R 7553. D–H, isolated left scapula of NHMUK PV R 7557e in: D, lateral; E, posterior; F, anterior; G, medioventral; H, lateroventral view. *Abbreviations*: acrp, acromion process; co, coracoid; cof, coracoid facet; gl, glenoid; hu, humerus; l., left; r., right; sc, scapula; scb, scapular blade. Scale bars represent 10 mm.

a roughly triangular outline in ventral view (Fig. 13G). A distinct acromial process is present on the anterolateral part of the ventral portion of the scapula (Fig. 13D), as is typical for non-crocodyliform crocodylomorphs. It forms a distinct ridge that originates on the anterior margin of the ventral portion of the scapula and from there curves posterodorsally. The lateral surface of the scapula posteroventral to the acromial process is gently concave. The entire ventral portion of the scapula is directed distinctly ventromedially relative to the scapular blade (Fig. 13E–F).

The scapular blade is tall and narrow in lateral view and very thin in anterior or posterior view (Fig. 13D–F). Distally it is expanded both anteriorly and posteriorly in lateral view (Fig. 13C–D). The anterior extension is less pronounced than the posterior one, and the former expansion is positioned further ventrally than the latter. The distal margin of the scapular blade is distinctly convex in lateral view. This configuration of the distal portion of the scapular blade is strongly reminiscent of that of *Saltoposuchus connectens* and *Hesperosuchus agilis* (Colbert 1952; Spiekman 2023). Both the anterior and posterior margin of the scapular blade are slightly concave in lateral view. The scapular blade is more than threefold taller than the ventral portion of the scapula.

Coracoid. The coracoid is a crescent-shaped bone (Fig. 14). Its dorsal margin mirrors that of the ventral margin of the scapula, with which it would have articulated, in that it is lateromedially wide posteriorly and becomes gradually narrower anteriorly, giving the margin a triangular outline in dorsolateral view (Fig. 14B). The glenoid, which is positioned directly posterior to the articular surface with the scapula, is slightly convex and roughly quadrangular in outline (Fig. 14B). Its articular surface
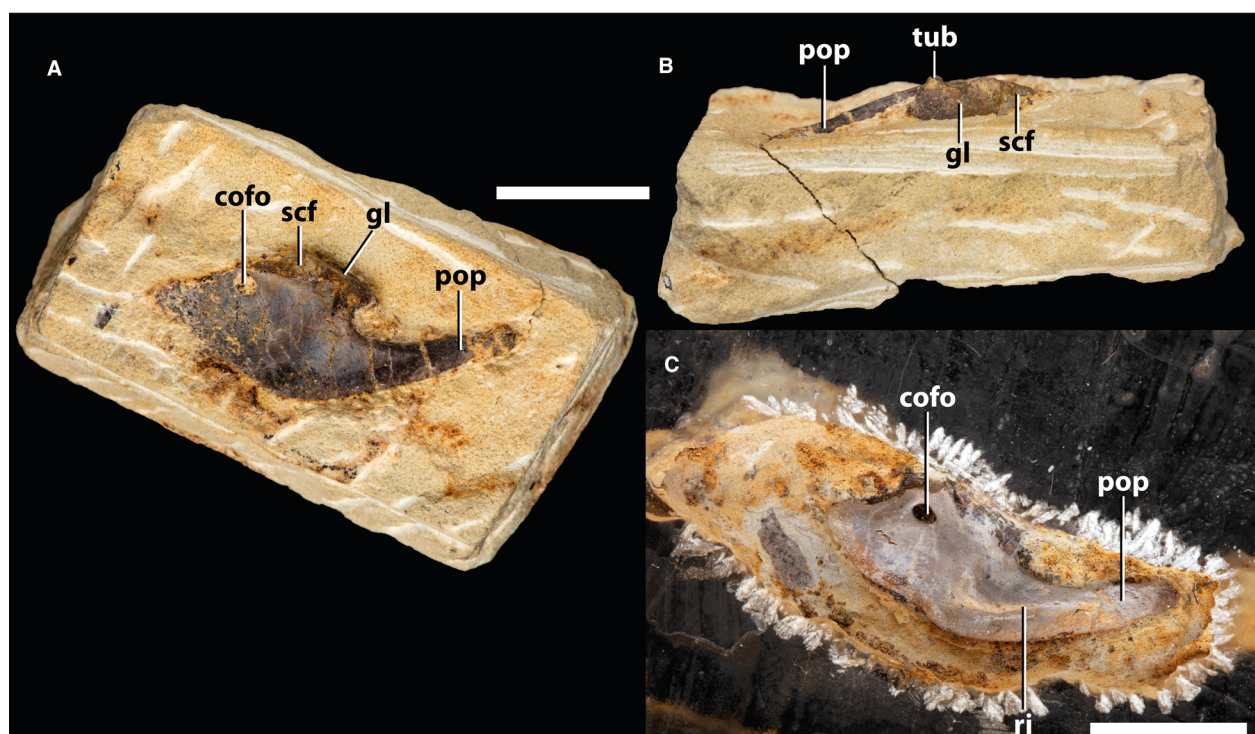
FIG. 14. Selected coracoids of *Terrestrisuchus gracilis*. A–B, right coracoid of NHMUK PV R 37785 in: A, mediodorsal; B, posterodorsal view. C, left coracoid of NHMUK PV R 37799 in lateroventral view. *Abbreviations*: cofo, coracoid foramen; gl, glenoid; pop, posterior process; ri, ridge; scf, scapular facet; tub, tubercle. Scale bars represent 10 mm.

faces posterodorsally and slightly laterally relative to the dorsal margin of the coracoid (Fig. 14A). On the mediodorsal surface of the coracoid, directly ventrolateral to the glenoid, a small but very pronounced tubercle is present (Fig. 14B). A similar tubercle also occurs in *Sphenosuchus acutus* (Walker 1990), *Dibothrosuchus elaphros* and *Junggarsuchus sloani* (Ruebenstahl *et al.* 2022). Near its dorsal end, the surface of the coracoid is pierced by the subcircular coracoid foramen, which is slightly longer anteroposteriorly than dorsoventrally tall (Fig. 14A, C). The anterior margin of the coracoid is rounded in lateral view and oriented anterodorsally to posteroventrally. Posteriorly the coracoid bears a long, posteriorly and slightly laterally directed process, which is approximately as long as the main body of the coracoid. This makes this process comparatively longer than that seen in *Trialestes romeri* (Lecuona *et al.* 2016), shorter than that of *Sphenosuchus acutus* (Walker 1990), much shorter than the rod-like posterior processes of *Dibothrosuchus elaphros* and *Junggarsuchus sloani* (Ruebenstahl *et al.* 2022), and similar in relative length to that in *Hesperosuchus agilis* and *Dromicosuchus grallator* (Colbert 1952; Walker 1970; Sues *et al.* 2003). It is curved with a convex ventral margin and concave dorsal margin in lateral view and terminates in a rounded tip posteriorly.

The lateroventral surface of the coracoid is smooth and distinctly convex anteroventral to the coracoid foramen (Fig. 14C). The lateroventral surface is characterized by a strongly pronounced ridge that is also present in *Sphenosuchus acutus*, *Dromicosuchus grallator*, *Pseudhesperosuchus jachaleri* and *Hesperosuchus agilis* (Colbert 1952; Bonaparte 1972; Walker 1990; Sues *et al.* 2003), but absent in *Trialestes romeri*, *Dibothrosuchus*

elaphros and *Junggarsuchus sloani*, and crocodyliforms (Sertich & Groenke 2010; Chamero *et al.* 2013; Leardi *et al.* 2015; Lecuona *et al.* 2016; Ruebenstahl *et al.* 2022). This ridge originates ventral to the glenoid, where it is poorly developed and oriented dorsoventrally. Ventral to this, at approximately the dorsoventral midpoint of the base of the posterior process, the ridge curves and is oriented posteriorly. At this transition the ridge is most strongly pronounced and directed laterally and slightly ventrally relative to the lateroventral surface of the coracoid. Posteriorly, the ridge gradually decreases in height and ultimately completely fades at approximately the anteroposterior midpoint of the posterior process. The ventral margin of the coracoid is slightly laterally inflected at the base of the posterior process, directly ventral to the most pronounced portion of the ridge. Consequently, a distinct concave groove is formed in between the ventral margin and the ridge. Articulated specimens of *Sphenosuchus acutus* and *Pseudhesperosuchus jachaleri* show that the interclavicle articulated in this groove in these taxa (Bonaparte 1972; Walker 1990). Crush (1984) considered this region to be the articular surface for an ossified sternum rather than the interclavicle. However, as outlined below, *Terrestrisuchus gracilis* did not have an ossified sternum.

Interclavicle. As in other archosaurs (Nesbitt 2011), the interclavicle of *Terrestrisuchus gracilis* lacks anterolateral processes and thus forms an elongate plate that is approximately sixfold longer than wide (Fig. 15). Its lateral margins are slightly convex. It cannot be determined which end of the bone represents the anterior and which the posterior end, because none of the known
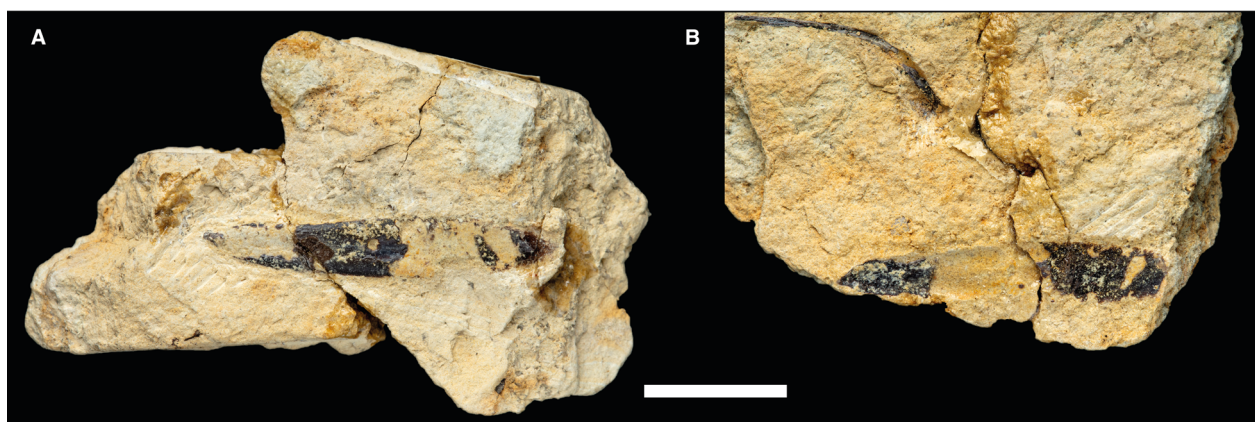
FIG. 15. The interclavicle of NHMUK PV R 37726 preserved over two slabs. A, NHMUK PV R 37726a in ventral view. B, NHMUK PV R 37726b in dorsal view. Scale bar represents 10 mm.

elements preserves both termini intact (Appendix S2). In NHMUK PV R 37726 both surfaces of the interclavicle are exposed. One side is gently convex, which is interpreted to be the ventral surface, and the opposing, dorsal surface is gently concave. In the larger element preserved in NHMUK PV R 7593 the ventral surface is more strongly convex.

Crush (1980) considered an interclavicle to be preserved only in NHMUK PV R 7553. The interclavicles preserved in NHMUK PV R 7591, NHMUK PV R 37726 and NHMUK PV R 7593 were interpreted to be elements of an ossified sternum. The main distinction made between these elements and the interclavicle identified by Crush (1980) in NHMUK PV R 7553 was that the latter was relatively narrower and had straight lateral margins, whereas those of the identified sternal elements were convex. In part, this identification was made based on observations by Walker, who had observed the presence of what he interpreted to be ossified sternal elements in *Sphenosuchus acutus* and *Pseudhesperosuchus jachaleri* (Crush 1980, p. 119). However, Walker (1990, p. 64) later reconsidered his interpretations and suggested that the sternal elements of *Terrestrisuchus gracilis* are interclavicles. Walker (1990) suggested that the more slender morphology and straight lateral margins of NHMUK PV R 7553 relative to the other specimens could be the result of incomplete ossification of this element in the small specimen. The overall size of NHMUK PV R 7553 is indeed comparatively small (Table S2). Furthermore, a partial and partially articulated pectoral girdle and front limb are preserved in NHMUK PV R 10002, a crocodylomorph specimen from Cromhall Quarry. Although it is not referable to *Terrestrisuchus gracilis* (Fraser *et al.* 2002; Spiekman *et al.* 2023), this specimen is morphologically similar to *Terrestrisuchus gracilis* from Pant-y-Ffynnon Quarry. It shows a close association between the right(?) coracoid and the interclavicle, without the presence of an ossified sternum. No ossified sternal plates are known for any early crocodylomorphs. Therefore, an ossified sternum is considered absent for *Terrestrisuchus gracilis*.

Humerus. Like all of the limb bones of *Terrestrisuchus gracilis*, the humerus is a slender element (Fig. 16). The proximal articular surface is rugose and strongly convex in anterior or posterior

view (Fig. 16A–B). On the posterior side of the humerus, this articular surface bulges over the smooth surface of the humerus directly distal to it on its lateral portion, close to the deltopectoral crest, as can also be seen in *Sphenosuchus acutus* (Walker 1990, fig. 43d) and *Hesperosuchus agilis* (Colbert 1952, fig. 22c). In contrast to *Dibothrosuchus elaphros* (Wu & Chatterjee 1993), there is no clear depression directly distal to the proximal head on the anterior surface. In proximal view, the anterior margin of the proximal head is convex medially and concave laterally, whereas the posterior margin is concave medially and convex laterally (Fig. 16E). The deltopectoral crest extends from the anterolateral margin of the proximal head. The crest increases in size distally as it curves anteriorly and eventually slightly medially. At its lateralmost extent, where the crest starts to curve somewhat medially, the crest is thickened to form a tuber on its posterolateral surface (Fig. 16A, C, E). A similar structure was also described for *Sphenosuchus acutus* (Walker 1990). This proximal portion of the crest is slightly convex in lateral or medial view. The deltopectoral crest reaches its apex, which is directed anteriorly and slightly medially, at *c.* 20% of the total length of the bone. Distal to this, the margin of the deltopectoral crest is slightly concave in lateral or medial view until it gradually fades into the humeral shaft distally. The overall shape of the deltopectoral crest in lateral or medial view is triangular.

The humeral shaft is very slightly anteriorly curved in lateral or medial view (Fig. 16C–D), which is similar to the humerus of *Dibothrosuchus elaphros* (Wu & Chatterjee 1993), but in contrast to the more sigmoidal humeri of *Sphenosuchus acutus*, *Trialestes romeri* and *Junggarsuchus sloani* (Walker 1990; Lecuona *et al.* 2016; Ruebenstahl *et al.* 2022). The shaft is thin walled and subcircular in cross-section. The angle formed between the proximal and distal ends of the humerus is 43°. On the distal portion of the shaft, the posterior surface bears a gently concave groove that extends and deepens distally and reaches the distal end of the bone (Fig. 16B), where it separates the two distal condyles in distal view (Fig. 16F). The distal end is slightly expanded relative to the shaft, both lateromedially and anteroposteriorly (Fig. 16A–D). The (medial) entepicondyle extends distinctly further distally than the (lateral) ectepicondyle, as in

FIG. 16. The left humerus NHMUK PV R 38851 in A, anterior; B, posterior; C, lateral; D, medial; E, proximal; and F, distal view. *Abbreviations*: dpc, deltopectoral crest; ect, ectepicondyle; ent, entepicondyle; gr, groove; tub, tuberosity. Scale bars represent: 10 mm (A–D); 5 mm (E, F).

Sphenosuchus acutus, *Hesperosuchus agilis* and *Dibothrosuchus elaphros* (Colbert 1952; Walker 1990; Wu & Chatterjee 1993). The ectepicondyle is considerably wider than the entepicondyle anteroposteriorly and it bears a convexity proximally on its posterolateral margin. The condyles are distally separated by a distinctly concave groove (Fig. 16B) as in most crocodylomorphs except *Trialestes romeri*, in which this groove is poorly developed (Lecuona *et al.* 2016).

Ulna. The ulna is a slender and elongate element (Fig. 17A). The proximal end of the ulna is anteriorly expanded and has a more rugose surface texture relative to the shaft. It is defined by a well-developed olecranon process on its posterior part (Fig. 17B–F). In addition, the proximal end also possesses small tubers or processes on its anterolateral (= lateral tuber *sensu* Nesbitt 2011) and anteromedial portions, as in other non-crocodyliform crocodylomorphs (Leardi *et al.* 2017). Thus, the ulna has a roughly triangular outline in proximal view (Fig. 17F). The anteromedial process is positioned slightly more distally than the anterolateral process. The anterior margin of

the proximal end, forming the margin between the anteromedial and anterolateral process, is slightly concave in proximal view and it articulates tightly with the posterior margin of the proximal end of the radius in NHMUK PV R 37634 (Fig. 17F). The medial margin, separating the anteromedial process and the olecranon, is similarly slightly concave in proximal view, whereas the lateral margin, between the olecranon and the anterolateral process, is very gently convex. The anteromedial process is more pronounced than the anterolateral process. It is squared in outline in proximal view, whereas the anterolateral process is rounded. The medial edge of the anteromedial process forms a lip that overhangs the shaft directly distal to it. The proximal surface is oriented posteroproximally to anterodistally, with the tallest or most proximal apex being formed by the tip of the olecranon process. The proximal surface is distinctly convex posteriorly and anterolaterally, whereas it is concave anteromedially.

The shaft of the ulna is smooth and straight to very slightly sigmoidal in lateral or medial view (Fig. 17A). *Terrestrisuchus gracilis* lacks the distinct ridge on the posterolateral surface of the proximal portion of the shaft present in *Trialestes romeri*
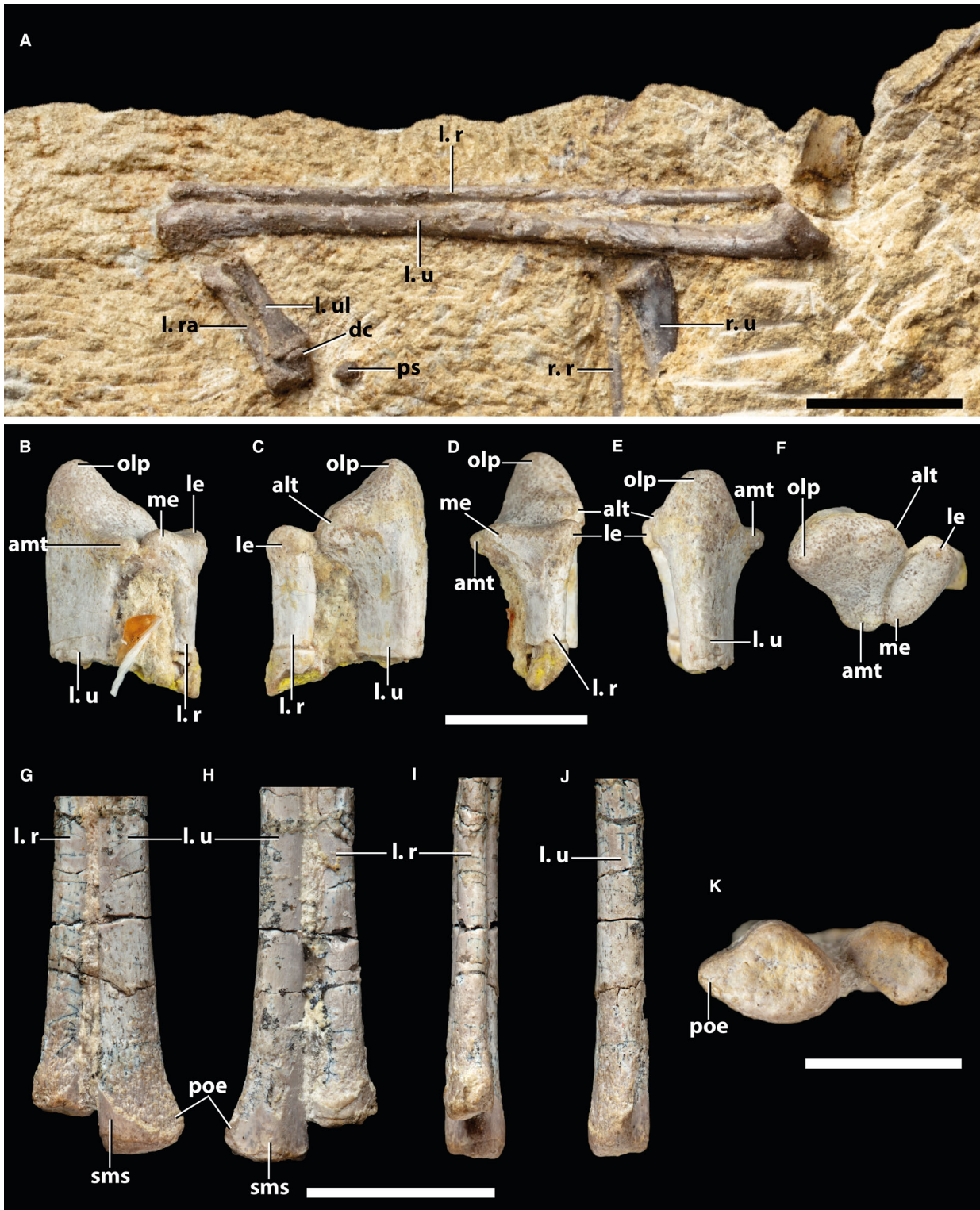
FIG. 17. Selected radii and ulnae of *Terrestrisuchus gracilis*. A, associated left radius and ulna of NHMUK PV R 7557b in lateral view and surrounding elements. B–F, the proximal ends of the associated left radius and ulna of NHMUK PV R 37634 in: B, medial; C, lateral; D, anterior; E, posterior; F, proximal view. G–K, the distal ends of the associated left radius and ulna of NHMUK PV R 7562 in: G, lateral; H, medial; I, anterior; J, posterior; K, distal view. *Abbreviations*: alt, anterolateral tuber; amt, anteromedial tuber; dc, distal carpal; l, left; le, lateral extension; me, medial extension; olp, olecranon process; poe, posterior extension; ps, pisiform; r, radius; r., right; ra, radiale; sms, smooth surface; u, ulna; ul, ulnare. Scale bars represent: 10 mm (A, G–J); 5 mm (B–F, K).

(Lecuona *et al.* 2016). Similar to the proximal end, the surface texture of the distal end of the ulna is distinct from that of the shaft. However, in contrast to being more rugose, the surface of the distal end is smoother than the surface of the shaft (Fig. 17G). In lateral view, the extent of this surface texture is oriented anteroproximally to posterodistally, with a curved, slightly concave margin. In medial view, this texture is restricted to the distal end of the ulna (Fig. 17H). The distal end is longer anteroposteriorly than it is wide lateromedially (Fig. 17G, H, J). In lateral view it is expanded posteriorly relative to the shaft, whereas on its anterior end the distal margin forms a roughly right angle with the anterior margin of the shaft (Fig. 17G). In distal view the medial margin of the posterior extension is concave, thus making the posterior extension quite lateromedially narrow (Fig. 17K). This concavity continues into a proximodistally short groove on the medial surface of the distal portion of the shaft. The distal surface bears a shallow central concavity on its distal end, whereas the edges of the distal surface, including that of the posterior process, are convex.

Radius. The radius is distinctly more slender than the ulna and completely straight in lateral view (Fig. 17A). It is slightly shorter than the ulna (Table S2). The proximal end is more than twofold wider lateromedially than long anteroposteriorly (Fig. 17B–F). In anterior view the lateral portion of the proximal end is slightly expanded relative to the shaft, whereas the medial portion is considerably more strongly expanded (Fig. 17D). This strong medial expansion of the proximal head was considered a synapomorphy for the crocodylomorph clade 'Group H', composed of *Hesperosuchus agilis* and *Dromicosuchus grallator*, recovered by Drymala & Zanno (2016). The unambiguous presence of this feature in *Terrestrisuchus gracilis* suggests that this feature is more common in early crocodylomorphs than previously considered. The rugose surface of the proximal end of the radius is restricted to the proximal margin and does not expand onto the shaft. The proximal surface is convex in lateral and medial view (Fig. 17B–C); in anterior view it is convex on its lateral and medial ends and slightly concave in its central portion (Fig. 17D). The proximal end is oval in proximal view, with short and distinctly convex medial and lateral margins, and considerably longer and slightly convex anterior and posterior margins (Fig. 17F).

The distal end of the radius is only very slightly expanded anteriorly and posteriorly relative to the shaft (Fig. 17G–H). In distal view the distal end of the radius has an oval shape that is oriented anterolaterally to posteromedially (Fig. 17K). The posterolateral and anteromedial sides are considerably longer than the anterolateral and posteromedial sides. The distal surface is slightly concave and set at a slight angle, extending furthest distally at its posteromedial end and being most proximal anterolaterally (Fig. 17G–H). The anterolateral, posteromedial and anteromedial margins are all distinctly convex in distal view, whereas the posterolateral margin is flat to slightly concave (Fig. 17K). On this surface, the radius would have articulated with the flattened anteromedial margin of the ulna. The smooth surface seen on the distalmost portion of the shaft in the ulna is also present in the radius, albeit to a lesser extent. The smooth surface is mainly present on the posterolateral and anteromedial sides of the element (Fig. 17G–H).

Radiale. The radiale is an elongate bone with a slightly expanded distal end and a more pronounced proximal head (Fig. 18A–F). The shaft length is a little less than threefold the maximum width of the proximal head. It is straight in anterior and posterior views, whereas it is gently curved in lateral and medial views with a gently concave anterior side and a slightly convex posterior side. The shaft is wider lateromedially than it is deep anteroposteriorly. The surface of the radiale is smooth but it bears a clear, mostly straight longitudinal crest that is oriented from the proximal end on the lateral side, directly distal to the proximolaterally oriented facet for the ulna, to the anterolateral side at the distal end (Fig. 18A–B). This ridge is possibly homologous with the longitudinal ridge on the posterolateral surface of the shaft in *Trialestes romeri* (Lecuona *et al.* 2016).

The proximal head of the radiale bears two clearly distinct articular surfaces, one of which faces entirely proximally (Fig. 18E). The surface of this facet is concave in its posteromedial portion, where it forms the main articular surface with the radius. On its lateral portion, the surface is convex and forms a slightly proximally raised process on its anterolateral extremity. The entire facet has a semi-circular outline in proximal view, being more than twofold wider lateromedially than deep anteroposteriorly. The anterior margin is strongly convex, whereas the posterior margin is convex laterally and medially, and concave in its central portion. The second articular surface is confluent with the first facet and is located on the posterolateral region of the proximal head (Fig. 18A, B, E). Its surface is proximolaterally oriented and would have articulated with the ulna. A similar, triangular articular surface for the ulna is also present in *Dibothrosuchus elaphros* (Wu & Chatterjee 1993; surface erroneously considered to articulate with the ulnare therein) and *Junggarsuchus sloani* (Ruebenstahl *et al.* 2022). Although the proximal end of the radiale is expanded towards the ulna in *Hallopus victor*, the exact morphology of its articular surfaces is unknown (Walker 1970). Such a separate articular surface is absent in *Trialestes romeri* (Lecuona *et al.* 2016). In the view perpendicular to its surface, the facet for the ulna has a roughly triangular outline (Fig. 17B). The articular surface is slightly concave. The posteromedial and lateral margins of the facet are delineated by clear ridges. The former is roughly straight, whereas the latter is convex and possesses a process at its lateralmost extension, close to its proximal end. It is pyramoidal in shape, with three concave faces sloping distally from the apex. Distal to the concave posteromedial face a clear subcircular fossa or depression is present on the shaft. The proximal face forms part of the articular facet, whereas the lateral and mediodistal faces are part of the shaft.

The distal end of the radiale is roughly square in outline in distal view, with all faces being roughly equally long (Fig. 18F). Of the four distinct margins, the anteromedial, posteromedial and anterolateral margins are all slightly convex, whereas the posterolateral margin bears a clear concavity. This concavity forms the distal end of a longitudinal trough that extends proximally along approximately one-third of the posterolateral surface of the shaft, which was interpreted as a muscle attachment site by Crush (1980). The distal end of the longitudinal ridge of the shaft forms the anterolateral margin of this trough. The distal end of the radiale is only very slightly expanded relative to the

FIG. 18. Selected carpal elements of *Terrestrisuchus gracilis*. A–F, left radiale of NHMUK PV R 7562 in: A, anterolateral; B, posterolateral; C, posteromedial; D, anterior; E, proximal; F, distal view. G–L, left ulnare of NHMUK PV R 7562 in: G, posteromedial; H, anterolateral; I, anteromedial; J, posterolateral; K, proximal; L, distal view. M–N, left pisiform of NHMUK PV R 7562 in: M, proximal or distal(?) view; N, the opposite orientation to M. O–R, left distal carpal of NHMUK PV R 7562 in: O, anterior; P, posterior; Q, lateral; R, medial view. S, associated left carpus of NHMUK PV R 7557b approximately in lateral view. *Abbreviations*: ac, anterior convexity; dc, distal carpal; fl, flange; l., left; lr, longitudinal ridge; lt, longitudinal trough; mc, medial convexity; plc, posterolateral convexity; ps, pisiform; r, radius; r., right; ra, radiale; rf, radius facet; tr, trough; u, ulna; uf, ulna facet; ul, ulnare. Scale bars represent: 5 mm (A–R); 10 mm (S).

shaft both in posterolateral or anteromedial views and in anterolateral or posteromedial views. The surface of the distal end bears another, roughly posterolaterally to anteromedially oriented, clearly concave trough. Consequently, the anteromedial and posterolateral edges of the distal end extend further distally than the posteromedial and anterolateral edges.

Ulnare. The ulnare is also an elongate element, albeit shorter than the radiale (Fig. 18G–L, S). The shaft is smooth without any clearly discernible ridges. It therefore does not possess the clear longitudinal ridge on the anterior surface of the ulnare present in *Trialestes romeri* (Lecuona *et al.* 2016). It is oval in cross-section, being widest anteromedially to posterolaterally and narrowest anterolaterally to posteromedially, which differs considerably from the L-shaped cross-section of the ulnare shaft described for *Hallopus victor* (Walker 1970). The proximal head is only slightly expanded anteriorly, medially and posterolaterally, relative to the shaft. It is triangular in proximal view, with the three corners of the head forming rounded convexities (Fig. 18K). The convexities on the anterior and medial portions are confluent with each other, whereas both are separated from the posterolateral convexity by a clear anterolaterally to posteromedially directed trough on the proximal surface. In proximal view, the anteromedial margin of the proximal head is slightly convex, whereas the posterior and lateral margins are clearly concave. The concavity on the lateral margin forms the proximal end of a short, longitudinally directed trough present on the lateral surface of the proximal part of the shaft.

The distal end of the ulnare is considerably larger than the proximal head and it is expanded mainly anteromedially to posterolaterally (Fig. 18G–H). This is similar to the condition in *Dibothrosuchus elaphros* and *Junggarsuchus sloani* (Wu & Chatterjee 1993; Ruebenstahl *et al.* 2022), but contrasts with *Trialestes romeri*, in which the proximal and distal ends of the ulnare are roughly similar in size (Lecuona *et al.* 2016). The latter condition might also occur in CMNH 29894 (Clark *et al.* 2000). Consequently, the distal end has a teardrop-shaped outline in distal view with two main faces: an anterolateral and a posteromedial face (Fig. 18L). The former is continuously and quite strongly convex. The latter is sinusoidal in outline with a distinctly concave anterior portion and a convex posterior portion. Because of this concavity, the anteromedial end of the distal end forms a flange. This concavity also forms the distal margin of a short, longitudinally oriented trough on the distal end of the shaft. The distal surface of the ulnare is generally concave except for the anteromedial end, which is gently convex.

Pisiform(?) & distal carpal. Besides the radiale and ulnare, carpal elements are rarely preserved in non-crocodyliform crocodylomorphs, and a (most likely) complete set of carpals has been described only for *Terrestrisuchus gracilis*, *Dibothrosuchus elaphros* and *Junggarsuchus sloani* to date (Crush 1980, 1984; Wu & Chatterjee 1993; Clark *et al.* 2000; Ruebenstahl *et al.* 2022). In the first two taxa two additional carpals are present, which have been interpreted as a pisiform (an element preserved directly proximal to the ulnare), and a single distal carpal considered to be a fusion of distal carpals 3 and 4. A similar configuration has also been described for the early crocodyliforms *Protosuchus richardsoni* and *Orthosuchus stormbergi* (Colbert & Mook 1952; Nash 1975). In contrast, no pisiform is known for *Junggarsuchus sloani* and this taxon possesses two to three distal carpals (Ruebenstahl *et al.* 2022). NHMUK PV R 7557b represents the only specimen of *Terrestrisuchus gracilis* that preserves a partially articulated carpus (Fig. 18S). In this specimen, the distal carpal is preserved in articulation with the left radiale and ulnare at their distal end, whereas the element identified by Crush (1980, 1984) as the pisiform is disarticulated and somewhat displaced from the other carpal elements. Therefore, the identification of this element as a pisiform cannot be corroborated confidently. Nevertheless, its identification is tentatively maintained based on the general similarity of this configuration to the majority of early terrestrial crocodylomorphs. Due to its articulation, the other element is confidently identified as a distal carpal. Despite this, its exact homology with the various distal carpal elements plesiomorphically present in archosaurs cannot be established, given that the ossification of the distal carpals is variable even among extant crocodylians and extinct crocodyliforms (Gregorovičová *et al.* 2018). Therefore, we identify this element simply as a distal carpal here in *Terrestrisuchus gracilis*.

The tentatively identified pisiform of NHMUK PV R 7557b is small and poorly preserved. The distal carpal is slightly larger and bulkier than the pisiform and, as exposed, has a roughly triangular outline. The pisiform and distal carpal are also present in NHMUK PV R 7562 and fully freed from matrix (Fig. 18M–R). Their association with the surrounding elements is unknown but, based on their overall size and shape, the flattened and smaller element is identified as the pisiform (Fig. 18M–N) and the larger, triangular element is identified as the distal carpal (Fig. 18O–R), *contra* Crush (1980). Our identification corresponds with the size and shape of these respective elements in NHMUK PV R 7557b, as well as the condition in *Dibothrosuchus elaphros*, in which the pisiform is also flat and disc-like and the distal carpal is slightly larger and rather block-like (Ruebenstahl *et al.* 2022).
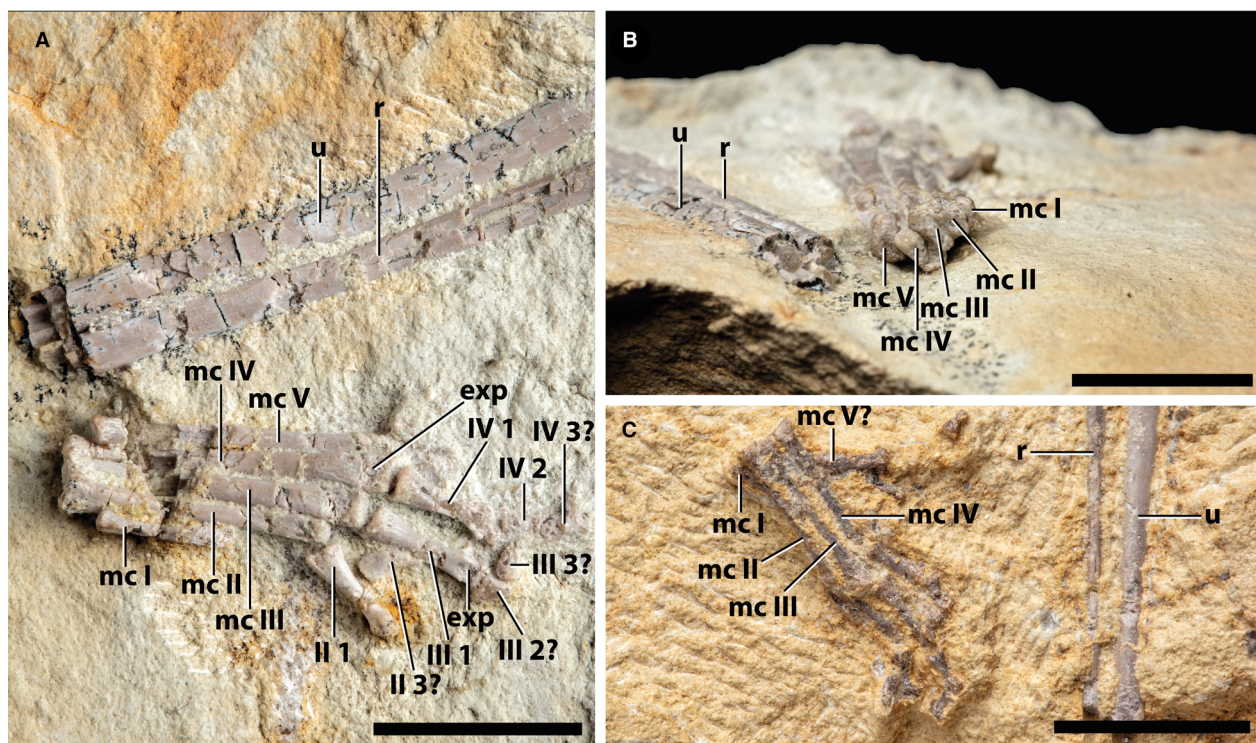
FIG. 19. Selected manus of *Terrestrisuchus gracilis*. Left manus of NHMUK PV R 7562 in A, dorsal; and B, proximal view. C, left manus of NHMUK PV R 7557b in dorsal view. *Abbreviations*: exp, extensor pit; mc, metacarpal; r, radius; u, ulna. Scale bars represent 10 mm.

The pisiform of NHMUK PV R 7557b has an irregular surface, indicating that it is incompletely preserved (Fig. 18S). The pisiform of NHMUK PV R 7562 is more completely preserved, but its exact orientation cannot be ascertained. The main surfaces of the element, which probably represent the proximal and distal sides, have an oval to roughly triangular outline (Fig. 18M–N). Of the three corners forming the triangular shape from this perspective, two are positioned in close proximity to each other. One of these forms a roughly right angle, whereas the angle formed by the other is obtuse. The margin separating these two adjacent corners is virtually straight. The third corner forms an acute angle. The margins connecting this corner to the two opposing corners diverge from each other, with one being virtually flat and the other gently convex.

The left distal carpal of NHMUK PV R 7557b is most likely to be exposed in lateral view, based on its tight articulation with the laterally exposed left ulnare (Fig. 18S). The orientation of the left distal carpal of NHMUK PV R 7562 is based on comparisons with this element. The distal carpal has a complex shape. Its proximal margin is roughly flat in anterior and posterior view (Fig. 18O–P). It has a large bulbous medial side that is strongly convex in anterior and posterior view, whereas the lateral side is tapered. The anterior(?) surface is roughly flattened (Fig. 18O) whereas the posterior(?) surface bears a deep concavity that is directed medioproximally to laterodistally and a prominent convexity on its proximolateral portion (Fig. 18P). The lateral side of the element is narrow and badly broken. The

distal surface of the distal carpal is composed of a lateromedially oriented ridge.

Manus. All metacarpals are slender and elongate (Fig. 19). Both the proximal and distal ends of the metacarpals, as well as the phalanges, are only slightly expanded relative to the shaft. The metacarpals of the best preserved, articulated manus, NHMUK PV R 7562, clearly overlap proximally (Fig. 19B). The cross-section of the metacarpals is oval, with the long axes of the proximal ends being oriented dorsolaterally to ventromedially, as in extant crocodylians (e.g. Klinkhamer *et al.* 2017). The proximal ends are quite narrow in metacarpals I–IV, but more rounded in metacarpal V. In NHMUK PV R 7562, shallow, poorly developed extensor pits can be discerned on the dorsal surface of the distal ends of metacarpals II, III and IV, as well as a more prominent pit on the first phalanges of digits II and III (Fig. 19A). Extensor pits have also been described for the metacarpals and phalanges of *Saltoposuchus connectens* and CMNH 29894 (Clark *et al.* 2000; Spiekman 2023).

As in all known non-crocodyliform crocodylomorphs, metacarpal I is considerably shorter than the other metacarpals, but it does contact carpal elements proximally, in contrast to the condition in *Junggarsuchus sloani* (Ruebenstahl *et al.* 2022). Metacarpal I is also considerably more slender (i.e. has a considerably smaller circumference of the shaft) than the other metacarpals. This character was previously considered to be unique to *Junggarsuchus sloani* but might be more widespread among non-crocodyliform crocodylomorphs than previously considered

(Clark *et al.* 2004; Leardi *et al.* 2017). Metacarpal IV represents the longest metacarpal in *Terrestrisuchus gracilis* (Table S2), whereas in all other non-crocodyliform crocodylomorphs for which these measurements are known (*Saltoposuchus connectens*, *Dibothrosuchus elaphros*, and *Junggarsuchus sloani*), as well as extant crocodylians, metacarpal III is longer than metacarpal IV (Wu & Chatterjee 1993; Ruebenstahl *et al.* 2022; Spiekman 2023). In NHMUK PV R 7562 metacarpal V is longer than metacarpals I and II and only slightly shorter than metacarpals III and IV (Fig. 19A). In contrast, a manual element preserved lateral to metacarpal IV in NHMUK PV R 7557b, ostensibly in the location of metacarpal V, is relatively much shorter than metacarpal V in NHMUK PV R 7562. This element is slightly displaced relative to the metacarpals and although its distal end appears intact, it is possible that its proximal end is either missing or covered by the fully articulated metacarpals (Fig. 19C). This element could also represent a displaced phalanx, in which case metacarpal V is not preserved in the left manus of NHMUK PV R 7557b. Both interpretations were also suggested by Crush (1980, pp. 67–68, fig. 36(II)).

The phalanges are incomplete in both NHMUK PV R 7557b and NHMUK PV R 7562 and therefore the manual phalangeal formula cannot be determined. In NHMUK PV R 7562 two phalanges are preserved in digit II, one of which is an ungual (Fig. 19A). Three phalanges are preserved in digit III, with the first phalanx being relatively long and well preserved, whereas the other two phalanges represent incomplete fragments. Digit IV preserves two relatively complete phalanges and possibly a small fragment of a third phalanx. No phalanges are preserved for digits I and V. In NHMUK PV R 7557b a small fragment is preserved, which might represent a phalanx of digit I (Fig. 19C). Three phalanges are preserved for each of digits II–IV. Digit V preserves two or three phalanges. No unguals can be discerned in NHMUK PV R 7557b.

All preserved phalanges are shorter than the metacarpals of the corresponding digit. Besides the well-excavated extensor pits present in the first phalanges of digit II (note that this phalanx is preserved in lateral view and thus the pit cannot be discerned in Fig. 19A) and digit III of NHMUK PV R 7562, small excavations are also present on the lateral and medial sides of the distal end of these elements, resulting in both sides slightly converging towards the distal end (Fig. 19A). The preserved ungual of NHMUK PV R 7562 (Fig. 19A, II 3?) is curved and terminates in a tapered but blunt tip distally. It is not enlarged relative to the other manual phalanges and preserves a shallow longitudinal groove on its exposed medial surface.

Ilium. The iliac blade is relatively low, with the height of the acetabular portion of the ilium being taller than the height between the supra-acetabular process and the dorsal margin of the iliac blade (Table S2), as in *Trialestes romeri* and *Dromicosuchus grallator* but unlike in *Hallopus victor* and *Dibothrosuchus elaphros* (Walker 1970; Wu & Chatterjee 1993; Sues *et al.* 2003; Lecuona *et al.* 2016). The dorsal margin of the iliac blade is roughly flat in lateral view (Figs 20A, 21A, E). It is lateromedially rounded and thin. Dorsal to the supra-acetabular crest, the dorsal margin of the iliac blade is somewhat expanded laterally and its lateral surface possesses dorsoventrally oriented

striations (Figs 20A–B, 21A, C). This represents an attachment site for the *M. iliotibialis* (Hutchinson 2001a). In NHMUK PV R 7561c and most other specimens, including the holotype, NHMUK PV R 7557, the dorsal margin of the iliac blade is straight in dorsal view (Fig. 21C). In contrast, in both ilia of NHMUK PV R 7562 and in NHMUK PV R 37788, the dorsal margin is curved laterally at the level of its thickened and rugose portion (Fig. 21G). This apparently represents a form of intraspecies variation independent of size, given that both the straight and curved margins are found in smaller sized specimens (NHMUK PV R 7557 and NHMUK PV R 37788, respectively) and larger sized specimens (e.g. NHMUK PV R 7561c and NHMUK PV R 7562) represented in the material (Table S2).

Terrestrisuchus gracilis possesses a long, slender, and gradually tapering preacetabular process (Figs 20, 21). It is oriented anteriorly and curves slightly ventrally and laterally on its distal portion. Consequently, the dorsal margin of the preacetabular process is convex in lateral view, whereas the ventral margin is concave (Fig. 21A). The preacetabular process is relatively longer (i.e. protrudes further anterior relative to the pubic peduncle) than in *Trialestes romeri* (Lecuona *et al.* 2016), and it has a gently rounded to sub-rectangular terminus (Fig. 20B–C).

The postacetabular process is moderately developed, posteriorly directed and gradually tapering. It is considerably dorsoventrally taller than the preacetabular process in lateral view (Fig. 21A). Its dorsal margin is slightly convex in lateral view, whereas its ventral margin is concave proximally and straight distally. The ventral portion of the medial surface of the postacetabular process bears a distinct anteroposteriorly oriented ridge that is identified as the medial shelf (Figs 20C, 21B–D, F, H; mr2 *sensu* Hutchinson 2001a). The crest of the shelf is directed medially and somewhat ventrally. The shelf originates on the medial surface of the acetabular region, where it would have articulated with a groove on the dorsal portion of the distal end of the second sacral rib (Fig. 7J, see description of sacral vertebrae above). The shelf extends to the posterior terminus of the postacetabular process (Fig. 21D). In its well-developed morphology this shelf is very similar to that described for *Trialestes romeri* (Lecuona *et al.* 2016, medioventral shelf therein), albeit not as distinctly ventrally curved in *Terrestrisuchus gracilis*.

The shelf forms the dorsomedial margin of a prominent, ventrally facing fossa, the brevis fossa (Figs 20C, 21B, D, F, H). A brevis fossa framed by a distinct medial shelf is best-known and most strongly developed in avemetatarsalian archosaurs, specifically in non-avian dinosaurs, but it is also well developed in some pseudosuchians, such as *Gracilisuchus stipanicicorum* (Hutchinson 2001a; Lecuona & Desojo 2012), and, to a lesser extent, in some ornithosuchids and proterochampsids (Hutchinson 2001a; von Baczko *et al.* 2019). Among Crocodylomorpha, a distinct brevis fossa is known only for *Trialestes romeri*, but it is possible that this feature occurred more widely (e.g. a prominent medial ridge on the medial surface of the postacetabular process was also reported for *Dromicosuchus grallator*, Sues *et al.* 2003). The brevis fossa forms an attachment site for the *M. caudofemoralis brevis*, which, in addition to the ventrolateral surface of the postacetabular process of the ilium, also attaches to the second sacral rib and first two proximal caudal vertebrae in extant crocodylians (Hutchinson 2001a). The
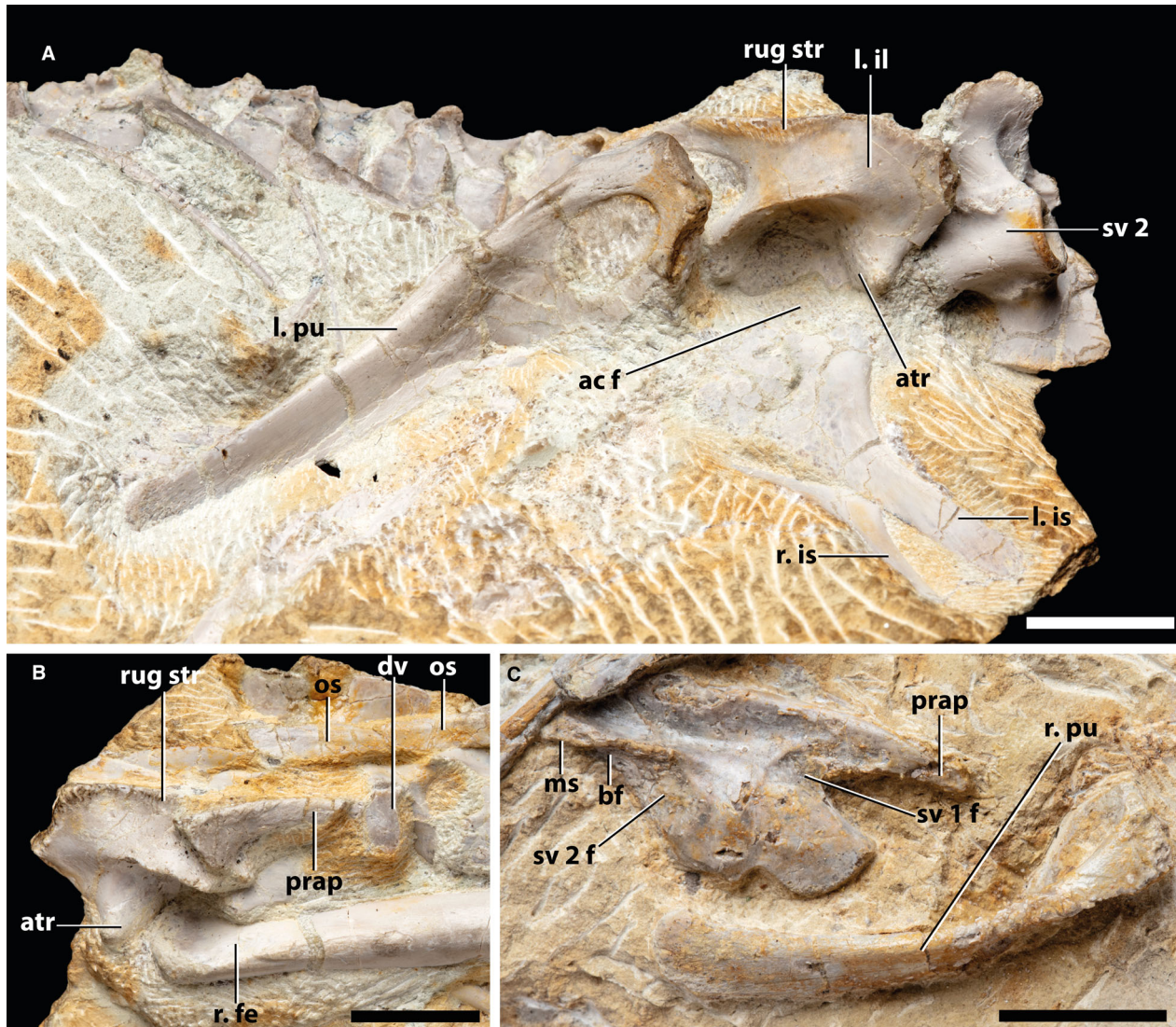
FIG. 20. Selected ilia of *Terrestrisuchus gracilis*. A, left ilium, exposed in lateral view, and associated elements, including a largely articulated left pubis and ischium, of NHMUK PV R 7562. B, right ilium, exposed in lateral view, and associated elements of NHMUK PV R 7562. C, left ilium, exposed in medial view, and associated elements of NHMUK PV R 7561a. *Abbreviations*: ac f, acetabular fenestra; atr, antitrochanter; bf, brevis fossa; dv, dorsal vertebra; fe, femur; il, ilium; is, ischium; l., left; ms, medial shelf; os, osteoderm; prap, preacetabular process; pu, pubis; r., right; rug str, rugose striations; sv, sacral vertebra; sv f, sacral vertebra facet. Scale bars represent 10 mm.

posteroventral margin of the brevis fossa is formed by a ridge that also forms the posteroventral margin of the ilium. This ridge is poorly developed and does not form a distinct brevis shelf, a feature that is present in many avemetatarsalians, including dinosaurs (Nesbitt 2011). Anteriorly, this ridge is quite prominent in *Terrestrisuchus gracilis*, forming the margin of a thin flange of bone posterior to the acetabulum. Here, this ridge is oriented anteroventrally to posterodorsally. Posterior to this, where the ridge forms the ventrolateral margin of the postacetabular process, it is more anteroposteriorly oriented and less clearly demarcated as a distinct ridge.

The lateral surface of the main body of the ilium is mainly composed of a well-excavated acetabulum (Figs 20, 21). The dorsal margin of the acetabulum is formed by a well-developed supraacetabular crest, which is oriented laterally. The supraacetabular crest fades posteriorly quite abruptly, just anterior to the posterior end of the acetabulum (Figs 20A, 21A, C). The crest extends considerably further anteriorly, being virtually straight and oriented posterodorsally to anteroventrally in lateral view, before fading as it reaches the pubic peduncle. In lateral view, the ventral margin of the ilium is slightly convex anteriorly, whereas it has a distinct notch in its posterior portion (Figs 20A, C, 21A, B, E, F). This indicates that the acetabulum was perforated by a small opening (Fig. 20A), as in other early crocodylomorphs (Crush 1984; Lecuona *et al.* 2016).

FIG. 21. Selected ilia of *Terrestrisuchus gracilis*. A–D, right ilium of NHMUK PV R 7561c in: A, lateral; B, medial; C, dorsal; D, ventral view. E–H, right ilium of NHMUK PV R 37788 in: E, lateral; F, medial; G, dorsal; H, ventral view. *Abbreviations*: atr, antitrochanter; bf, brevis fossa; ms, medial shelf; poap, postacetabular process; prap, preacetabular process; rug str, rugose striations; sac cr; supraacetebular crest; sc rug, subcircular rugosity; sv f, sacral vertebra facet. Scale bars represent: 10 mm (A–D); 5 mm (E–H).

The posteroventral surface of the acetabulum is slightly rugose, which represents the antitrochanter (Figs 20A–B, 21A, D, E, H). Tentative iliac antitrochanters have also been identified in *Kayentasuchus walkeri* and *Dromicosuchus grallator* among non-crocodyliform crocodylomorphs (Clark & Sues 2002; Sues *et al.* 2003). In addition, a clear subcircular rugosity is present on the anterior portion of the acetabulum (Fig. 21A), which might also represent a muscle or ligament attachment site. This subcircular rugosity is not known for any other non-crocodyliform crocodylomorph.

The anterior margin of the main body of the ilium is straight ventrally and concave dorsally in lateral view and angled at approximately 50° relative to the horizontal level (Figs 20C, 21A). The anteroventral corner of the ilium, which forms the pubic peduncle, is moderately expanded lateromedially and

anteroposteriorly (Fig. 21A, D). The pubic peduncle is turned laterally in ventral view as in *Dromicosuchus grallator* and *Trialestes romeri* (Fig. 21D; Sues *et al.* 2003; Lecuona *et al.* 2016). The posteroventral margin of the ilium is concave in lateral view and oriented anteroventrally to posterodorsally at an angle of 120° relative to the horizontal plane (Fig. 21A). This orientation is also seen in *Dromicosuchus grallator* and *Dibothrosuchus elaphros* (Wu & Chatterjee 1993; Sues *et al.* 2003) but differs from the posteroventrally to anterodorsally oriented posteroventral margin of the ilium in *Trialestes romeri* (Lecuona *et al.* 2016). The posteroventral corner of the ilium, forming the ischial peduncle, is slightly lateromedially expanded and oriented posterolaterally in ventral view as in *Dromicosuchus grallator* and *Trialestes romeri* (Fig. 21D; Sues *et al.* 2003; Lecuona *et al.* 2016).

The medial surface of the ilium is characterized by the rugose and slightly depressed articular facets for the ribs of the two sacral vertebrae (Figs 20C, 21B, F). The facet for the first sacral vertebra is oval in medial view and oriented anteroventrally to posterodorsally on the anteroventral portion of the main body of the ilium, which corresponds to the anteroventral portion of the acetabulum. The articular surface for the second sacral vertebra is comparatively smaller but more deeply excavated and rugose. It is also oval in shape and oriented anteroventrally to posterodorsally. The medial surface of the acetabulum is lateromedially convex, whereas the medial surface of the iliac blade is mostly flat. A distinct concavity is formed on the medial surface of the postacetabulum between the medially projected medial shelf and the medially facing surface of the iliac blade. Additionally, a shallow fossa is formed anterodorsal to the articular facet for the first sacral rib. The dorsal margin of this fossa is formed by a poorly developed anteroposteriorly directed ridge, which occurs in a wide range of archosaurs (mr1 *sensu* Hutchinson 2001a).

Pubis. The pubic shaft forms an elongate, flattened plate (Fig. 22). It is oriented anteroventrally and curves very slightly posteriorly in lateral view. The two main, smooth surfaces of the plate are directed anterodorsally and posteroventrally, respectively. The pubic shaft is gently bowed, so that the anterodorsal surface is slightly convex and the posteroventral surface, slightly concave in lateral view (Fig. 22B), as in *Saltoposuchus connectens* (Spiekman 2023). The lateral margin of the pubic shaft is anteroposteriorly thin and rounded. The pubic shaft would have contacted its counterpart medially for most of its proximodistal length through the thin, medial pubic apron (Crush 1984), which is even thinner anteroposteriorly than the lateral margin. In anterior or posterior view, the lateral margin is somewhat concave, whereas the medial margin is straight (Fig. 22C). The pubic shaft is considerably longer than the length of the iliac blade and that of the ischial shaft (Fig. 20A, Table S2). The pubic shaft only narrows very gradually distally but does not taper; its distal end is gently rounded (Fig. 22A, C). Therefore, there is no expanded 'pubic boot' in *Terrestrisuchus gracilis*, in contrast to the tentatively identified pubic shaft of *Hallopus victor* and the pubis of the indeterminate crocodylomorph UCMP 129740 (Walker 1970; Parrish 1991). The distalmost portion of the posterior surface of the pubic shaft is somewhat rugose in the left pubis of NHMUK PV R 7562, probably forming an attachment site for *M. puboischiofemoralis externus* (Hutchinson 2001a).

The proximal region of the pubis is composed of a curved plate, a large obturator foramen, and two proximal articular surfaces (Fig. 22B, D). The obturator foramen is large and oval (Fig. 22A), similar to that seen in *Saltoposuchus connectens* (Spiekman 2023). It is longest anteroventrally to posterodorsally. In this plane the foramen is a little less than twofold longer than tall. The proximal pubic region is oriented anterolaterally to posteromedially, and consequently, the obturator foramen is not fully obscured by the pubic shaft in anterior view (Fig. 22C), in contrast to *Saltoposuchus connectens*. The anterior margin of the proximal pubis bears a faint pubic tubercle (Fig. 22A–B), similar to the condition in *Trialestes romeri* and *Saltoposuchus connectens*

(Lecuona *et al.* 2016; Spiekman 2023). The lateral margin is thickened in this part of the pubis, and directly anteromedial to the tubercle this surface bears a shallow concavity. Another concave surface is positioned proximomedially to the tubercle. The latter surface is subtriangular in lateral view, widening proximally. The tubercle and the two associated concave surfaces represent attachment sites for ligaments and *M. obliquus abdominus* and *M. ambiens*, respectively (Hutchinson 2001a). Distally, the tubercle transitions into a small ridge that is placed on the lateral margin of the pubis, which extends approximately until the level of the anteriormost margin of the obturator foramen. This small ridge is demarcated medioventrally by a shallow and short groove that is oriented parallel to it (Fig. 22A–B).

The proximal or dorsal surface of the pubis possesses a rugose and concave facet for the articulation with the pubic peduncle of the ilium (Fig. 22B). In proximal view this facet forms an elongate oval that is oriented anteromedially to posterolaterally. Directly posterolateral to this facet there is a rugose, slightly convex, and crescent-shaped surface that faces posterodorsally as well as laterally. This is the small acetabular contribution of the pubis. The posterior margin of the pubis is positioned almost directly posterior to the obturator foramen. Dorsally, it is separated from the acetabular contribution of the pubis by a shallow groove that is subtriangular in outline in lateral view, expanding anteriorly (Fig. 22B). The posterior margin is oriented dorsoventrally and it is slightly concave in lateral view. It forms the articular surface with the ischium. In posterior view this facet is widest dorsally and tapers ventrally. Further ventrally, the margin curves anteroventrally. It is unclear whether this represents an original section of the margin or whether the posterior margin is partially broken off ventrally in NHMUK PV R 7562 (Fig. 22B).

Ischium. The ischium is composed of a proximal portion and a long, plate-like, posteroventrally directed ischial shaft (Fig. 23). The shaft possesses two main surfaces, which are both flat: one is directed ventrally and the other dorsally. Like the pubic shaft, the ischial shaft slightly reduces in width distally but does not taper (Fig. 23A–B). Instead, the distal end is rounded off. This is similar to the morphology observed in *Trialestes romeri* (Lecuona *et al.* 2016), but differs from the expanded distal end of the ischium in *Hallopus victor* (Walker 1970). The ventral surface of the distal end of the ischial shaft is rugose (Fig. 23A), probably representing an attachment site for *m. puboischiofemoralis externus* (Hutchinson 2001a). In contrast, the dorsal surface of the distal end is smooth. The lateral margin of the ischial shaft is somewhat thickened and rounded proximally, but it becomes very thin distally. The medial margin would have connected to its antimere across most of its length (Crush 1984). The medial margin is thin along its entire proximodistal length (Fig. 23D). Both the lateral and medial margins are straight on their distal halves and concave proximally (Fig. 23B). The dorsal surface of the ischial shaft bears a low ridge proximally, which is directed distomedially from the lateral margin of the shaft. It probably represents a continuation of the posterior margin of the proximal portion of the ischium and it fades as it reaches the lateromedial midpoint of the ischial shaft.
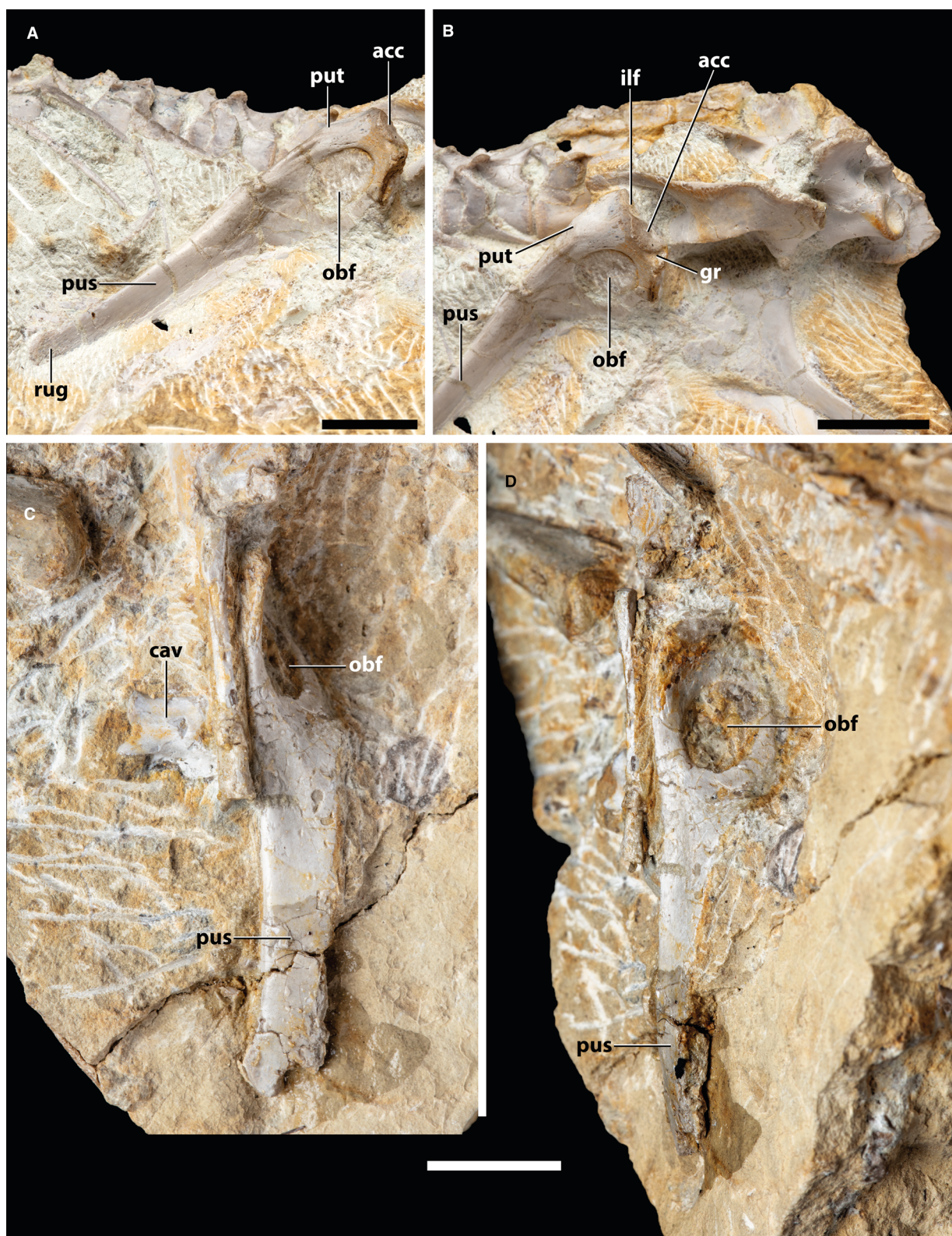
FIG. 22. Selected pubes of *Terrestrisuchus gracilis*. A–B, the left pubis and associated elements of NHMUK PV R 7562; left pubis in: A, lateroventral; B, laterodorsal view. C–D, the larger of the two right pubes and associated elements of NHMUK PV R 7561b; right pubis in: C, anterior; D, medial view. *Abbreviations*: acc, acetabular contribution of pubis; cav, caudal vertebra; ilf, ilium facet; gr, groove; obf, obturator foramen; pus, pubic shaft; put, pubic tubercle; rug, rugosity. Scale bars represent 10 mm.
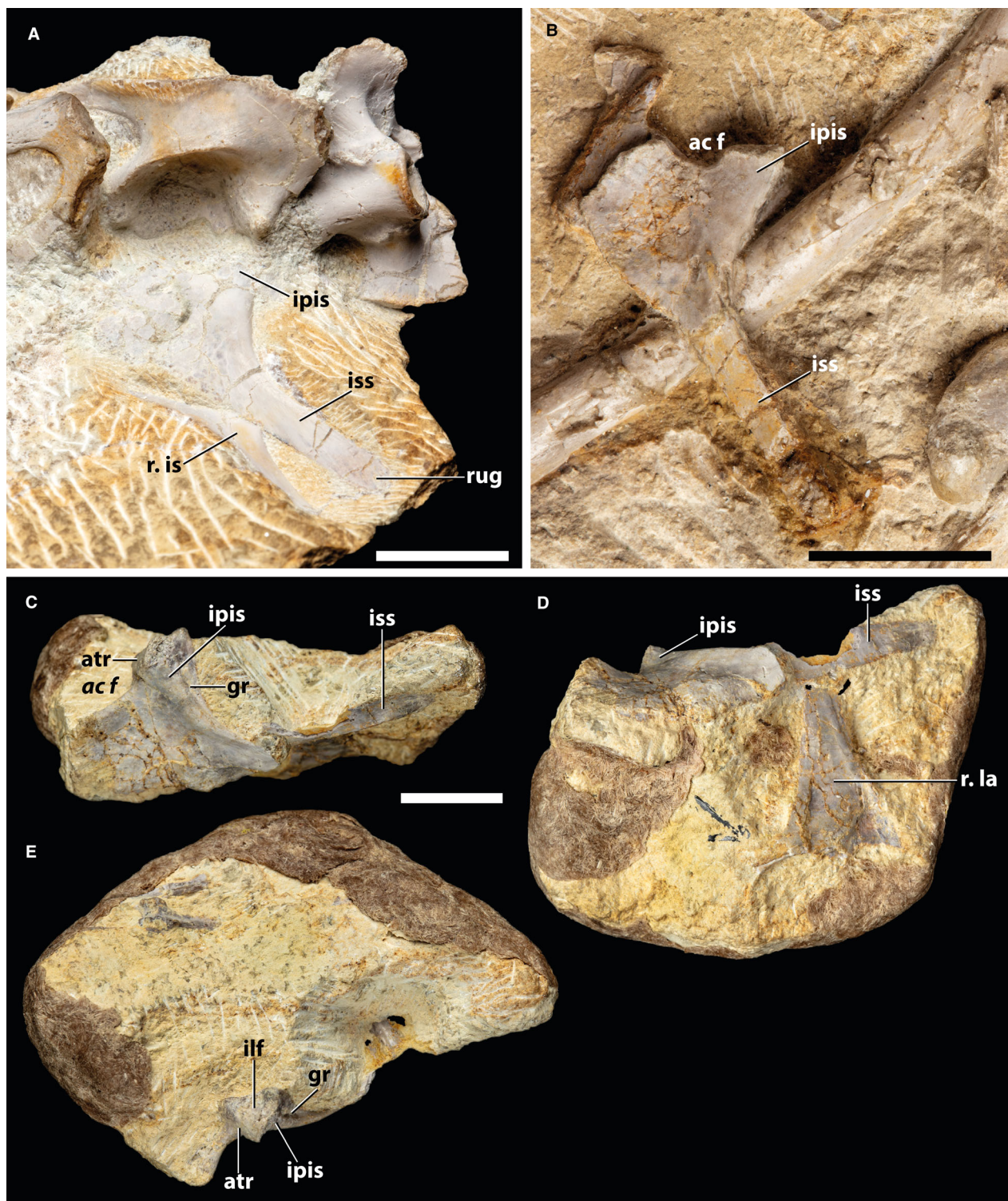
FIG. 23. Selected ischia of *Terrestrisuchus gracilis*. A, both ischia and associated elements of NHMUK PV R 7562, the left ischium is exposed in lateroventral view, and the right ischium is partially exposed in medial view. B, left ischium of NHMUK PV R 7561a, exposed in lateroventral view, and associated elements. C–E, left ischium of NHMUK PV R 37728 and associated elements; left ischium in: C, lateral; D, ventral; E, dorsal view. *Abbreviations*: ac f, acetabular fenestra; atr, antitrochanter; gr, groove; ilf, ilium facet; ipis, iliac peduncle of the ischium; is, ischium; iss, ischial shaft; la, lacrimal; r., right; rug, rugosity. Scale bars represent 10 mm.

The iliac peduncle of the ischium projects dorsally relative to the rest of the ischium in lateral view (Fig. 23C). On its dorsal surface it possesses a crescent-shaped articular facet for the ilium (Fig. 23E), similar to that seen in *Saltoposuchus connectens* (Spiekman 2023). This facet faces dorsally and slightly anteriorly. Its surface is formed by raised posteromedial and anteromedial portions with a distinct concavity between them. The surface directly anterolaterally to this facet forms a platform and is confluent with the former. It is slightly convex and directed dorsally, anteriorly and slightly laterally. It represents the ischial contribution of the antitrochanter (Fig. 23C, E). An antitrochanter is absent on the ischia of *Saltoposuchus connectens* and *Trialestes romeri* (Lecuona *et al.* 2016; Spiekman 2023). The ischial antitrochanter is roughly rectangular in outline and demarcated anteriorly and laterally by a sharp ridge. This antitrochanter cannot be discerned in the left ischia of NHMUK PV R 7562 and NHMUK PV R 7561a, which represent smaller specimens compared with the ischium of NHMUK PV R 37728 (Table S2). Although these specimens do not preserve this region as well as in NHMUK PV R 37728, it is likely that the antitrochanter was less well developed in smaller individuals of *Terrestrisuchus gracilis*.

The dorsal margin of the ischium is separated by a distinct notch from the antitrochanter positioned posterior to it. This margin, which forms the posteroventral border of the perforated acetabulum as in *Trialestes romeri* (Lecuona *et al.* 2016), is distinctly concave in lateral view and is oriented anteroventrally to posterodorsally. The posterior margin of the ischium proximal to the ischial shaft is characterized by a distinct longitudinal groove (Fig. 23C, E). In posterior view this margin is thickest proximally and it tapers gradually distally until it transitions into the posterolateral margin of the ischial shaft. The dorsoventrally oriented anterior margin of the ischium articulated with the pubis. It is poorly preserved in all available specimens and was not completely fused in any of the known specimens. The ventral margin of the ischium proximal to the ischial shaft is gently convex in lateral view and oriented anterodorsally to posteroventrally.

Femur. The femur of *Terrestrisuchus gracilis* is elongate and gracile (Fig. 24A). It is slightly shorter than the tibia and fibula, based on the complete right femur and left tibia and fibula of NHMUK PV R 37600 (Table S2). This feature possibly also occurs in *Macelognathus vagans* (Göhlich *et al.* 2005), but is more typical of pterosaurs, lagerpetids, and some small theropods and early ornithischians (Nesbitt 2011). The proximal head of the femur is inturned and directed mostly medially and slightly anteriorly to articulate with the pelvic acetabulum (Fig. 20B). Ventrally, this inturned head is not very strongly offset, but it is instead connected to the shaft by a gradually concave ventromedial surface. This represents the condylar fold (*sensu* Brochu 1992; Nesbitt *et al.* 2006), which is a crocodylomorph synapomorphy. In proximal view, the head is oval to subtriangular in outline, with a wider medial portion and a narrower lateral portion (Fig. 24G). The medial margin of the head is convex in proximal view and is characterized by a small anteromedial tuber and a considerably larger posteromedial tuber (Fig. 24A). The lateral margin is convex anteriorly, which

represents the anterolateral tuber, and concave posteriorly in proximal view (Fig. 24G).

The lateral margin of the proximal head transitions distally into a ridge (Fig. 24A–B). In NHMUK PV R 7562 the surface directly anterolateral to this ridge is slightly depressed and rugose. Further distally, this ridge thickens into a more clearly defined, elongate tubercle (Fig. 24B). In NHMUK PV R 37600a this ridge is differentiated from the shaft medially by a shallow longitudinal groove that runs parallel to the ridge (Fig. 24A). The ridge and associated rugosity represent the pseudointernal trochanter first identified by Walker (1970) for *Hallopus victor*, which is widely present among non-crocodyliform crocodylomorphs (e.g. Sues *et al.* 2003; Göhlich *et al.* 2005; Pol *et al.* 2013). Although Crush (1980, 1984) described this lateral ridge, he did not consider it homologous to the pseudointernal trochanter. Another muscle attachment site is widely present in non-crocodyliform crocodylomorphs (e.g. *Almadasuchus figarii, Macelognathus vagans, Dromicosuchus grallator, Kayentasuchus walkeri, Hallopus victor*; Pol *et al.* 2013): the lesser trochanter (*sensu* Walker 1970). This structure is absent in all available specimens of *Terrestrisuchus gracilis*. The presence of femoral muscle scars is strongly ontogenetically variable in archosaurs (Griffin 2018), and therefore it is uncertain whether the lesser trochanter was truly absent in *Terrestrisuchus gracilis*. The fourth trochanter forms a low, mound-like tuberosity as is typical for crocodylomorphs (Fig. 24A, E, F) and is located relatively proximal to the head, about one-quarter of the way down the femur. The anteromedial surface of the fourth trochanter bears a shallow concavity (the medial pit of Hutchinson 2001b) and the trochanter is oriented slightly proximoanteriorly to distoposteriorly across the medial surface of the shaft.

The shaft has a continuous anterior curvature along its proximal half, as well as a slight lateral curvature in posterior or lateral view (Fig. 24A–B). This corresponds to the morphology seen in other non-crocodyliform crocodylomorphs (e.g. *Dromicosuchus grallator, Kayentasuchus walkeri, Hallopus victor*), but differs from the sigmoidal curvature present in crocodyliforms (Clark & Sues 2002; Sues *et al.* 2003).

The distal end of the femur is characterized by prominent fibular (lateral) and tibial (medial) condyles (Fig. 24H–L), as well as an additional prominent process posterior to the lateral condyle, the crista tibiofibularis (Nesbitt 2011). The crista tibiofibularis forms a prominent posterior extension in distal view (Fig. 24L). It is separated from the lateral condyle by a shallow groove, which is oriented anteromedially to posterolaterally on the distal surface. The medial condyle is at the same distal level as the crista tibiofibularis, whereas the lateral condyle extends slightly further distally (Fig. 24H–I), as in *Hesperosuchus agilis* and *Dromicosuchus grallator* (Parrish 1991; Sues *et al.* 2003). In the hallopodids *Macelognathus vagans* and *Almadasuchus figarii* the lateral condyle extends further distally than the medial condyle to a much larger extent (Göhlich *et al.* 2005; Pol *et al.* 2013). The lateral and medial condyle are separated by a shallow anteroposteriorly directed groove on the distal surface (Fig. 24L). In distal view the anterior margins of the medial and lateral condyles are distinctly convex and separated by a clear concavity that is deepest slightly medial to the lateromedial midpoint of the anterior margin. This concavity reaches a short

FIG. 24. Selected femora of *Terrestrisuchus gracilis*. A, right femur of NHMUK PV R 37600a in posterior view. B, right femur, exposed in lateral view, and associated elements of NHMUK PV R 7562. C–G, proximal end of the right femur of NHMUK PV R 37878 in: C, anterior; D, posterior; E, medial; F, lateral; G, proximal view. H–L, distal end of the right femur of NHMUK PV R 37636 in: H, posterior; I, anterior; J, medial; K, lateral; L, distal view. *Abbreviations*: alt, anterolateral tuber; amt, anteromedial tuber; crtf, crista tibiofibularis; gr, groove; lc, lateral condyle; lr, longitudinal ridge; mc, medial condyle; pmt, posteromedial tuber; pst, pseudointernal trochanter; 4th tr, fourth trochanter. Scale bars represent: 30 mm (A); 10 mm (B, H–K); 5 mm (C–G, L).

distance onto the anterior surface of the femur near its distal end, and it is framed on either side by a longitudinal ridge that is confluent with one of the condyles. The ridge on the medial side is most strongly developed. In distal view, the medial margin of the distal end is roughly flat to very slightly convex and anteroposteriorly directed. In NHMUK PV R 37875 the lateral margin of the crista tibiofibularis is rounded, whereas it is almost flat in NHMUK PV R 37636. The lateral margin of the crista tibiofibularis forms almost a right angle with the posterior margin of the lateral condyle in NHMUK PV R 37636, whereas in NHMUK PV R 37875 this angle is considerably more obtuse. This variation is possibly attributable to size differences, given that neither specimen is compressed in this region. The morphology seen in NHMUK PV R 37636 has also been reported for *Dromicosuchus grallator* (Nesbitt 2011, char. 319). Posteriorly the medial condyle forms a relatively sharp apex in distal view on its posteromedial corner (Fig. 24L). In contrast, the posterior margin of the lateral condyle is gently rounded. The medial condyle is separated from the crista tibiofibularis by a notch on the posterior margin in distal view. The posterior surface of the shaft is flat to slightly concave between the two distal condyles.

Tibia. The tibia is an elongate element with a virtually straight shaft, except for a slight medial curvature of the distal portion (Fig. 25A). In contrast, the tibia is considerably curved in most non-crocodyliform crocodylomorphs, including *Saltoposuchus connectens* (Colbert 1952; Walker 1990; Spiekman 2023). The tibia is slightly more slender than the femur and considerably more robust than the fibula (Fig. 25A; Table S2). The proximal and distal ends are expanded relative to the shaft. As in *Dromicosuchus grallator* (Sues *et al.* 2003), the proximal end is strongest expanded posteromedially, whereas the distal end is expanded anterolaterally to posteromedially.

The proximal surface of the proximal end is mostly flat but strongly convex anteriorly (Fig. 25D). The posterolateral corner of the proximal surface, which forms the lateral condyle that would have articulated with the proximal portion of the fibula, is very slightly concave (Fig. 25F). In several other non-crocodyliform crocodylomorphs (e.g. *Dromicosuchus grallator*, *Hesperosuchus agilis*, *Sphenosuchus acutus*) this depression is considerably more distinct (Sues *et al.* 2003; Nesbitt 2011). The proximal end is sloped anteroproximally to posteroventrally. In proximal view the tibia has a roughly straight lateral margin (Fig. 25F), which lacks the notch present in *Saltoposuchus connectens* (Spiekman 2023). The anterior margin forms an acute angle with the lateral margin. It is slightly convex and medially it is confluent with the similarly convex medial margin. The medial margin is rounded posteriorly on the expanded

posteromedial corner of the proximal head. In proximal view the lateral condyle forms a posteriorly directed mound-like expansion on the posterolateral corner of the proximal end. It is separated from the posteromedial expansion by a distinct notch on the posterior margin of the proximal end. The anterior surface of the tibia directly distal to the proximal head is distinctly convex, particularly anterolaterally. The medial and posterior surfaces are concave and overhung by the proximal head. The lateral surface directly distal to the proximal head is flat.

The distal end of the tibia is expanded anterolaterally to posteromedially. The posteromedial side reaches slightly further distally than the anterolateral side (Fig. 25G–J), as in *Hesperosuchus agilis*, *Dromicosuchus grallator* and *Macelognathus vagans* (Colbert 1952; Sues *et al.* 2003; Göhlich *et al.* 2005). The distal surface of the anterolateral side, as well as the anterior third of the anteromedial surface, are strongly convex. The posteromedial side is very weakly convex, whereas the posterolateral side is weakly concave between the posteromedial and anterolateral portions. The posterolateral half of the distal surface is sloped anterodistally to posteroproximally. In distal view the posteromedial and anterolateral halves of the distal end are separated by a distinct groove on the posterolateral margin (Fig. 25K), which also occurs in other non-crocodyliform crocodylomorphs (Nesbitt 2011). The anterolateral and posteromedial margins of the distal end are strongly convex, whereas the anteromedial margin is most convex medially and only slightly convex laterally.

Fibula. The fibula is more slender than the tibia (Fig. 26). In lateral and medial view the proximal head is slightly expanded posteriorly and, as a result, the surface directly distal to the head is concave in this region (Fig. 26C). The proximal head is oval in outline in proximal view, with the longest margins being lateral and medial (Fig. 26D). The anterior and posterior margins are strongly convex and the medial margin is slightly convex. The lateral margin cannot be observed in any of the available specimens. The proximal surface is mostly flat, but it has a shallow concavity in its centre (Fig. 26D).

The proximal portion of the fibular shaft is thickened anteriorly due to the presence of the low ridge, which forms an attachment site for the *M. iliofibularis* (Huene 1921; anterior trochanter *sensu* Sereno 1991). The ridge forms a poorly differentiated longitudinal crest along the anterolateral side of the fibula (Fig. 26B, C, E). This crest is slightly thickened laterally, with the lateral surface directly adjacent to it being slightly concave. The anterior half of the shaft is slightly curved anteriorly, whereas the rest of the shaft is straight (Fig. 26A–B). This differs from the strongly sigmoidally curved fibula of *Saltoposuchus connectens* (Spiekman 2023). The fibula is also straight in *Trialestes*

FIG. 25. Left tibia of NHMUK PV R 7566, in A, posterior view. B–F, the proximal end in B, anterior; C, posterior; D, lateral; E, medial; and F, proximal view. G–K, the distal end in G, anteromedial; H, posterolateral; I, posteromedial; J, anterolateral; and K, distal view. *Abbreviations*: als, anterolateral side; gr, groove; latc, lateral condyle; no, notch; pme, posterior expansion; pms, posteromedial side. Scale bars represent: 20 mm (A); 5 mm (B–J).

romeri (Lecuona *et al.* 2016). The cross-section of the shaft is oval, with the shaft being slightly longer anteroposteriorly than lateromedially.

The distal surface of the distal end bears a concavity on its medial portion for the articulation of the astragalus (Nesbitt 2011), but it is otherwise flat (Fig. 26A). The outline of the distal end is roughly oval in distal view.

Astragalus. The astragalus is a complex bone, consisting of a proximolaterally directed process, which contains the articular surfaces for the fibula (proximolaterally) and part of the tibia (proximomedially), a laterally projected peg for articulation with the calcaneum, and a large block-like medial portion that

proximally articulated with the tibia (Fig. 27). The peg forms a ball-and-socket joint with the deeply excavated articular surface on the calcaneum (see below). As such, the articulation between astragalus and calcaneum is typical of crocodylomorphs (the so-called 'crocodile-normal' ankle joint, Cruickshank 1979; Sereno 1991), with the possible exception of *Trialestes romeri* (Lecuona *et al.* 2016).

The proximolateral process is square (Fig. 27A, C, D). The fibular facet on its proximolateral surface is slightly concave and trapezoidal in outline (Fig. 27C), in contrast to the rectangular outline seen in, for instance, *Trialestes romeri* and *Hesperosuchus agilis* (Lecuona *et al.* 2016). Its posterior margin is the longest, whereas its anterior margin is the shortest; the medial and lateral margins
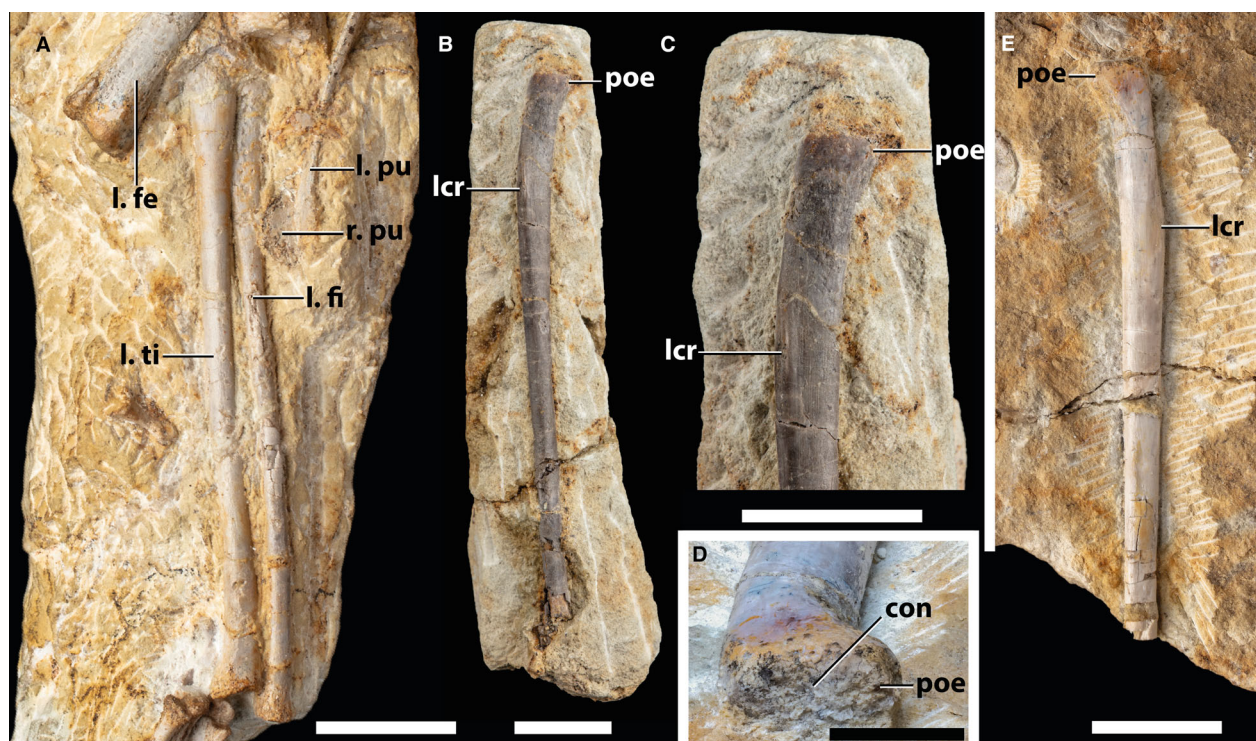
FIG. 26. Selected fibulae of *Terrestrisuchus gracilis*. A, left fibula, exposed in anterior or anteromedial view, and associated elements of NHMUK PV R 37600b. B, partial left fibula missing the distal end of NHMUK PV R 37898 in lateral view; C, close up of the proximal portion of the same element. D–E, partial left fibula missing the distal end of NHMUK PV R 38297 in: D, proximal; E, medial view. *Abbreviations*: con, concavity; fe, femur; fi, fibula; l., left; lcr, longitudinal crest; poe, posterior expansion; pu, pubis; r., right; ti, tibia. Scale bars represent: 20 mm (A); 10 mm (B, C, E); 5 mm (D).

are subequal and intermediate in length. The fibular facet is slanted medially to posterolaterally on its posterolateral portion.

The majority of the proximal surface of the astragalus forms the complex tibial facet (Fig. 27C, E). The lateral portion of this facet is formed on the proximomedial surface of the proximolateral process. This surface is slanted both proximoposteriorly to distoanteriorly and proximolaterally to distomedially, and it can best be observed in anterior and proximal view (Fig. 27A, C). The proximal surface of the astragalus forms the remainder of the tibial facet and it is deeply excavated, forming a bowl-like concavity (Fig. 27C, E). The anterior margin of the tibial facet forms a thin but distinct lamina along the proximal margin of the astragalus in anterior view (Fig. 27A). It is oriented proximolaterally to distomedially. This anterior lamina is virtually straight along most of its length but it curves slightly more proximally on its lateral portion on the proximolateral process of the astragalus. The medial and posterior margins of the tibial facet are distinctly raised. In proximal view the medial margin is strongly convex, whereas the shape of the posterior margin is more complex: it is concavoconvex, being distinctly convex medially and concave laterally before reaching the proximolateral process of the astragalus (Fig. 27C). In posterior view the medial portion of the posterior margin is semi-circular (concave) in outline (Fig. 27D). Laterally, the posterior margin curves strongly proximally to form the posteromedial margin of the proximolateral process.

The laterally projected peg of the astragalus is placed on the distolateral portion of the bone (Fig. 27A, D). It has a complex shape, being convex distoanteriorly and concave proximoposteriorly, where it forms the main articulation facet for the calcaneum, in lateral view (Fig. 27B). The lateral terminus of the peg is positioned distoposteriorly. The peg is separated from the proximolateral process of the astragalus by the posterior groove, which extends along the posterolateral surface of the astragalus in an anterolateral to posteromedial direction and, as such, the groove is clearly visible in lateral and posterior views (Fig. 27B, D).

The distomedial portion of the astragalus forms a large bulbous expansion. In medial view this expansion is distinctly convex anteriorly, whereas it is slightly concave posterodistally and its posteroproximal margin, which forms the medial margin of the tibial facet, is straight (Fig. 27E). Its medial surface bears a small but distinct pit. The posterior surface of the bulbous expansion is slightly concave because of the expanded margins on the proximal and distal ends of the surface (Fig. 27D). Laterally, this surface is separated from the posterior groove by a slight convexity. The anterior surface of the bulbous expansion is distinctly convex and forms the distomedial portion of the anterior surface of the astragalus (Fig. 27A). The remainder of the anterior surface is formed by a large concavity (= the anterior hollow of Nesbitt 2011), which is framed distomedially by the bulbous expansion, proximally by the anterior lamina, and
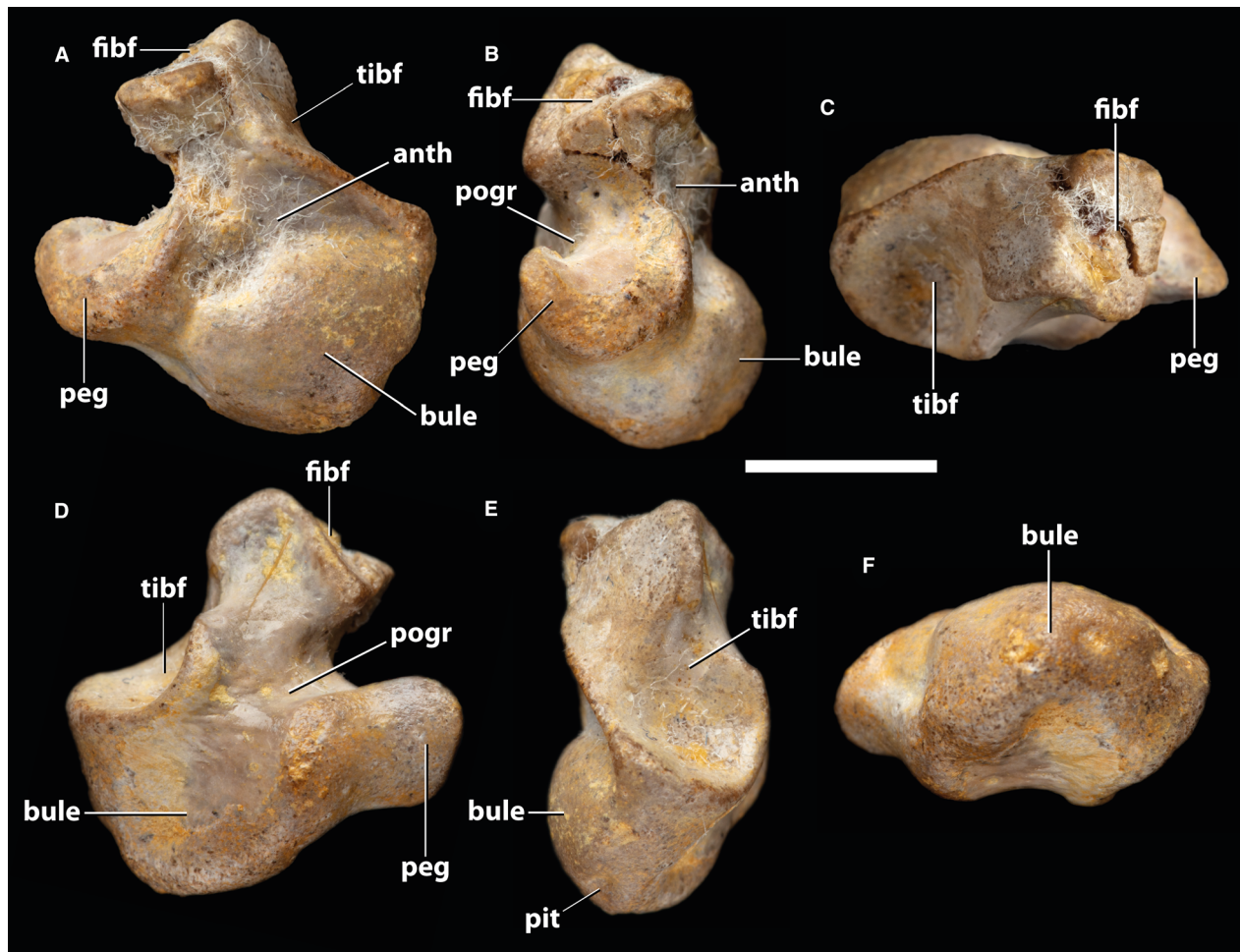
FIG. 27. Right astragalus of NHMUK PV R 37789 in: A, anterior; B, lateral; C, proximal; D, posterior; E, medial; F, distal view. *Abbreviations*: anth, anterior hollow; bule, bulbous expansion; fibf, fibular facet; pogr, posterior groove; tibf, tibial facet. Scale bar represents 5 mm.

laterally by the medial margin of the laterally oriented peg. This concavity is more deeply excavated and extends further medially than in *Trialestes romeri* (Lecuona *et al.* 2016). The distal surface of the astragalus is convex medially due to the presence of the bulbous expansion (Fig. 27F). Laterally, the laterally directed peg forms a surface on the distal surface that is continuously curved anteromedially to posterolaterally in distal view. This curved surface wraps around the laterally oriented peg to form the posterior surface of the peg in posterior view. Anteriorly, this surface is connected with the anterior hollow via a shallow groove (Fig. 27A).

Calcaneum. The calcaneum is composed of a main body and a large calcaneal tuber (Fig. 28), as in all other crocodylomorphs (Nesbitt 2011). The main body bears a very deep excavation on its medial surface, which represents the socket for the laterally projecting peg of the astragalus (Fig. 28E). A deeply excavated articular surface for the astragalar peg is present in most non-crocodyliform crocodylomorphs, except possibly *Trialestes romeri* (Lecuona *et al.* 2016). In medial view the outline of the socket is

subcircular (Fig. 28E), as in *Macelognathus vagans* (Göhlich *et al.* 2005). The socket is most deeply excavated on its anterior portion; this deeper excavation is quite abrupt and can therefore clearly be distinguished from the rest of the socket. The posterior margin of the astragalar facet is formed by a distinct medially directed lip. In anterior view this lip is slightly wider than the anterior surface of the calcaneum (Fig. 28A). The lip follows the curvature of the margin of the astragalar facet, and therefore has a concave anterior surface and a convex posterior surface. The medial end of the lip is continuously rounded. This lip was interpreted by Göhlich *et al.* (2005) as an insertion site for the distal ligament of *m. flexor hallucis*.

The anterodistal surface of the calcaneum is virtually flat in lateral and medial view. This surface is the articular facet for distal tarsal 4 (Fig. 28E). The anteroproximal and proximal surface of the main body is convex, being continuously rounded in lateral and medial view (= hemicylindrical calcaneal condyle of Sereno 1991). This surface formed a sliding articular surface for the fibula (Fig. 28E). Together with the ball-and-socket joint formed between the calcaneum and astragalus, this surface
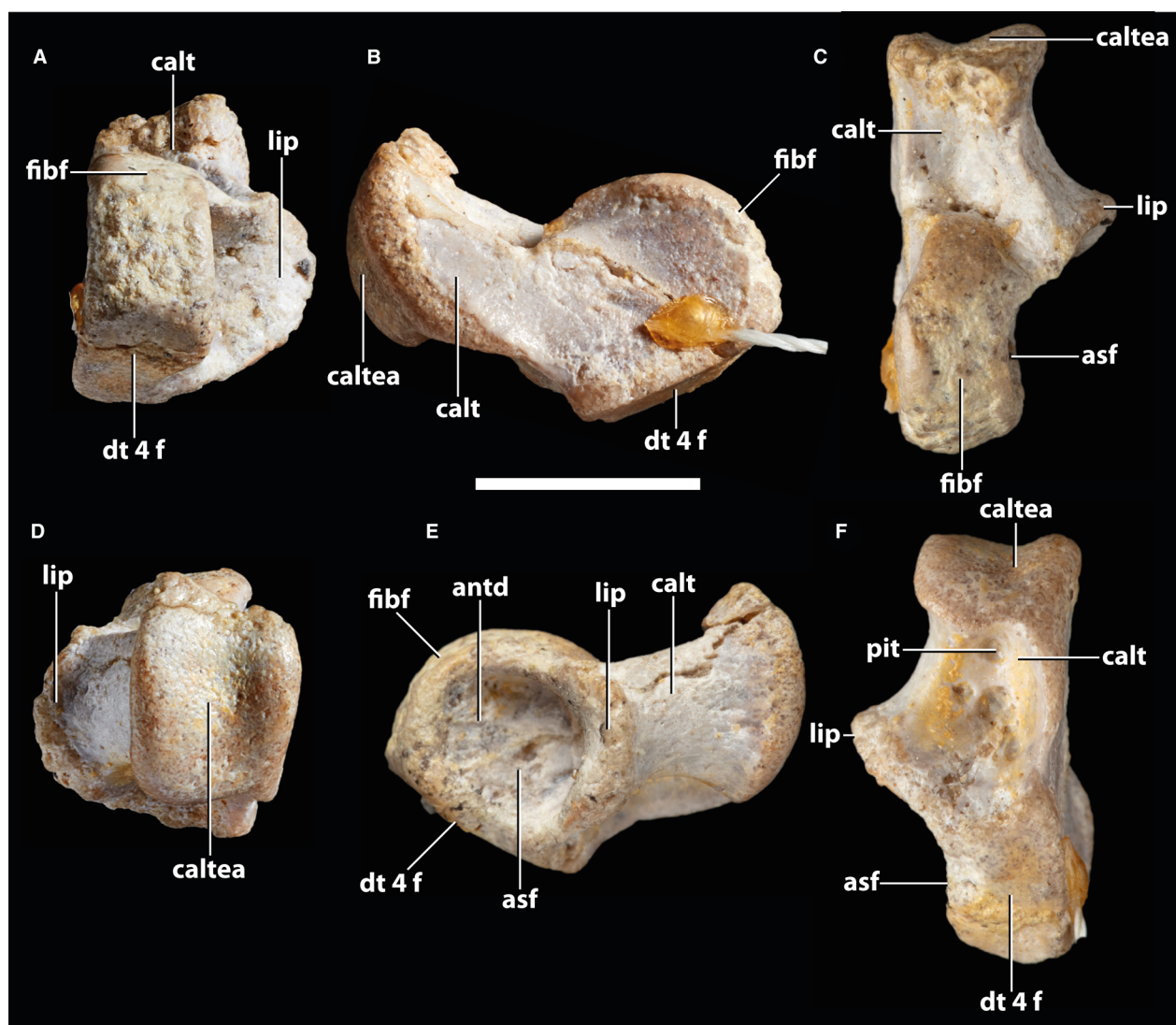
FIG. 28. Right calcaneum of NHMUK PV R 37782 in: A, anterior; B, lateral; C, proximal; D, posterior; E, medial; F, distal view. *Abbreviations*: antd, anterior depression; asf, astragular facet; calt, calcaneal tuber; caltea, calcaneal tendon attachment site; dt 4 f, distal tarsal 4 facet; fibf, fibular facet. Scale bar represents 5 mm.

allowed for the majority of the rotation of the calcaneum, and through it also the distal tarsals and pes, relative to the astragalus and epipodials. The lateral surface of both the main body and calcaneal tuber is continuous, smooth and flat to very slightly concave (Fig. 28B), as in *Saltoposuchus connectens* and *Macelognathus vagans* (Göhlich *et al.* 2005; Spiekman 2023), but in contrast to the more distinctly concave lateral surface of the calcaneum in *Dromicosuchus grallator* (Sues *et al.* 2003). The calcaneal tuber is perpendicular to the astragalar facet, and was oriented directly posterior relative to the main axis of the body, as in other non-crocodyliform crocodylomorphs (Walker 1970; Sues *et al.* 2003; Göhlich *et al.* 2005; Lecuona *et al.* 2016). This configuration is indicative of an erect posture in early crocodylomorphs that is shared with some notosuchians (e.g. Gomani 1997; Pol 2005), but which contrasts with the posterolaterally directed calcaneal tuber and semi-erect posture of

eusuchians, including extant crocodylians (Parrish 1987). The proximal surface of the calcaneal tuber is deeply excavated at its base (i.e. directly posterior to the main body of the calcaneum) (Fig. 28C). In proximal view both the lateral and medial margins of the calcaneal tuber form distinct laminae that are raised relative to the centre of the proximal surface of the tuber, as in *Saltoposuchus connectens* (Spiekman 2023). The lateral margin is anteroposteriorly directed and straight. The medial margin is concave and posterolaterally to anteromedially directed, such that it anteriorly connects to the calcaneal lip. The concavity is subrectangular in proximal view, being anteroposteriorly longer than lateromedially wide.

The distal surface of the calcaneal tuber is similarly characterized by a strongly depressed surface bordered by raised medial and lateral margins (Fig. 28F). Similar concavities on both the proximal and distal surfaces of the tuber are present in *Trialestes*

romeri (Lecuona *et al.* 2016). The concavity on the distal surface possesses up to seven clear pits in it (Fig. 28F), which were suggested by Crush (1980) to be indicative of muscle insertion. The lateral margin is most distinctly raised and forms a clear lamina that is slightly convex in distal view. The distal concavity has similar proportions to its counterpart on the proximal surface of the calcaneal tuber.

The posterior end of the calcaneal tuber is proximodistally expanded in lateral or medial view (Fig. 28B, E), particularly proximally, as in other crocodylomorphs (Sereno 1991). On its anterior portion the calcaneal tuber is wider lateromedially than tall proximodistally, as in other pseudosuchians (Sereno 1991). The posterior surface of the calcaneal tuber served as an attachment site for the calcaneal tendon (Fig. 28B, D), which attaches to the *M. gastrocnemius*. It bears a proximodistally oriented depression along its entire height that is positioned slightly laterally to the lateromedial midline of the posterior surface (Fig. 28D). The posterior surface of the tuber is distinctly convex in lateral and medial view (Fig. 28B, E), as in *Saltoposuchus connectens* and *Macelognathus vagans* (Göhlich *et al.* 2005; Spiekman 2023). This contrasts with the posterior surface of the tuber in *Trialestes romeri*, which is concave with a distally located projection (Lecuona *et al.* 2016).

Distal tarsals. As in other pseudosuchians, the ankle of *Terrestrisuchus gracilis* possesses two distal tarsals: distal tarsal 3 and 4, as can be discerned from the holotype NHMUK PV R 7557 (Fig. 29; Appendix S2). The maximum width of distal tarsal 3 is about twofold smaller than that of distal tarsal 4 (Table S2). It is elliptical and elongate, being considerably lateromedially wider than both proximodistally tall and anteroposteriorly deep (Fig. 29G–L).

Distal tarsal 4 is slightly smaller in width and height than the astragalus and calcaneum (Table S2). It consists of two flattened expansions that are perpendicular to each other (Fig. 29A–F), as in YPM 41198 (Nesbitt 2011). These two flattened expansions represent an anteriorly placed surface with proximally and distally directed faces and a posteriorly placed surface with laterally and medially directed faces. The lateral and proximal faces represent the articular surfaces for metatarsal V and the calcaneum, respectively (Sereno 1991; Nesbitt 2011). The articular surface for metatarsal V on the lateral surface of distal tarsal 4 is quite deeply excavated, in contrast to the flattened surface present in YPM 41198 (Nesbitt 2011). The calcaneal facet on the proximal surface forms a flattened subcircular platform. On the posteromedial portion of the medial surface a clear concavity is present that has two or three smaller pits inside it. These excavations, which were indicated as foramina by Nesbitt (2011), are also present in several pseudosuchian-line archosaurs, including YPM 41198 (Nesbitt 2011).

Pes. All metatarsals are long and slender (Fig. 30). Metatarsal III is the longest, but it is only slightly longer than metatarsal II (Table S2). Metatarsals I and IV are distinctly shorter, with the latter being a bit longer than the former. Metatarsal V is poorly developed and considerably shorter, being less than half the length of metatarsals II and III and slightly more than half the length of metatarsals I and IV. This configuration is common among early crocodylomorphs, although in *Trialestes romeri* metatarsal V is similar in length to the other metatarsals, and metatarsals III and IV form the longest metatarsals (Lecuona *et al.* 2016). The midshaft diameters of metatarsals II, III and IV are subequal in width. In contrast, the diameter of the midshaft in metatarsal I is slightly narrower, whereas it is considerably narrower in the reduced metatarsal V. A narrower metatarsal I relative to metatarsals II–IV also occurs in the ornithosuchid *Riojasuchus tenuisceps* and is common in avemetatarsalians (Sereno 1991). In *Hallopus victor*, metatarsal I is apparently very thin and splint-like (Walker 1970).

The articulated pes of NHMUK PV R 37600b shows that metatarsals I–IV were tightly bunched (Fig. 30A), overlapping each other for at least their proximal halves, with the lateral side of each metatarsal overlapping the medial side of the metatarsal directly lateral to it, and being only slightly separated at their distal ends, as in *Macelognathus vagans* and possibly *Sphenosuchus acutus* (Walker 1990; Göhlich *et al.* 2005). In contrast, metatarsal V is positioned posterior to metatarsals IV and III, and it can thus not be observed in anterior view, but only in posterolateral view (Fig. 30B).

The proximal ends of metatarsals I–IV are considerably lateromedially and slightly posteriorly expanded compared with the shaft (Fig. 30A), albeit not as strongly as in *Sphenosuchus acutus* (Walker 1990). They are oval in proximal view and, like the metacarpals, their long axes are oriented dorsolaterally or anterolaterally to plantomedially relative to the main body axis, as in extant crocodylians (e.g. Klinkhamer *et al.* 2017). The lateral and medial portions of the proximal head are slightly convex, and they are separated by a shallow concavity on the proximal surface. The distal ends of metatarsals I–IV are not expanded and are therefore subrectangular in anterior view. Their medial side bears a distinct concavity, which represents a ligamental pit (Fig. 30A), as in *Sphenosuchus acutus* (Walker 1990). The anterior surface of the shaft directly proximal to the distal end also possesses a clear lateromedially oriented excavation on these four metatarsals. Their distal surface is roughly flat. The posterior portion of the distal end is slightly expanded relative to the shaft and, as such, the posterior margin of the shaft is distally slightly concave in lateral or medial view. The metatarsal shaft has a thin cortex and is approximately circular in cross-section.

The morphology of metatarsal V differs distinctly from that of the other four metatarsals. Its proximal end is approximately fourfold wider than its shaft at mid-length due to a predominantly medial and slightly anteroposterior expansion (Fig. 30B). The proximal head is slanted lateroproximally to mediodistally. It is subtriangular in proximal view, narrowing medially. The proximal surface is slightly convex in lateral or medial view. The shaft gradually narrows distally along most of its length, before widening somewhat towards its distal end. The distal end is rounded and bulbous.

With the possible exception of the small ungual of the third digit, all phalanges are accounted for between the right pes of NHMUK PV R 7557a (Spiekman *et al.* 2023, fig. 1) and the left pes of NHMUK PV R 37600b (Fig. 30), and the phalangeal formula is 2-3-4-4-2. The phalanges are all several times shorter than the metatarsals of the corresponding digit. The non-terminal
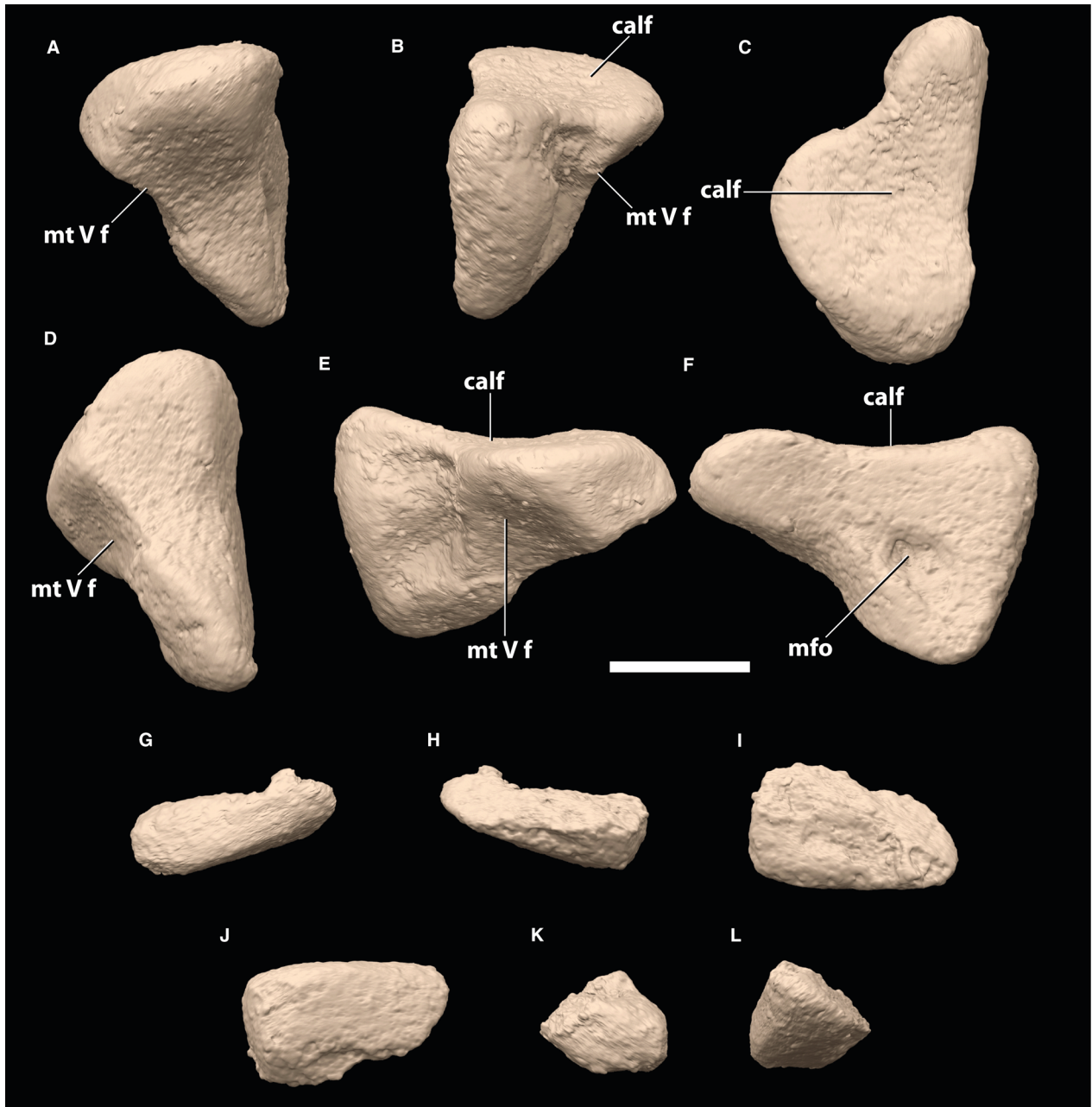
FIG. 29. Digital renderings of the right distal tarsals of NHMUK PV R 7557d. A–F, distal tarsal 4 in: A, anterior; B, posterior; C, proximal; D, distal; E, lateral; F, medial view. G–L, distal tarsal 3 in: G, ?anterior; H, ?posterior; I, ?proximal; J, ?distal; K, ?lateral; L, ?medial view. *Abbreviations*: calf, calcaneal facet; mfo, medial foramen; mtVf, metatarsal V facet. Scale bar represents 2 mm.

phalanges of metatarsals I–IV are slightly expanded on both their proximal and distal ends. Proximally, they are equally expanded in all orientations and, as such, their proximal end is subcircular in proximal view; the distal end is expanded only lateromedially. The proximal surface of the phalanges is slightly concave. The distal ends bear clear extensor pits on their medial and lateral sides (Fig. 30A). Consequently, the lateral and medial margins of the distal end converge slightly distally, and the lateral and medial surfaces are concave. The dorsal surface directly proximal to the

distal end also bears a shallow concavity. The posterior surface of the distal end is flat.

The unguals of digits I and II are considerably larger than those of the other digits, but they are nevertheless considerably smaller than the preceding phalanges of the same digit (Fig. 30A). They are also conspicuously curved, with a strongly convex dorsal margin and concave plantar margin in lateral or medial view. Distally, these unguals terminate in a relatively sharp tip. The ungual of digit III is incompletely preserved in

FIG. 30. Left pes of NHMUK PV R 37600b in: A, dorsal; B, lateral view. *Abbreviations*: dt, distal tarsal; exp, extensor pit; fi, fibula; l., left; mt, metatarsal; ti, tibia. Scale bars represent: 20 mm (A); 10 mm (B).

NHMUK PV R 37600b and might have been similarly developed as in digits I and II. The ungual of digit IV is short and blunt, forming a rounded apex in dorsal or lateral view. The two phalanges of digit V are preserved in articulation with right metatarsal V in NHMUK PV R 7557a (Spiekman *et al.* 2023, fig. 1). Both the non-terminal phalanx and the ungual are much smaller than the phalanges of the other digits, with the diminutive ungual of digit V being four- to fivefold smaller than the preceding phalanx. The proximal and distal ends of the non-terminal phalanx are very slightly expanded and rounded. The distal end of the ungual is gently rounded.

Histological description

In one specimen, a partial tibia (NHMUK PV R 37652), bacterial invasion has entirely destroyed the bone tissue, and no features can be discerned clearly. The medullary cavity is filled with sparry calcite cement in all specimens. Calcite crystals are smallest closest to the bone, and become larger in the centre of the medullary cavity. The preservation of the endosteal margin is variable, and it has probably been weathered due to exposure that also allowed for the subsequent calcite infilling during diagenesis. In all specimens, the cortex is relatively thin.
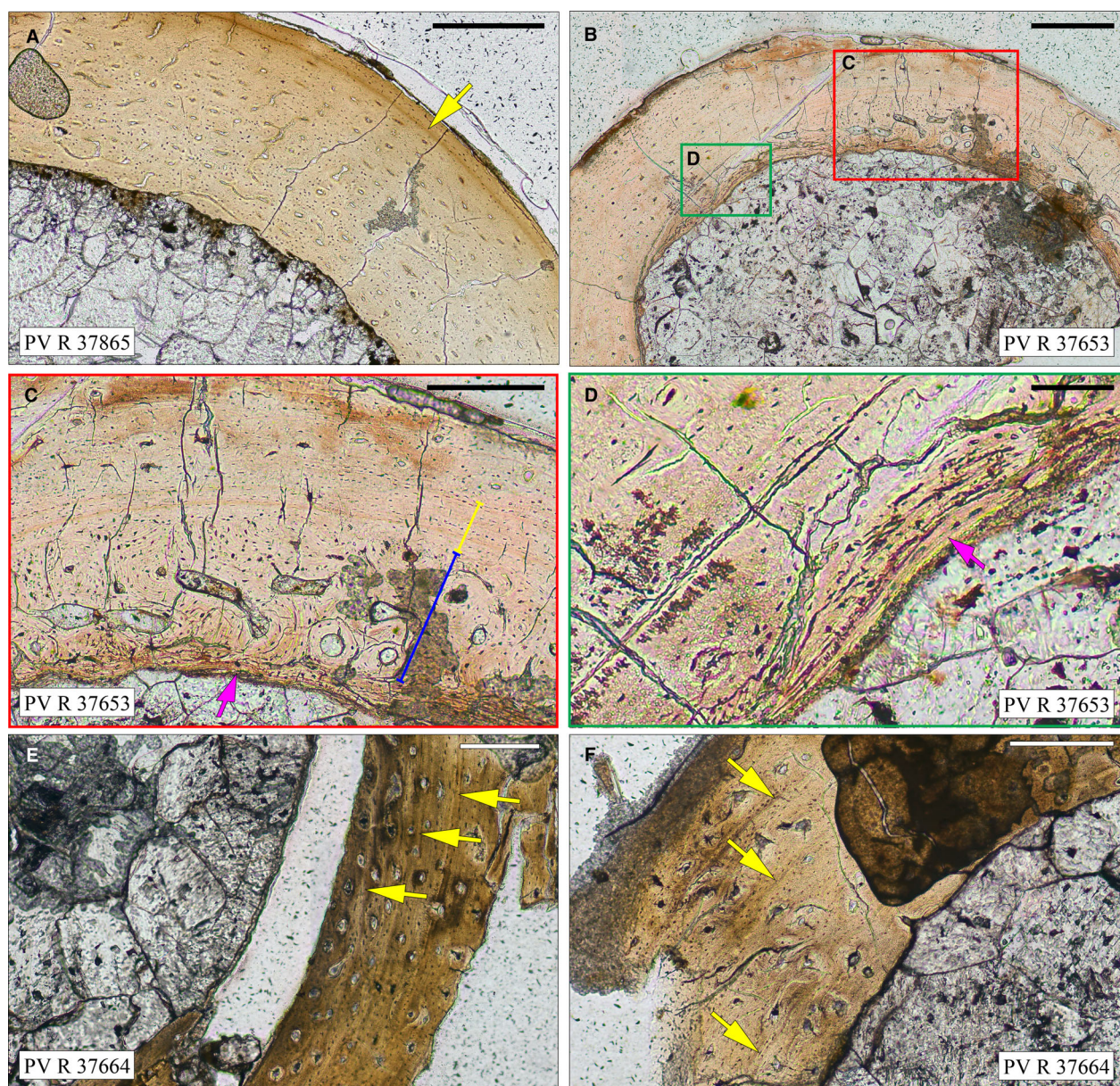
FIG. 31. Histological thin-sections of three individuals of *Terrestrisuchus gracilis*. A, cross-section through the femur of NHMUK PV R 37685; the yellow arrow indicates a single line of arrested growth (LAG). B–D, cross-section through the tibia of NHMUK PV R 37653: in B, the locations of the higher-magnification sections in C and D are shown by the red and green boxes respectively; C–D, endosteal bone is indicated by a purple arrow; C, a remodelled region of the inner cortex is indicated by the blue line, while an annulus is indicated by the yellow line. E–F, cross-section through the tibia of NHMUK PV R 37664. LAGs are indicated with yellow arrows. Scale bars represent: 250 μm (A, C, E, F); 500 μm (B); 200 μm (D).

In the femur, NHMUK PV R 37865 (Fig. 31A), the cortex is composed entirely of fibrolamellar bone. Primary osteons are evenly distributed throughout the cortex and are arranged longitudinally, although near the outer cortex they become flattened and the vascularity slightly decreases. A single line of arrested growth (LAG) is present close to the periosteal margin of the bone (Fig. 31A, yellow arrow). The histological characteristics of this femur are similar to those of a humerus attributed to *Terrestrisuchus* sp. by de Ricqlès *et al.* (2003).

In the best preserved tibia, NHMUK PV R 37653 (Fig. 31B–D), a layer of endosteal bone can be seen extending around parts of the endosteal margin of the cortex (Fig. 31C–D, purple arrow). This layer is composed of parallel-fibred bone and is poorly vascularized (Fig. 31D). Endosteal bone lining the medullary cavity was also observed in a humerus attributed to *Terrestrisuchus* sp. by de Ricqlès *et al.* (2003). The majority of the inner cortex is composed of fibrolamellar bone with large, equally spaced, longitudinal primary osteons, but one section of the inner cortex has been

remodelled, and is formed of fibrolamellar bone forming circumferential rings around large secondary osteons (Fig. 31C, region indicated by blue line). The outer cortex is composed of parallel-fibred bone with small, sparse simple vascular canals, and the boundary between the inner and outer cortex is marked by a low-vascularity annulus (Fig. 31C, region indicated by yellow line).

A second sectioned tibia (NHMUK PV R 37664; Fig. 31E–F) is not as well preserved. It has been damaged by bacterial alteration, and only parts of the original bone tissues can be seen. However, where preserved, it can be seen that the cortex is predominantly composed of fibrolamellar bone, with longitudinal primary osteons distributed throughout it. Vascularity is greatest in the inner cortex and decreases outwards. Three continuous LAGs appear to be present, marked by dark lines (Fig. 31E–F, yellow arrows). These are evenly spaced throughout the cortex.

DISCUSSION

Ontogenetic status & growth rates

None of the three histological sections studied preserve an external fundamental system, indicating that all of the animals were still growing at time of death. Fibrolamellar bone with longitudinal primary osteons appears to predominate early in growth, and the cortex of both NHMUK PV R 37865 (Fig. 31A) and NHMUK PV R 37664 (Fig. 31E–F) is composed of this bone tissue, indicating that these animals were still growing relatively fast and that they were not skeletally mature at time of death. In contrast, NHMUK PV R 37653 has parallel-fibred bone in the outer cortex and a partly remodelled inner cortex (Fig. 31C), indicating that this animal was probably from a later ontogenetic stage than the others. NHMUK PV R 37865 preserves one LAG in the rapidly deposited fibrolamellar cortex (Fig. 31A), while NHMUK PV R 37664 preserves three LAGs (Fig. 31E–F). In contrast, NHMUK PV R 37653 preserves an annulus that marks the boundary between the remodelled bone and the outer cortex (Fig. 31C). De Ricqlès et al. (2003) suggested that pseudosuchian archosaurs generally had a lamellar–zonal growth pattern, a cyclical pattern in which fibrolamellar bone gives way to parallel-fibred annuli, which terminate in a LAG. This growth pattern was observed in the early diverging crocodylomorph Hesperosuchus (de Ricqlès et al. 2008). LAGs observed in our samples of Terrestrisuchus are not underlain by annuli, suggesting relatively high growth rates for a pseudosuchian, as also suggested by de Ricqlès et al. (2003).

None of the Terrestrisuchus specimens that have so far been histologically sampled appear to be skeletally mature, and it is possible that all of the preserved specimens of this taxon are sub-adult or younger, and the lamellar–zonal pattern of tissue organization might have

been established as the animals reached skeletal maturity (de Ricqlès et al. 2008). However, the closely related crocodylomorph Saltoposuchus connectens also has a cortex composed of fibrolamellar bone with no evidence of a lamellar–zonal pattern (Spiekman 2023). The histologically sampled specimen of this taxon did not constitute an early ontogenetic stage, indicating that saltoposuchid crocodylomorphs probably had genuinely higher growth rates than later crocodyliforms (Spiekman 2023). The presence of fibrolamellar bone and elevated growth rates in saltoposuchids contrasts with the recent findings of Botha et al. (2023), who concluded that all early crocodylomorphs predominantly exhibit parallel-fibred or lamellar bone tissue in middle to late ontogeny and thus had growth patterns comparable with Jurassic crocodyliforms. Interestingly, saltoposuchid crocodylomorphs extended into the Early Jurassic in the form of Litargosuchus leptorhynchus (Clark & Sues 2002; Spiekman 2023), suggesting that 'fast-growing' crocodylomorphs might even have survived the end-Triassic mass extinction. Alternatively, the mixed presence of predominantly fibrolamellar and parallel-fibred bone tissue might also be reflective of highly variable growth regimes among early crocodylomorphs, as has been observed in a wide range of Triassic Archosauromorpha (Botha-Brink & Smith 2011; Jaquier & Scheyer 2017).

LAGs are thought to be due to pauses in growth related to resource-poor intervals, and are usually considered to occur annually, hence they have been used to estimate the age of animals at time of death (Bailleul et al. 2019). In Terrestrisuchus, two specimens that are histologically relatively immature have different numbers of LAGs in the inner cortex, while one specimen that appears histologically more mature has no LAGs in the inner cortex at all. This discrepancy could be interpreted in a number of ways. It could indicate developmental plasticity in Terrestrisuchus such that different individuals took different lengths of time to reach maturity and for growth to slow. Developmental plasticity of this type has been identified in the early sauropodomorph dinosaur Plateosaurus (Sander & Klein 2005), and was used to suggest an ectothermic metabolism in this dinosaur, given that all extant amniotes that show this sort of development are ectothermic and their growth rates are strongly affected by environmental factors (Sander & Klein 2005). Under this scenario, NHMUK PV R 37664 was 4 years of age but still growing rapidly when it died, while NHMUK PV R 37653 was a maximum of 1 year old, but its growth had slowed significantly at time of death, and it would presumably have reached a smaller adult body size.

Conversely, the discrepancy in the number of LAGs in the inner cortex could indicate that LAGs (and annuli) in Terrestrisuchus were not always deposited annually, but instead were laid down during resource-poor intervals,
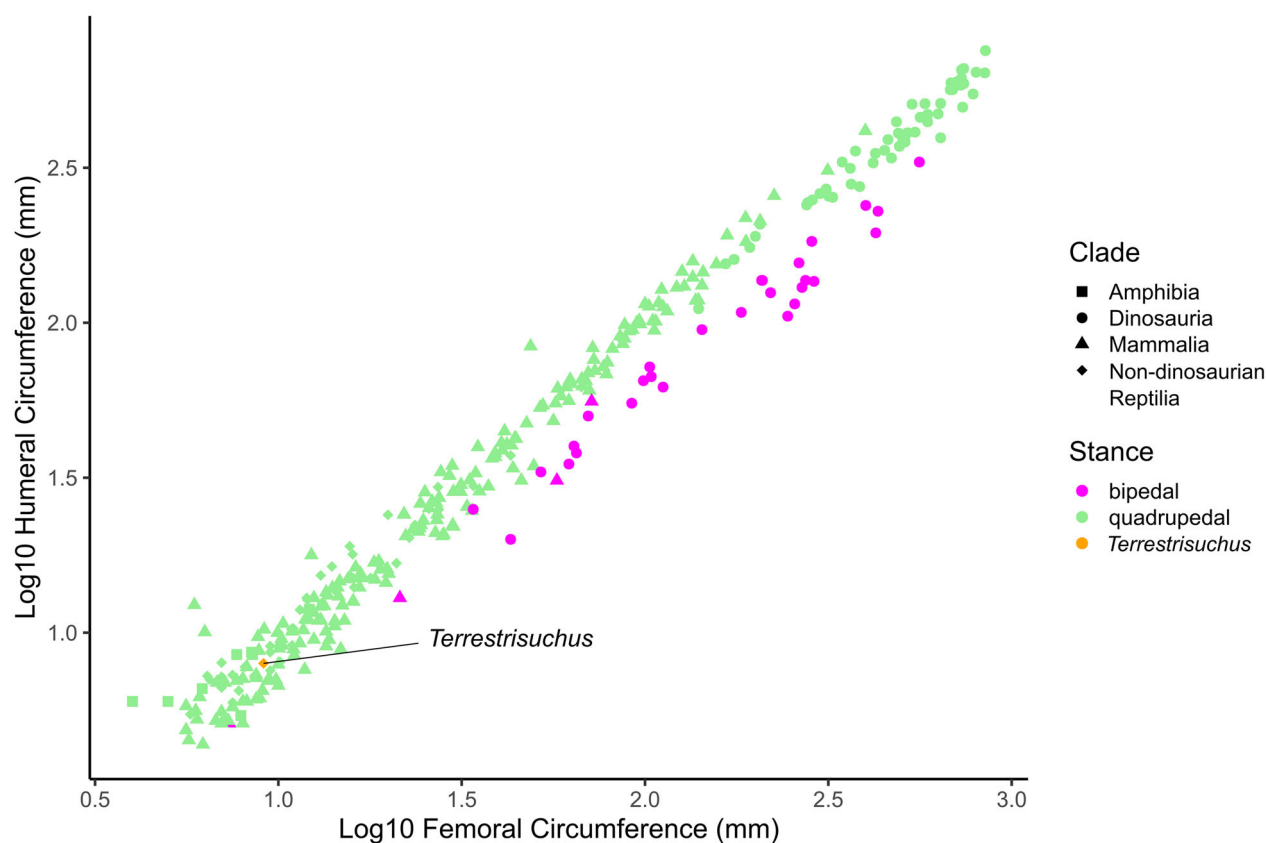
FIG. 32. A plot showing the relationship between femoral and humeral circumference in a range of quadrupedal and bipedal amphibians, dinosaurs, mammals and non-dinosaurian reptiles. *Terrestrisuchus gracilis* is indicated in pink, and lies within a region of small quadrupeds. Data from McPhee *et al.* (2018).

which may have occurred more frequently than once per year. Woodward (2019) identified 'localized vascular changes' (LVCs) in the tibiae of individuals of the dinosaur *Maiasaura* thought to be less than 1 year old, which were interpreted as a slowing in growth rate due to temporary but repeated stress, and were not expressed annually. Under this scenario, LAGs observed in the inner cortex of *Terrestrisuchus* could relate to frequent environmental stress in early ontogeny, equivalent to LVCs observed in *Maiasaura*.

Stance in Terrestrisuchus gracilis

When the humeral and femoral shaft circumferences of *Terrestrisuchus gracilis* (NHMUK PV R 7557) were added to the dataset of McPhee *et al.* (2018), *Terrestrisuchus* was found to plot firmly in the quadrupedal region, along with a number of small-bodied amphibians, mammals and reptiles (Fig. 32). This result is consistent with most previous assessments of the stance of *Terrestrisuchus*, which considered it a cursorial, terrestrial quadruped (e.g. Crush 1980; Sereno & Wild 1992; Irmis *et al.* 2013).

However, Gônet *et al.* (2023) found the taxon to be a biped or facultative biped based on femoral cortical thickness. Our histological analysis indicates that, at least in some specimens, the innermost region of the cortex is eroded, which may have led to thinning of the cortex after death. Furthermore, all specimens of *Terrestrisuchus* that we have examined to date appear to be skeletally immature, and this may also have resulted in a thinner cortex than in adult specimens. A caveat, however, of this analysis is that the McPhee *et al.* (2018) dataset is depauperate in small-bodied bipedal taxa, and indeed any bipedal taxa that are not dinosaurs. This is a consequence of a scarcity of bipeds among extant terrestrial taxa rather than incomplete sampling.

Nevertheless, other morphological observations lend strong additional support to the interpretation of *Terrestrisuchus gracilis* as a quadruped. The radiale and ulnare are strongly elongate, resulting in a long and stiffened carpus (Fig. 18). Furthermore, the metacarpals are tightly bunched in articulated specimens (Fig. 19), forming a single functional unit. Combined, these features suggest a distal forelimb that was clearly weight bearing and digitigrade, thus implying a quadrupedal posture, as was also

inferred by Crush (1980) based on similar observations. A digitigrade configuration of the carpus and manus has also been described for *Trialestes romeri* (tentatively), *Saltoposuchus connectens*, CMNH 29894, *Hallopus victor* and *Junggarsuchus sloani* (Walker 1970; Sereno & Wild 1992; Clark *et al.* 2000, 2004; Lecuona *et al.* 2016; Spiekman 2023), which might suggest that most, if not all, small-bodied non-crocodyliform crocodylomorphs were quadrupedal.

CONCLUSION

The postcranial anatomy of the small-bodied and highly gracile crocodylomorph *Terrestrisuchus gracilis* is documented, representing the most detailed postcranial description of a non-crocodyliform crocodylomorph to date. The presacral vertebrae lack hypapophyses (Figs 2–6). The anterior and mid dorsal ribs have a marked longitudinal crest along the anterior margin of the rib shaft (Fig. 4). There is no distinct lumbar region (Fig. 6). The vertebral count of the tail cannot be determined, but it was probably roughly similar to that seen in *Protosuchus richardsoni*, *c.* 35 caudal vertebrae (Colbert & Mook 1952), rather than the previously estimated count of *c.* 70 (Crush 1980, 1984). *Terrestrisuchus gracilis* had a single paired row of paramedian osteoderms, which are relatively small, mostly unsculptured, and leaf shaped (Fig. 11).

The known specimens of *Terrestrisuchus gracilis* do not preserve an ossified sternum (*contra* Crush 1980, 1984). The proximal head of the radius is strongly expanded medially, suggesting that this feature is more widespread in early crocodylomorphs than previously thought (Fig. 17B, D, E). The ilium has a long and slender preacetabular process (Fig. 20). The femur has a strongly inturned proximal head (Fig. 23A–D). The tibia and fibula are slightly longer than the femur (Table S2), a feature shared with *Macelognathus vagans* and certain avemetatarsalian archosaurs (Göhlich *et al.* 2005; Nesbitt 2011). In contrast to most early crocodylomorphs, the tibia and fibula are virtually straight (Figs 25A, 26A–B).

The carpus is characterized by an elongate radiale and ulnare (Fig. 18). Together with the closely bundled metacarpals and metatarsals of the fore- and hindlimbs (Figs 18, 30), this suggests a digitigrade posture, as has also been inferred for other crocodylomorphs (Irmis *et al.* 2013). The astragalocalcaneal articulation reflects the classical crurotarsal ankle joint (e.g. Sereno 1991; Appendix S1), and the posteriorly directed calcaneal tuber (Fig. 28C) is indicative of a fully erect posture (Parrish 1987). The unguals of both the manus and pes are poorly developed (Figs 19, 30). The pedal phalangeal formula is 2-3-4-4-2.

The inferred quadrupedal posture of *Terrestrisuchus gracilis* is corroborated by a statistical analysis of humeral and femoral shaft circumferences (Fig. 32), using a dataset with a broad sample of tetrapods (McPhee *et al.* 2018). Analysis of the long bone histology of several *Terrestrisuchus gracilis* specimens shows that all specimens were probably immature at the time of death, as indicated by the absence of both an external fundamental system and extensive bone remodelling (Fig. 31). The sample is dominated by fibrolamellar bone tissue with longitudinal primary osteons, although one specimen (NHMUK PV R 37653) has parallel-fibred bone in the outer cortex and a partly remodelled inner cortex. The overall histological pattern is similar to that recently described for the larger saltoposuchid *Saltoposuchus connectens* (Spiekman 2023).

Author contributions. **Conceptualization** SNF Spiekman (SNFS), RJ Butler (RJB), SCR Maidment (SCRM); **Data Curation** SNFS, SCRM, V Fernandez; **Formal Analysis** SNFS, RJB, SCRM; **Funding Acquisition** SNFS, RJB, SCRM; **Investigation** SNFS, SCRM; **Methodology** SNFS, RJB, SCRM; **Project Administration** SNFS, SCRM; **Resources** SNFS, SCRM; **Supervision** RJB, SCRM; **Validation** SNFS, RJB, SCRM; **Visualization** SNFS, SCRM; **Writing – Original Draft Preparation** SNFS, SCRM; **Writing – Review & Editing** SNFS, RJB, SCRM.

DATA ARCHIVING STATEMENT

Scan data for this study are archived in MorphoSource: NHMUK PV R 7591a https://doi.org/10.17602/M2/M518680; NHMUK PV R 7557d, distal tarsal 3 (https://doi.org/10.17602/M2/M622526), distal tarsal 4 (https://doi.org/10.17602/M2/M622507), calcaneum (https://doi.org/10.17602/M2/M622548), astragalus (https://doi.org/10.17602/M2/M622517).

Editor. Stephan Lautenschlager

SUPPORTING INFORMATION

Additional Supporting Information can be found online (https://doi.org/10.1002/spp2.1577):

Table S1. Scanning parameters used for the ankle bones of NHMUK PV R 7557.
Table S2. Postcranial measurements of *Terrestrisuchus gracilis*.
Appendix S1. Digital rendering of the astragalus–calcaneum articulation of *Terrestrisuchus gracilis* based on the ankle bones of NHMUK PV R 7557.
Appendix S2. Overview of the postcranial elements of *Terrestrisuchus gracilis* present in NHMUK collections.
Appendix S3. Files and script used to conduct the stance analysis.

REFERENCES

Allen, R. C. 2010. The anatomy and systematics of *Terrestrisuchus gracilis* (Archosauria, Crocodylomorpha). PhD thesis, Northern Illinois University, USA.

Bailleul, A. M., O'Connor, J. and Schweitzer, M. H. 2019. Dinosaur paleohistology: review, trends and new avenues of investigation. *PeerJ*, **7**, e7764.

Ballell, A., Rayfield, E. J. and Benton, M. J. 2020. Osteological redescription of the Late Triassic sauropodomorph dinosaur *Thecodontosaurus antiquus* based on new material from Tytherington, southwestern England. *Journal of Vertebrate Paleontology*, **40**, e1770774.

Benton, M. J. 2021. The origin of endothermy in synapsids and archosaurs and arms races in the Triassic. *Gondwana Research*, **100**, 261–289.

Bonaparte, J. F. 1972. Los tetrápodos del sector superior de la Formación Los Colorados, La Rioja, Argentina (Triásico Superior). 1 Parte. *Opera Lilloana*, **22**, 1–183.

Botha-Brink, J. and Smith, R. M. H. 2011. Osteohistology of the Triassic archosauromorphs *Prolacerta*, *Proterosuchus*, *Euparkeria*, and *Erythrosuchus* from the Karoo Basin of South Africa. *Journal of Vertebrate Paleontology*, **31**, 1238–1254.

Botha, J., Weiss, B. M., Dollman, K., Barrett, P. M., Benson, R. B. and Choiniere, J. N. 2023. Origins of slow growth on the crocodilian stem lineage. *Current Biology*, **33**, 4261–4268.

Brochu, C. A. 1992. Ontogeny of the postcranium in crocodylomorph archosaurs. MSc thesis, University of Texas at Austin, USA.

Brochu, C. A. 2003. Phylogenetic approaches toward crocodylian history. *Annual Review of Earth & Planetary Sciences*, **31**, 357–397.

Buckley, G. A., Brochu, C. A., Krause, D. W. and Pol, D. 2000. A pug-nosed crocodyliform from the Late Cretaceous of Madagascar. *Nature*, **405**, 941–944.

Chamero, B., Buscalioni, Á. D. and Marugán-Lobón, J. 2013. Pectoral girdle and forelimb variation in extant Crocodylia: the coracoid–humerus pair as an evolutionary module. *Biological Journal of the Linnean Society*, **108**, 600–618.

Clark, J. M. 1986. Phylogenetic relationships of the crocodylomorphs archosaurs. PhD thesis, University of Chicago, USA.

Clark, J. M. and Sues, H.-D. 2002. Two new basal crocodylomorph archosaurs from the Lower Jurassic and the monophyly of the Sphenosuchia. *Zoological Journal of the Linnean Society*, **136**, 77–95.

Clark, J. M., Sues, H.-D. and Berman, D. S. 2000. A new specimen of *Hesperosuchus agilis* from the Upper Triassic of New Mexico and the interrelationships of basal crocodylomorph archosaurs. *Journal of Vertebrate Paleontology*, **20**, 683–704.

Clark, J. M., Xu, X., Forster, C. A. and Wang, Y. 2004. A Middle Jurassic 'sphenosuchian' from China and the origin of the crocodylian skull. *Nature*, **430**, 1021–1024.

Colbert, E. H. 1952. A pseudosuchian reptile from Arizona. *Bulletin of the American Museum of Natural History*, **99**, 561–592.

Colbert, E. H. and Mook, C. C. 1952. The ancestral crocodilian *Protosuchus*. *Bulletin of the American Museum of Natural History*, **97**, 143–182.

Cope, E. D. 1869–1870. Synopsis of the extinct Batrachia, Reptilia and Aves of North America. *Transactions of the American Philosophical Society*, **14**, 1–252.

Cruickshank, A. R. I. 1979. The ankle joint in some early archosaurs. *South African Journal of Science*, **75**, 168–178.

Crush, P. J. 1980. An early, terrestrial, crocodile from South Wales. PhD thesis, University College London, UK.

Crush, P. J. 1984. A late upper Triassic sphenosuchid crocodilian from Wales. *Palaeontology*, **27**, 131–157.

Cuff, A. R., Demuth, O. E., Michel, K., Otero, A., Pintore, R., Polet, D., Wiseman, A. L. A. and Hutchinson, J. R. 2022. Walking – and running and jumping – with dinosaurs and their cousins, viewed through the lens of evolutionary biomechanics. *Integrative & Comparative Biology*, **62**, 1281–1305.

de Buffrénil, V. and Quilhac, A. 2021. Bone tissue types: a brief account of currently used categories. 147–190. *In* de Buffrénil, V., de Ricqlès, A. J., Zylberberg, L. and Padian, K. (eds) *Vertebrate skeletal histology and paleohistology*. CRC Press, 8 pp.

de Buffrénil, V., Clarac, F., Fau, M., Martin, S., Martin, B., Pellé, E. and Laurin, M. 2015. Differentiation and growth of bone ornamentation in vertebrates: a comparative histological study among the Crocodylomorpha. *Journal of Morphology*, **276**, 425–445.

de Ricqlès, A. J., Padian, K. and Horner, J. R. 2003. On the bone histology of some Triassic pseudosuchian archosaurs and related taxa. *Annales de Paléontologie*, **89**, 67–101.

de Ricqlès, A. J., Padian, K., Knoll, F. and Horner, J. R. 2008. On the origin of high growth rates in archosaurs and their ancient relatives: complementary histological studies on Triassic archosauriforms and the problem of a "phylogenetic signal" in bone histology. *Annales de Paléontologie*, **94**, 57–76.

Drymala, S. M. and Zanno, L. E. 2016. Osteology of *Carnufex carolinensis* (Archosauria: Pseudosuchia) from the Pekin Formation of North Carolina and its implications for early crocodylomorph evolution. *PLoS One*, **11**, e0157528.

Dufeau, D. L. and Witmer, L. M. 2015. Ontogeny of the middle-ear air–sinus system in *Alligator mississippiensis* (Archosauria: Crocodylia). *PLoS One*, **10**, e0137060.

Fernandez, V. 2024. Terrestrisuchus. MorphoSource dataset. https://www.morphosource.org/projects/000518675

Fish, F. E. 1984. Kinematics of undulatory swimming in the American alligator. *Copeia*, **4**, 839–843.

Fraser, N. C., Padian, K., Walkden, G. M. and Davis, A. L. M. 2002. Basal dinosauriform remains from Britain and the diagnosis of the Dinosauria. *Palaeontology*, **45**, 79–95.

Galton, P. M. and Kermack, D. 2010. The anatomy of *Pantydraco caducus*, a very basal sauropodomorph dinosaur from the Rhaetian (Upper Triassic) of South Wales, UK. *Revue de Paléobiologie*, **29**, 341–404.

Galton, P. M., Yates, A. M. and Kermack, D. 2007. *Pantydraco* n. gen. for *Thecodontosaurus caducus* Yates, 2003, a basal sauropodomorph dinosaur from the Upper Triassic or Lower Jurassic of South Wales, UK. *Neues Jahrbuch für Geologie und Paläontologie-Abhandlungen*, **243**, 119–125.

Gatesy, S. M. 1991. Hind limb movements of the American alligator (*Alligator mississippiensis*) and postural grades. *Journal of Zoology*, **224**, 577–588.

Gauthier, J. A. and Padian, K. 2020. Archosauria. 1187–1193. *In* de Queiroz, K., Cantino, P. D. and Gauthier, J. A. (eds) *Phylonyms: A companion to the Phylocode*. CRC Press.

Georgi, J. A. and Krause, D. W. 2010. Postcranial axial skeleton of *Simosuchus clarki* (Crocodyliformes: Notosuchia) from the Late Cretaceous of Madagascar. *Journal of Vertebrate Paleontology*, **30**, 99–121.

Godoy, P. L., Bronzati, M., Eltink, E., Marsola, J. C. D. A., Cidade, G. M., Langer, M. C. and Montefeltro, F. C. 2016. Postcranial anatomy of *Pissarrachampsa sera* (Crocodyliformes, Baurusuchidae) from the Late Cretaceous of Brazil: insights on lifestyle and phylogenetic significance. *PeerJ*, **4**, e2075.

Godoy, P. L., Benson, R. B., Bronzati, M. and Butler, R. J. 2019. The multi-peak adaptive landscape of crocodylomorph body size evolution. *BMC Evolutionary Biology*, **19**, 167.

Göhlich, U. B., Chiappe, L. M., Clark, J. M. and Sues, H.-D. 2005. The systematic position of the Late Jurassic alleged dinosaur *Macelognathus* (Crocodylomorpha: Sphenosuchia). *Canadian Journal of Earth Sciences*, **42**, 307–321.

Gomani, E. M. 1997. A crocodyliform from the Early Cretaceous dinosaur beds, northern Malawi. *Journal of Vertebrate Paleontology*, **17**, 280–294.

Gônet, J., Bardin, J., Girondot, M., Hutchinson, J. R. and Laurin, M. 2023. Locomotor and postural diversity among reptiles viewed through the prism of femoral microanatomy: palaeobiological implications for some Permian and Mesozoic taxa. *Journal of Anatomy*, **242**, 891–916.

Gow, C. E. and Kitching, J. W. 1988. Early Jurassic crocodilomorphs from the Stormberg of South Africa. *Neues Jahrbuch für Geologie und Paläontologie-Monatshefte*, **1988**, 517–536.

Gregorovičová, M., Kvasilová, A. and Sedmera, D. 2018. Ossification pattern in forelimbs of the Siamese Crocodile (*Crocodylus siamensis*): similarity in ontogeny of carpus among crocodylian species. *The Anatomical Record*, **301**, 1159–1168.

Griffin, C. T. 2018. Developmental patterns and variation among early theropods. *Journal of Anatomy*, **232**, 604–640.

Griffin, C. T., Stocker, M. R., Colleary, C., Stefanic, C. M., Lessner, E. J., Riegler, M., Formoso, K., Koeller, K. and Nesbitt, S. J. 2021. Assessing ontogenetic maturity in extinct saurian reptiles. *Biological Reviews*, **96**, 470–525.

Groh, S. S., Upchurch, P., Barrett, P. M. and Day, J. J. 2020. The phylogenetic relationships of neosuchian crocodiles and their implications for the convergent evolution of the longirostrine condition. *Zoological Journal of the Linnean Society*, **188**, 473–506.

Hay, O. P. 1930. *Second bibliography and catalogue of the fossil vertebrata of North America*. Carnegie Institution of Washington, 1074 pp.

Hill, R. V. 2010. Osteoderms of *Simosuchus clarki* (Crocodyliformes: Notosuchia) from the Late Cretaceous of Madagascar. *Journal of Vertebrate Paleontology*, **30**, 154–176.

Hoffstetter, R. and Gasc, J.-P. 1969. Vertebrae and ribs of modern reptiles. 201–310. *In* Gans, C., Bellairs, A. D. A. and Parsons, T. S. (eds) *Biology of the reptilia*. Academic Press.

Huene, F. R. von 1921. Neue Pseudosuchier und Coelurosaurier aus dem Württembergischen Keuper. *Acta Zoologica*, **2**, 329–403.

Hutchinson, J. R. 2001a. The evolution of pelvic osteology and soft tissues on the line to extant birds (Neornithes). *Zoological Journal of the Linnean Society*, **131**, 123–168.

Hutchinson, J. R. 2001b. The evolution of femoral osteology and soft tissues on the line to extant birds (Neornithes). *Zoological Journal of the Linnean Society*, **131**, 169–197.

Irmis, R. B., Nesbitt, S. J. and Sues, H.-D. 2013. Early Crocodylomorpha. *Geological Society, London, Special Publications*, **379**, 275–302.

Jaquier, V. P. and Scheyer, T. M. 2017. Bone histology of the Middle Triassic long-necked reptiles *Tanystropheus* and *Macrocnemus* (Archosauromorpha, Protorosauria). *Journal of Vertebrate Paleontology*, **37**, e1296456.

Johnson, M. M., Young, M. T. and Brusatte, S. L. 2020. The phylogenetics of Teleosauroidea (Crocodylomorpha, Thalattosuchia) and implications for their ecology and evolution. *PeerJ*, **8**, e9808.

Keeble, E., Whiteside, D. I. and Benton, M. J. 2018. The terrestrial fauna of the Late Triassic Pant-y-ffynnon Quarry fissures, South Wales, UK and a new species of *Clevosaurus* (Lepidosauria: Rhynchocephalia). *Proceedings of the Geologists' Association*, **129**, 99–119.

Klein, N., Foth, C. and Schoch, R. R. 2017. Preliminary observations on the bone histology of the Middle Triassic pseudosuchian archosaur *Batrachotomus kupferzellensis* reveal fast growth with laminar fibrolamellar bone tissue. *Journal of Vertebrate Paleontology*, **37**, e1333121.

Klinkhamer, A. J., Wilhite, D. R., White, M. A. and Wroe, S. 2017. Digital dissection and three-dimensional interactive models of limb musculature in the Australian estuarine crocodile (*Crocodylus porosus*). *PLoS One*, **12**, e0175079.

Korneisel, D. E., Vice, R. and Maddin, H. C. 2022. Anatomy and development of skull–neck boundary structures in the skeleton of the extant crocodylian *Alligator mississippiensis*. *The Anatomical Record*, **305**, 3002–3015.

Leardi, J. M., Pol, D., Novas, F. E. and Suárez Riglos, M. 2015. The postcranial anatomy of *Yacarerani boliviensis* and the phylogenetic significance of the notosuchian postcranial skeleton. *Journal of Vertebrate Paleontology*, **35**, e995187.

Leardi, J. M., Pol, D. and Clark, J. M. 2017. Detailed anatomy of the braincase of *Macelognathus vagans* Marsh, 1884 (Archosauria, Crocodylomorpha) using high resolution tomography and new insights on basal crocodylomorph phylogeny. *PeerJ*, **5**, e2801.

Leardi, J. M., Pol, D. and Clark, J. M. 2020. Braincase anatomy of *Almadasuchus figarii* (Archosauria, Crocodylomorpha) and a review of the cranial pneumaticity in the origins of Crocodylomorpha. *Journal of Anatomy*, **237**, 48–73.

Lecuona, A. and Desojo, J. B. 2012. Hind limb osteology of *Gracilisuchus stipanicicorum* (Archosauria: Pseudosuchia). *Earth & Environmental Science Transactions of the Royal Society of Edinburgh*, **102**, 105–128.

Lecuona, A., Ezcurra, M. D. and Irmis, R. B. 2016. Revision of the early crocodylomorph *Trialestes romeri* (Archosauria, Suchia) from the lower Upper Triassic Ischigualasto Formation of Argentina: one of the oldest-known crocodylomorphs. *Papers in Palaeontology*, **2**, 585–622.

Legendre, L. J., Guénard, G., Botha-Brink, J. and Cubo, J. 2016. Palaeohistological evidence for ancestral high metabolic rate in archosaurs. *Systematic Biology*, **65**, 989–996.

Lovegrove, J., Newell, A. J., Whiteside, D. I. and Benton, M. J. 2021. Testing the relationship between marine transgression and evolving island palaeogeography using 3D GIS: an example from the Late Triassic of SW England. *Journal of the Geological Society*, **178**, jgs2020-158.

Mannion, P. D., Chiarenza, A. A., Godoy, P. L. and Cheah, Y. N. 2019. Spatiotemporal sampling patterns in the 230 million year fossil record of terrestrial crocodylomorphs and their impact on diversity. *Palaeontology*, **62**, 615–637.

Mansfield, J. H. and Abzhanov, A. 2010. Hox expression in the American alligator and evolution of archosaurian axial patterning. *Journal of Experimental Zoology Part B: Molecular & Developmental Evolution*, **314**, 629–644.

McPhee, B. W., Benson, R. B., Botha-Brink, J., Bordy, E. M. and Choiniere, J. N. 2018. A giant dinosaur from the earliest Jurassic of South Africa and the transition to quadrupedality in early sauropodomorphs. *Current Biology*, **28**, 3143–3151.

Nash, D. S. 1975. The morphology and relationships of a crocodilian, *Orthosuchus stormbergi*, from the Upper Triassic of Lesotho. *Annals of the South African Museum*, **67**, 227–329.

Nesbitt, S. J. 2011. The early evolution of archosaurs: relationships and the origin of major clades. *Bulletin of the American Museum of Natural History*, **352**, 1–292.

Nesbitt, S. J., Irmis, R. B., Lucas, S. G. and Hunt, A. P. 2005. A giant crocodylomorph from the Upper Triassic of New Mexico. *Paläontologische Zeitschrift*, **79**, 471–478.

Nesbitt, S. J., Turner, A. H., Erickson, G. M. and Norell, M. A. 2006. Prey choice and cannibalistic behaviour in the theropod *Coelophysis*. *Biology Letters*, **2**, 611–614.

Padian, K. and Lamm, E.-T. 2013. *Bone histology of fossil tetrapods: Advancing methods, analysis, and interpretation*. University of California Press.

Parrish, J. M. 1987. The origin of crocodilian locomotion. *Paleobiology*, **13**, 396–414.

Parrish, J. M. 1991. A new specimen of an early crocodylomorph (cf. *Sphenosuchus* sp.) from the Upper Triassic Chinle Formation of Petrified Forest National Park, Arizona. *Journal of Vertebrate Paleontology*, **11**, 198–212.

Patrick, E. L., Whiteside, D. I. and Benton, M. J. 2019. A new crurotarsan archosaur from the Late Triassic of South Wales. *Journal of Vertebrate Paleontology*, **39**, e1645147.

Pintore, R., Houssaye, A., Nesbitt, S. J. and Hutchinson, J. R. 2022. Femoral specializations to locomotor habits in early archosauriforms. *Journal of Anatomy*, **240**, 867–892.

Pol, D. 2005. Postcranial remains of *Notosuchus terrestris* Woodward (Archosauria: Crocodyliformes) from the Upper Cretaceous of Patagonia, Argentina. *Ameghiniana*, **42**, 21–38.

Pol, D., Leardi, J. M., Lecuona, A. and Krause, M. 2012. Postcranial anatomy of *Sebecus icaeorhinus* (Crocodyliformes, Sebecidae) from the Eocene of Patagonia. *Journal of Vertebrate Paleontology*, **32**, 328–354.

Pol, D., Rauhut, O. W. M., Lecuona, A., Leardi, J. M., Xu, X. and Clark, J. M. 2013. A new fossil from the Jurassic of Patagonia reveals the early basicranial evolution and the origins of Crocodyliformes. *Biological Reviews*, **88**, 862–872.

Reilly, S. M. and Elias, J. A. 1998. Locomotion in *Alligator mississippiensis*: kinematic effects of speed and posture and their relevance to the sprawling-to-erect paradigm. *Journal of Experimental Biology*, **201**, 2559–2574.

Rio, J. P., Mannion, P. D., Tschopp, E., Martin, J. E. and Delfino, M. 2020. Reappraisal of the morphology and phylogenetic relationships of the alligatoroid crocodylian *Diplocynodon hantoniensis* from the late Eocene of the United Kingdom. *Zoological Journal of the Linnean Society*, **188**, 579–629.

Ruebenstahl, A. A., Klein, M. D., Yi, H., Xu, X. and Clark, J. M. 2022. Anatomy and relationships of the early diverging Crocodylomorphs *Junggarsuchus sloani* and *Dibothrosuchus elaphros*. *The Anatomical Record*, **305**, 2463–2556.

Sander, P. M. 2000. Longbone histology of the Tendaguru sauropods: implications for growth and biology. *Paleobiology*, **26**, 466–488.

Sander, P. M. and Klein, N. 2005. Developmental plasticity in the life history of a prosauropod dinosaur. *Science*, **310**, 1800–1802.

Schaeffer, B. 1941. The morphological and functional evolution of the tarsus in amphibians and reptiles. *Bulletin of the American Museum of Natural History*, **78**, 395–472.

Sereno, P. C. 1991. Basal archosaurs: phylogenetic relationships and functional implications. *Journal of Vertebrate Paleontology*, **11**, 1–53.

Sereno, P. C. and Wild, R. 1992. *Procompsognathus*: theropod, "thecodont" or both? *Journal of Vertebrate Paleontology*, **12**, 435–458.

Sertich, J. J. and Groenke, J. R. 2010. Appendicular skeleton of *Simosuchus clarki* (Crocodyliformes: Notosuchia) from the late Cretaceous of Madagascar. *Journal of Vertebrate Paleontology*, **30**, 122–153.

Seymour, R. S., Bennett-Stamper, C. L., Johnston, S. D., Carrier, D. R. and Grigg, G. C. 2004. Evidence for endothermic ancestors of crocodiles at the stem of archosaur evolution. *Physiological & Biochemical Zoology*, **77**, 1051–1067.

Skinner, M., Whiteside, D. I. and Benton, M. J. 2020. Late Triassic island dwarfs? Terrestrial tetrapods of the Ruthin fissure (South Wales, UK) including a new genus of procolophonid. *Proceedings of the Geologists' Association*, **131**, 535–561.

Spiekman, S. N. 2023. A revision and histological investigation of *Saltoposuchus connectens* (Archosauria: Crocodylomorpha) from the Norian (Late Triassic) of south-western Germany. *Zoological Journal of the Linnean Society*, **199**, 354–391.

Spiekman, S. N. F., Ezcurra, M. D., Butler, R. J., Fraser, N. C. and Maidment, S. C. R. 2021. *Pendraig milnerae*, a new small-sized coelophysoid theropod from the Late Triassic of Wales. *Royal Society Open Science*, **8**, 210915.

Spiekman, S. N. F., Fernandez, V., Butler, R. J., Dollman, K. N. and Maidment, S. C. R. 2023. A taxonomic revision and cranial description of *Terrestrisuchus gracilis* (Archosauria, Crocodylomorpha) from the Upper Triassic of Pant-y-Ffynnon Quarry (southern Wales). *Papers in Palaeontology*, **9**, e1534.

Stefanic, C. M. and Nesbitt, S. J. 2019. The evolution and role of the hyposphene–hypantrum articulation in Archosauria: phylogeny, size and/or mechanics? *Royal Society Open Science*, **6**, 190258.

Stubbs, T. L., Pierce, S. E., Rayfield, E. J. and Anderson, P. S. 2013. Morphological and biomechanical disparity of crocodile-line archosaurs following the end-Triassic extinction. *Proceedings of the Royal Society B*, **280**, 20131940.

Stubbs, T. L., Pierce, S. E., Elsler, A., Anderson, P. S., Rayfield, E. J. and Benton, M. J. 2021. Ecological opportunity and the rise and fall of crocodylomorph evolutionary innovation. *Proceedings of the Royal Society B*, **288**, 20210069.

Sues, H.-D., Olsen, P. E., Carter, J. G. and Scott, D. M. 2003. A new crocodylomorph archosaur from the Upper Triassic of North Carolina. *Journal of Vertebrate Paleontology*, **23**, 329–343.

Toljagić, O. and Butler, R. J. 2013. Triassic–Jurassic mass extinction as trigger for the Mesozoic radiation of crocodylomorphs. *Biology Letters*, **9**, 20130095.

Turner, M. L. and Gatesy, S. M. 2023. Inner workings of the alligator ankle reveal the mechanistic origins of archosaur locomotor diversity. *Journal of Anatomy*, **242**, 592–606.

Vickaryous, M. K. and Hall, B. K. 2008. Development of the dermal skeleton in *Alligator mississippiensis* (Archosauria, Crocodylia) with comments on the homology of osteoderms. *Journal of Morphology*, **269**, 398–422.

von Baczko, M. B., Desojo, J. B. and Ponce, D. 2019. Postcranial anatomy and osteoderm histology of *Riojasuchus tenuisceps* and a phylogenetic update on Ornithosuchidae (Archosauria, Pseudosuchia). *Journal of Vertebrate Paleontology*, **39**, e1693396.

Walker, A. D. 1970. A revision of the Jurassic reptile *Hallopus victor* (Marsh), with remarks on the classification of crocodiles. *Philosophical Transactions of the Royal Society B*, **257**, 323–372.

Walker, A. D. 1990. A revision of *Sphenosuchus acutus* Haughton, a crocodylomorph reptile from the Elliot Formation (Late Triassic or Early Jurassic) of South Africa. *Philosophical Transactions of the Royal Society B*, **330**, 1–120.

Whiteside, D. I., Duffin, C. J., Gill, P. G., Marshall, J. E. A. and Benton, M. J. 2016. The Late Triassic and Early Jurassic fissure faunas from Bristol and South Wales: stratigraphy and setting. *Palaeontologia Polonica*, **67**, 257–287.

Wickham, H. 2016. *ggplot2: Elegant graphics for data analysis*. Springer-Verlag.

Wilson, J. A. 1999. A nomenclature for vertebral laminae in sauropods and other saurischian dinosaurs. *Journal of Vertebrate Paleontology*, **19**, 639–653.

Wilson, J. A., Michael, D. D., Ikejiri, T., Moacdieh, E. M. and Whitlock, J. A. 2011. A nomenclature for vertebral fossae in sauropods and other saurischian dinosaurs. *PLoS One*, **6**, e17114.

Wiseman, A. L. A., Bishop, P. J., Demuth, O. E., Cuff, A. R., Michel, K. B. and Hutchinson, J. R. 2021. Musculoskeletal modelling of the Nile crocodile (*Crocodylus niloticus*) hindlimb: effects of limb posture on leverage during terrestrial locomotion. *Journal of Anatomy*, **239**, 424–444.

Woodward, H. N. 2019. *Maiasaura* (Dinosauria: Hadrosauridae) tibia osteohistology reveals non-annual cortical vascular rings in young of the year. *Frontiers in Earth Science*, **7**, 50.

Wu, X.-C. and Chatterjee, S. 1993. *Dibothrosuchus elaphros*, a crocodylomorph from the Lower Jurassic of China and the phylogeny of the Sphenosuchia. *Journal of Vertebrate Paleontology*, **13**, 58–89.

Zittel, K. A. 1887–1890. *Handbuch der palaeontologie. Palaeozoologie. Band 3. Vertebrata*. R. Oldenbourg.